1995

Dynamic balance and walking control of biped mechanisms

James J. Troy
Iowa State University

Dynamic balance and walking control of biped mechanisms

by

James J. Troy

A Dissertation Submitted to the

Graduate Faculty in Partial Fulfillment of the

Requirements for the Degree of

DOCTOR OF PHILOSOPHY

Department: Mechanical Engineering
Major: Mechanical Engineering

Approved:

Signature was redacted for privacy.

In Charge of Major Work

Signature was redacted for privacy.

For the Major Department

Signature was redacted for privacy.

For the Graduate College

Iowa State University
Ames, Iowa

1995

TABLE OF CONTENTS

LIST OF FIGURES

LIST OF TABLES

NOMENCLATURE

The following is a listing and description of some of the variables used in this dissertation. Additional variables, superscripts, and subscripts may be defined within the text.

m	mass
I, I_c	moment of inertia, moment of inertia about CG
l, l_c	length, length to CG
μ	friction coefficient
ρ	viscous damping coefficient
M	moment or torque
F	general force
G	ground reaction force
k	feedback gain or spring rates
${}^i_jR$	3×3 rotation matrix
${}^i_jT$	4×4 homogeneous transformation matrix
t	time
τ	torque
$\mathbf{g}$	gravity
q_i	generalized coordinate variable
θ	angular position
$\omega, \dot{\theta}$	angular velocity
$\alpha, \ddot{\theta}$	angular acceleration
x, y, z	cartesian positions
$\dot{x}, \dot{y}, \dot{z}$	cartesian velocities
$\ddot{x}, \ddot{y}, \ddot{z}$	cartesian accelerations

ACKNOWLEDGEMENTS

I would like to thank my advisor Marty Vanderploeg for giving me the chance to work on a topic that has interested me for a long time. I would also like to thanks Professors Bernard, Flugrad, Huston, Luecke, and Pierson for serving on my committee.

I also thank my friends and colleagues in the Visualization Laboratory, from the early days when the lab consisted of a couple of graphics computers crammed in the corner of the old mainframe room, to the present — for our technical and philosophical discussions as well as for needed distractions.

And finally, I thank my parents for believing in me and for their many words of encouragement.

1. INTRODUCTION

What is a biped? A biped is any system that uses two legs for support and/or locomotion. The research presented here focuses on the development of feedback control systems for locomotion of two and three dimensional, dynamically balanced, biped mechanisms. The objective of this research is to develop interactive simulations of dynamic biped systems using feedback control for balancing and walking.

The main areas to be discussed are: the development of system equations of motion, manual and automatic actuator control, and interactive computer graphics. Additional concerns include: optimization, interface devices, manual control methods.

1.1 Motivation

Why study biped locomotion? Aside from general curiosity into the visually elegant, but mathematically complex field of bipedal systems, there are several practical reasons to investigate this topic. Among the most important is the relative ease with which legged vehicles can traverse a discontinuous surface. Other practical aspects include the ability to maneuver in restricted spaces, and the relatively low impact that legs have on the environment. But, to answer this question in more detail we first need to take a brief look at the limitations of other types of ground transportation.

Wheeled locomotion is a relatively simple form of transportation. In its most basic form, a torque is applied through a single joint and motion is produced. To stop a wheeled vehicle from moving, restrict its rotation by applying a brake. The system is inherently stable, easy to describe mathematically, and relatively easy to build. Wheeled vehicles require a relatively level and uniform surface on which to move. Only obstacles of limited size can be tolerated,

orientation control is usually very limited, and stability is determined by the systems physical parameters.

Tracked vehicles operate under essentially the same principles as wheeled vehicles. The track itself is just a movable surface that the vehicle lays down to get relatively consistent traction no matter where it goes. By providing itself with a uniform surface, a tracked vehicle increases its operational environment, but the burden of carrying its own surface decreases its efficiency. Orientation techniques for tracked vehicles are clumsy and can be damaging to the surface environment (anyone who has seen a tracked vehicle turn on a grass field knows the damage they can cause).

Legged locomotion, and bipedal locomotion in particular, is a much different concept. Several complex operations must be performed simultaneously to achieve a walking cycle, as well as to just maintain position. In addition, several types of sensory feedback inputs are required. A steady stream of visual, balance, and tactile information is necessary to maintain control. Bipeds are inherently unstable systems that require active control to behave in a stable manner. Legged systems are not limited by the need for a continuous surface. Even a very discontinuous surface, like steps or rocks, will serve as a sufficient surface for a biped. As along as some set of platforms exist that are spaced within the biped's step length, the surface qualifications are met.

1.2 Disciplines Involved

Research in the area of biped locomotion is a multi-disciplinary field that usually breaks down into one of three areas: 1. robotics and controls, 2. computer graphics, and 3. biomechanics. Each field has a different perspective and different goals. Robotics and controls research usually deal with non-graphical computer simulation or with actual hardware devices. Computer graphics animation of biped motion is more involved with the way the results looks instead of the physical accuracy of how the motion is obtained. Most biomechanics research deals with analysis of data collected by observing human locomotion in a gait laboratory. This project will combine some elements from all three fields.

1.2.1 Robotics and Control Systems

The primary focus of the research presented here is in the area of robotics and control, and subsequently the majority of work presented will be concentrated in this area. Most of the development in this area involves creating a mathematical models of the system using multibody dynamics and synthesizing control systems to drive these models. This is the most mathematically grounded of the three disciplines, but possessing the necessary mathematical tools does not guarantee that a set of procedures can be developed for controlling the system. Several types of models will be discussed ranging from simple planar bipeds to more complex 3D devices. The control systems discussed range from completely manual, to semi-automatic, to completely automatic control.

1.2.2 Computer Graphics Simulation and Animation

In the field of computer simulation and animation, the main sources of motion generation are usually kinematic positioning and keyframe interpolation. Recently, inverse kinematics has become more commonplace, but for complicated multibody system models this motion generation tool still lacks the necessary realism required for accurate simulation. Experienced computer animators frequently obtain realistic looking motion through their own intuition, or by trial and error. Often intuition can lead the animator down a path that may look realistic or plausible, but one that is totally inaccurate, and in some cases dangerously misleading. The only *real* solution to problems where accurate motion is essential is through multibody dynamics. The trouble with creating motion in this manner is in the development of the system equations of motion and in the joint actuator feedback control that moves the system. Developing graphically interactive, feedback control for this type of system, specifically, the locomotion control of bipedal mechanisms, is one of the main goals of this project.

1.2.3 Biomedical

Studying locomotion of biological organisms provides a great source of information about the type of performance that is possible. The chance to observe a working example of bipedal locomotion provides insight for the design of mechanical systems.

The field of biomedical research tends to focus on experimental data analysis. As a result, mathematical equations are usually of the empirically variety, the product of a statistical analysis of experimental data obtained from many human subjects. Developments in this area involve methods of obtaining experimental three-dimensional motion data, muscle modeling, and energy expenditure analysis.

Although the techniques that will be presented here can be extended to human motion analysis, it is important to note that this research is not intended to be a complete model of human bipedal locomotion. Instead, it describes an approach for obtaining general bipedal motion. Some aspects of the model and control techniques may result in motion that is very similar to human locomotion, other aspects may not. Certainly until muscle modeling and a system model with all human degrees-of-freedom are included, the control scheme could only represent a subset of a system that can duplicate the results of a human control system. This is not to say that such a mathematical model would not be a useful tool for human locomotion simulation and analysis. Even when an incomplete mathematical model is assembled using human physiological parameters, motion very similar to experimentally obtained human data should result.

1.3 Stages of Development

Development consists of three stages: modeling, control, and interactive simulation. Modeling starts with planar (2D) monoped models and progresses through several evolutionary steps to spatial (3D) biped systems. Control system design begins with simple manual control techniques and proceeds to automatic balancing control, steady-state walking, and transitional modes. Computer graphics simulation allows the multibody systems to be displayed and interactively controlled in real-time.

1.3.1 System Models

The initial multibody mechanisms that will be discussed include a series of planar monopeds (one legged mechanisms). These models serve as simplified testing systems for some of the basic balancing and control development techniques. Several types of planar bipeds will

then be presented that include both sagittal plane (side view) and frontal plane biped mechanisms. Spatial (3D) biped models of increasing complexity will then be developed.

1.3.2 Control Methods

As stated earlier, the main goal of this project is to develop feedback control methods to balance on one or both feet, and to initiate and sustain a steady-state walking gait cycle. In addition, the control system should be able to transition between balancing and walking, change velocity, and react appropriately to varying terrain.

A series of interactive control techniques ranging from manual torque input to automatic gait cycle generation will be discussed. Two distinct automatic control methods will be presented: optimal control methods for balancing modes, and state machines for walking control.

1.3.3 Interactive Graphical Simulation

Real-time interactive simulation software has been developed to allow the user to operate the biped models within a 3D virtual environment. Aspects involved in combining interactive computer graphics with multibody dynamics and feedback control will be presented.

1.4 Overview

1.4.1 Chapter Summary

A literature review of similar work and issues related to biped systems, physically based modeling, controls, and biomechanics is presented in Chapter 2. Additional Background on human walking and running gait cycles will be discussed in Chapter 3.

A chapter on physically based modeling discusses the details of the multibody monoped and biped models developed for this research, as well as techniques for obtaining solutions using numerical integration. Linear and nonlinear equations of motion for the planar and spatial bipeds are developed.

Control systems that deal with balance, walking, and transitions are then presented. Linearized equations of motion from the modeling section are used in obtaining full state feedback matrices for balancing control. State machines are presented for the control of biped walking cycles.

Graphs, images, and other performance data for the monoped and biped systems are given in the Results chapter. Comparisons to data collected from human walking will be made. Position and ground reaction force data obtained from a human walking is compared to data generated from one of the more complex biped models developed for this research.

Contributions to the field of biped locomotion as well as possible applications and recommendations for future work are summarized in the last chapter.

Appendices A, B, C, and D contain preliminary and supplemental models used for initial system design and control system development, numerical method examples, software summary, and color images, respectively.

1.4.2 Interactive Media

An interactive version of this document containing text, images, and animations will be made available at the time of publication and initially served on the Iowa State University Visualization Laboratory World-Wide Web (WWW) site[1] located at: `http://www.vis-lab.iastate.edu`.

1. Since electronic repositories are somewhat volatile, this address may not be valid in a few years. See the Iowa State University site at: `http://www.iastate.edu` for directory information.

2. LITERATURE REVIEW

Sufficient overlap exists in many areas of current research in biped systems which sometimes prevents categorizing work into just one field. However several distinct classes can be defined. Research in the area of biped locomotion usually breaks down into one of three areas: 1. biomechanics, 2. computer graphics and simulation, and 3. robotics and controls. By merging elements from each of these fields, a more complete understanding of biped locomotion can be obtained. Other supplemental fields include: kinematics, inverse kinematics, dynamics, optimization, and numerical methods.

2.1 Biomechanics

Biomechanics work usually deals with experimental data collected by observing human locomotion in a gait laboratory. Some specific areas include: locomotion acquisition and analysis; metabolic energy expenditure; collection, analysis, and electrical stimulation of muscle.

Inman et al. [60] provides an overall summary of many of the issues dealing with human walking, from statistical summaries for various walking parameters to metabolic energy expenditure, to normal and pathological gait analysis. Rose and Gample [115] extend this work to cover additional topics including, computerized acquisition of human performance data and electrical muscle stimulation. Dufek et al. [31] present ground force reaction data obtained from force plate measurements and then converted into joint torques using inverse dynamics.

Dempster [28] and later Clauser et al. [22] obtained data for various parameters of the human body. Hatze [44] used these measurements to formulate equations to approximate the

mass, volume, and center of mass position given other more easily obtainable parameters, like segment length.

Human muscle models were developed by Yamaguchi [143, 144] for use in dynamic simulation and control. Mena et al. [88] analyze muscle control of the swing leg during gait. They use a very simplified dynamic model and come to the conclusion that "both the thigh and shank behaved essentially as constrained pendula during swing, requiring no muscular control, while the foot required an active muscular moment to maintain foot-floor clearance." Unfortunately, other researchers have come to the opposite conclusion using the same basic procedures. These differing views on the use of multibody dynamics is one of the unfortunate occurrences within the biomedical literature.

Hay [45] presents theories and analysis behind running, jumping, and other type of athletic motions.

2.2 Computer Graphics and Simulation

Computer graphics and animation of biped devices has relied mainly on keyframing motion, and more recently on kinematics and dynamics. Interactive simulation involves computing solutions and displaying graphical results in real-time (or near real-time).

Badler and Phillips [8] discuss some of the basic concepts involved in controlling human-like mechanisms in a computer graphics environment. Badler et al. [9] at the University of Pennsylvania have created interactive graphical software called *Jack* for analysis and simulation of human movement. Most functions are kinematic operations. Levels of interaction and control of models in a virtual environment have also been studied by Zelder [146].

An interactive software package called *Lifeforms* by Bruderlin and Calvert [18] uses a knowledge base of several stored motion sequences that can be kinematically altered to produce a desired motion. Bruderlin and Calvert have also published results for dynamic walking, which will be discussed in the next section.

Baraff [13-15] discusses contact between colliding objects and real-time calculation of collision forces for interactive simulation environments. An interactive 2D simulation environment capable of running in real-time has been developed (with a 3D system in the works).

2.2.1 Dynamics and Control

Dynamics and control are two very closely related topics. In fact, simulated control could not exist without dynamics models. Because of this fact, much of the work in these two areas overlaps.

Bruderlin and Calvert [16, 17] use a simplified dynamics model to create walking cycles for use in computer animation. The main divergences from a more realistic model are the assumptions that: 1. a virtual telescopic stance leg consisting of a single mass element can be used instead of a revolute jointed two segment double pendulum leg, and 2. that the swing and stance leg dynamics are uncoupled, in that the swing leg dynamics are calculated independently of the rest of the system. They claim that this second assumption can be justified (but without any qualitative comparison data) for their planar model. Although this claim may prove to have only moderate impact on the appearance of the output motion of the planar case, it would have disastrous consequences for a spatial (3D) model. The missing hip torque, that would have been produced by the swing leg, is necessary in order to cancel the yaw rotation about the vertical axis (normal to the transverse plane) produced by the stance leg. The resulting motion would be completely unnatural.

Craig [24], Hollerbach [58], and Lewis et al. [76] present inverse dynamics (computed torque) methods. Orin et al. [104] use Newton-Euler methods to obtain equations of motion. Walker and Orin [141] discuss methods for converting the numerical formulations of the inverse dynamics solutions to a form that can be numerically integrated for simulation purposes. Walker and Orin [141] also compare four dynamics methods for execution time. The best method takes symmetry of the inertia matrix into account and uses a recursive method for computing mass, center of mass, and moment of inertia of the composite system.

Lin and Yae [77] present a recursive linearization of multibody dynamics for control design that uses linearization proceeding from the outermost link inward. Burdick [20], presents an efficient manipulator dynamic equations in symbolic form. Simplification rules are used during the process of equation generation and offers improvement over Lagrangian derivation methods.

Golliday and Hemami [39] develop 3-link planar biped using Lagrangian formulation for impulsive motion. Gait calculations involve four sets of equations for the left-right and single-double support phases. The double support phase consists of a single time step in which angular velocity changes instantaneously.

Hemami and Zheng [52] develop a biped system that can handle many types of constraint circumstances. The system deals with many possible conditions, but always uses a joint constraint foot instead of compliant foot. Sagittal plane biped simulation has been researched by Hemami et al [46-54], standing and sitting by Hemami and Jaswa [50], and frontal plan biped simulation for two and three link models by Hemami et al. [54].

Climbing and descending slopes is discussed by Townsend and Tsay [126], and by Zheng [150]. Biped foot placement is discussed by Raibert [111], Townsend [125], and Redfern and Schumann [114]. Biped double support phase is discussed by Narikiyo and Ito [99], Shih et al. [118], and Shih and Gruver [119].

Many neural network control papers in the area of biped locomotion control have been published. Typical of many papers in this area is the one by Miller [90], which uses a neural network to train a 3-D, 10-axis robot for quasi-static balance by shifting weight from one foot to the other. The system has dynamic balance for lifting the foot off floor and placing it in a new location. The control method does not appear to be able to produce an elegant human-like gait since the system can only take short steps. The mechanism shifts between statically stable balanced postures, which seems to be its main method of locomotion. No dynamic model of device was used. Frontal and lateral coupling was ignored and general purpose walking was not achieved. Another neural network controlled biped, by Kitamura and Kurematsu [70] and

Kitamura et al. [71], use a 2D model based on controlling the system center of gravity to follow the motion of an inverted pendulum. A neural network is used to find the inverse kinematic solution for positioning the foot (which seems unnecessary since this solution can be found much more efficiently using analytical methods). Another neural network is used for the control system to force the system center of gravity to follow the inverted pendulum model.

2.2.2 Motion Capture

Motion capture is probably the simplest method available for obtaining realistic looking motion for animating human systems. In some ways motion capture can be considered to be dynamics, since the motion is taken from systems that move based on physical forces. This method consists of outfitting a human actor with some type of joint position senors or markers and having him/her perform a task while position data is collected. These marker positions are then processed to obtain joint angles. Two distinct types of motion capture exits. The first method uses motion captured from humans and is used directly as input data for body segment positioning -- no dynamics model or control system is needed. The second method uses motion capture data as the tracking input to a positioning system in which some type of kinematic or controlled dynamic system model is used.

Getting accurate motion data is a difficult process. Various methods ranging from joint marker lights to drilling into bones for solid position markers have been tried. Guo et al. present [41] an automatic method to digitize data from video, which does not require fixing position sensors or markers to body segments as required by usual gait analysis methods. A kinematic 2D model to resolve the self-occlusion problems usually associated with this type of image processing.

Hemami et al. [48] used a similar method to obtain the desired path for input to a control system for a multibody dynamic model. Marker points were digitized from sagittal plane video. Fourier series analysis was performed to obtain equations for the joint paths, which were then differentiated twice to obtain joint angular velocity and angular acceleration func-

tions. These position, velocity, and acceleration functions are used as inputs to inverse dynamics equations to obtain the desired joint torques. Feedback was used to correct deviations from the nominal path.

2.3 Robotics and Controls

Robotics and controls research in biped locomotion usually deals with non-interactive computer simulation or with actual hardware devices. On the other side of the dynamics spectrum is the research being done with hardware. Hardware devices can take the form of robotic mechanisms of exoskeleton devices for human use.

2.3.1 Robotic devices

These mechanisms can be divided into two types: static and dynamic. Static devices are usually slow moving machines that require the projected center of gravity (CG) to be within the support polygon created by the contact positions of the feet. Dynamic machines allow the projected CG to move outside the support polygon, resulting in a more useful and faster moving device.

One very simple dynamic machine is the passive walking machine built be McGeer [83]. This device walks down slopes with no external energy source. Another simple dynamic machine built by Jameson [63] uses gyroscopic forces to maintain its posture while a simple leg system propels the device forward.

More complex dynamic locomotion devices have been built by Raibert et al. [109-112]. These include hopping monopeds and bipeds as shown in Figure 2.1. Other hopping machine have been built by Dunn and Howe [32], and by M'Closkey and Burdick [84]. These types of systems have also been simulated by others like Kearney and Hanson [68]. These systems typically balance by hopping in place instead of using a control system that can maintain a stabilized stationary position. Although complex looking motion sequences have been developed

for these types of mechanisms, like the gymnastic biped by Hodgins and Raibert [56], biped motion using this type of dynamic system does not resemble normal human locomotion.

Several researchers in Japan have built biped mechanisms of various degrees of complexity, some of which are shown in Figure 2.2. These research projects includes static, dynamic, and quasi-dynamic robots ranging from simple 3-link systems to 7-link systems with 10 input controls. Some of these include the walking biped mechanisms built by Furusho and Masubuchi [33], Furusho and Sano [34-35], Mita et al. [91], Miura and Shimoyama [92], and Takanishi et al. [122, 123]. Miura [93] summarizes several biped research projects conducted in Japan dating back to 1970.

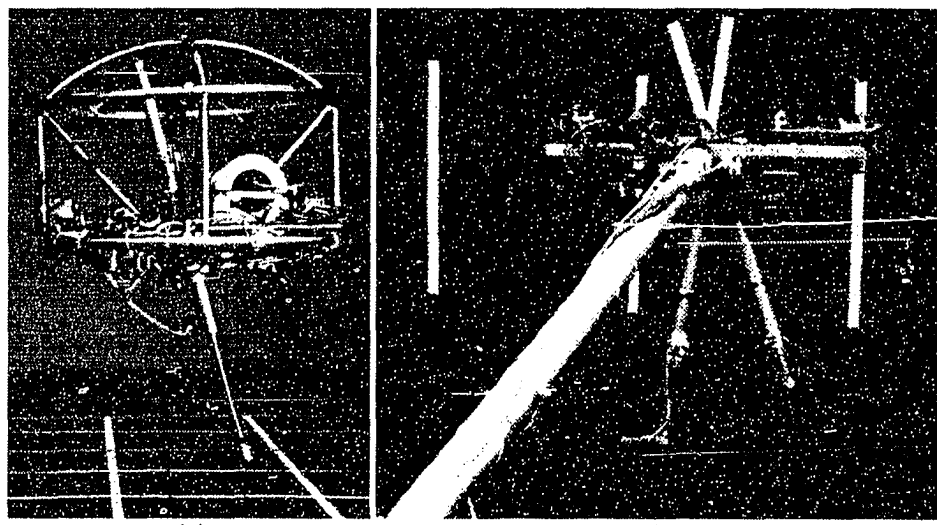

(a) (b)

Figure 2.1 Dynamic hopping robots[1]: (a) monoped, (b) biped

1. Images from *Legged Robots that Balance* [111]

Saito et al. [116] present a two-link brachiation robot that moves by swinging to foot holds under the surface plane instead of above it, similar to a long-armed ape swinging its body like a pendulum. System energy management is done by tracking center of gravity. The system can't move statically unless a substantial torque is allowed at the contact point. The control system was developed by heuristic control methods where motion is generated by trial and error without any knowledge of system dynamics.

Although most research in bipedal locomotion is conducted in a laboratory setting, some work has been done in less ideal environments. Manko [82] discusses aspects of legged locomotion non-ideal surfaces, specifically soil modeling and natural terrain environments. Kajita [64] also deals with environments outside a laboratory setting.

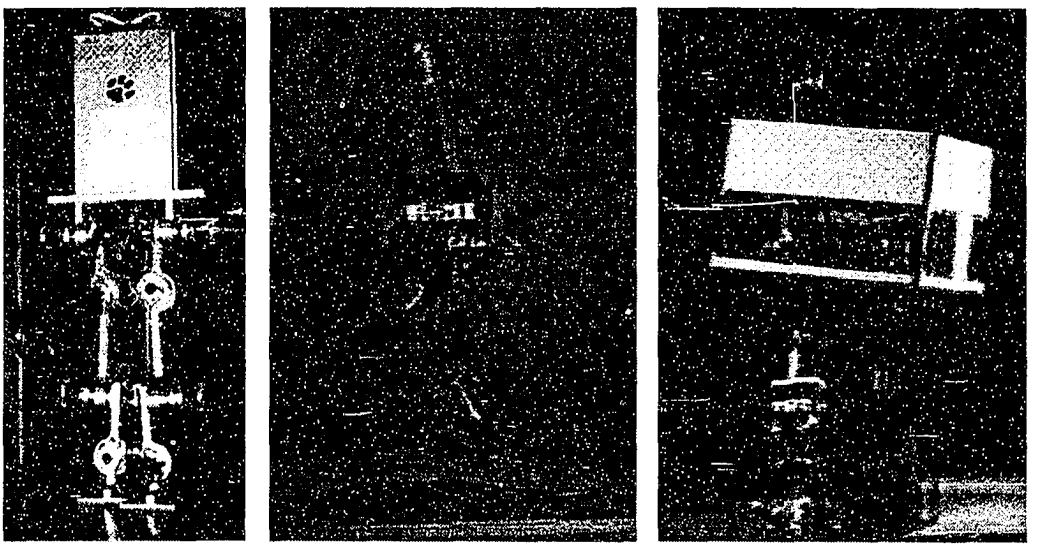

(a) (b) (c)

Figure 2.2 Biped machines: (a) CURBi[1], (b) WL-12RD[2], (c) WL-10RD[3]

1. Ohio State University "CURBi" biped (image courtesy of IEEE Robotics and Automation Magazine)
2. Waseda University "WL-12RD" biped (image courtesy of University Video Communications)
3. Waseda University "WL-10RD" biped (image courtesy of University Video Communications)

2.3.2 Exoskeleton devices

Exoskeleton devices are mechanisms that attach to the legs of a human subject in which leg movement controlled by external torque inputs. Some of these systems resemble a suit of armor that the person must climb into, other are less intrusive and are similar to putting on a pair of pants. In addition to providing several theoretical studies on human locomotion Vokobratovic et al. [134-138] presents several exoskeleton mechanisms for assisting bipedal locomotion of paralyzed subjects. Miyamoto et al. [94] also developed devices for providing movement to paralyzed lower limbs. Unfortunately, all of these devices suffer from the problem of a limited self contained power supply.

3. BACKGROUND

In order to help clarify the vocabulary used in this field, an introduction to some of the basic issues involved with bipedal systems is presented here. The first topic deals with the system naming conventions, the second introduces the terminology involved with biped walking and running cycles.

3.1 Coordinate Systems Descriptions

Describing the system parameters for bipedal waking is a complex task involving multiple coordinate systems. Two vastly different naming systems appear in the literature, one in the biomedical field and one in the engineering field.

The reference plane definitions for the human body in the standard anatomical position are shown in Figure 3.1. The three viewing planes are: the sagittal, or side view plane, which will be aligned with the xy-axes in 2D model definitions and the xz-axes in the 3D definitions; the frontal (or coronal) plane, which will be aligned with the yz-axes in the 3D system models; and the transverse plane, which is aligned with the xy-axes in the 3D definitions.

Lower limb joint rotation terminology is given in Figure 3.2. In the sagittal plane, the hip and knee rotations are flexion and extension, and the ankle rotation are plantar flexion and dorsiflexion. In the frontal plane, the hip rotations are adduction and abduction, and the ankle rotations are inversion and eversion. This naming system takes a little getting used to, especially for those who are used to a right-handed set of mutually perpendicular unit vectors. One reason for this confusion is the fact that the term *flexion* is used for both clockwise and counter-clockwise rotations.

The decision was made that for the work presented in this dissertation, these rotation terms will be used sparingly. Instead, the more consistent terminology associated with engineering mechanics will be used, where positive rotations are always counter-clockwise and negative rotations are always clockwise around the rotation axis (i.e., the right-hand rule).

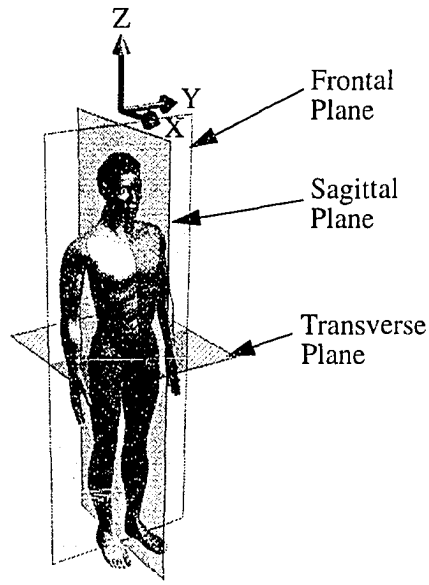

Figure 3.1 Human body reference planes in the standard anatomical position

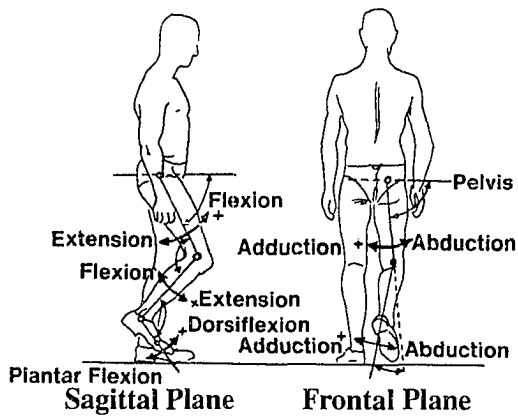

Figure 3.2 Biomedical naming convention for angular motion[1]

1. Angular motion definition image from *Human Walking* [60]

3.2 Biped Locomotion Terminology

The walking and running cycles consist of several well defined phases, as described in Figure 3.3. Bipedal locomotion cycles consist of two independently controlled single leg cycles. Symmetry between the leg cycles means that the cycles are identical except for a phase offset, which is usually 50% of the cycle time. Although symmetry between legs is not required, most non-pathological gaits are symmetric.

The stance phase is the portion of the cycle of each leg in which that leg is in contact with the surface, and supporting some portion of the load. In the walking cycle, the stance phase of each leg occupies approximately 60% of the total cycle time. The swing phase is the portion of the cycle in which the leg is not supporting any load and is moving into position for the next stance cycle. The portion of the walking cycle for each leg in the swing phase is approximately 40%. The walking cycle can also be described as being divided into two support phases: double and single support. The double support phase occurs when both feet are on the ground and share the support load, occupies approximately 25% of the total walking gait cycle. Single support occupies the remainder of the time, approximately 75% of the total walking cycle.

The running cycle has a flight phase where both legs are off the ground. The portion of the running cycle in the flight phase depends on speed, and ranges from approximately 30-60% of the total cycle time [45]. A double support phase does not exist in the running cycle.

The transition between the swing and stance phases consists of first extending the leg from its retracted position to prepare for surface contact. This foot contact is referred to as heel strike left (HSL) and heal strike right (HSR), or more generally as foot touchdown (TD). At the other end of the stance cycle, the transition from stance to swing consists of a pre-swing phase where the heel leaves the surface but the toe remains in contact. The point where the toe breaks contact is the start of the swing cycle. This point is referred to as toe off left (TOL) and toe off right (TOR), or more generally as lift-off (LO).

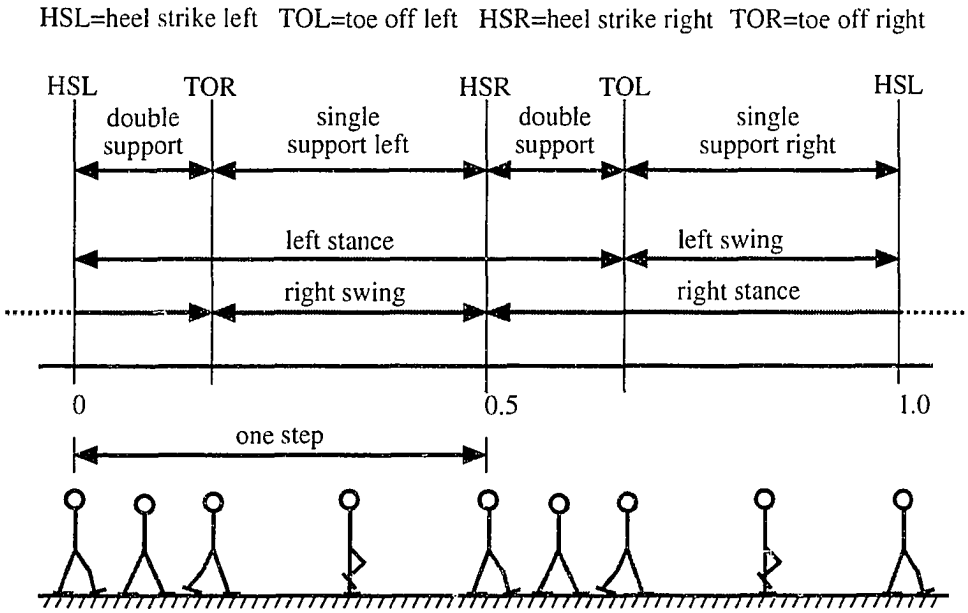

(a)

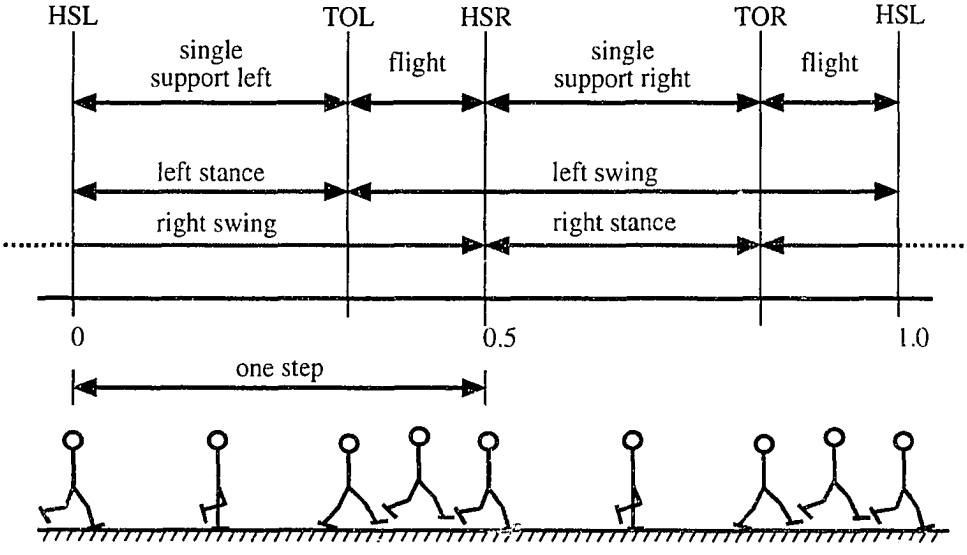

(b)

Figure 3.3 Symmetric steady-state gait cycles: (a) walking; (b) running

Typical walking step rates for humans are 80-100 steps/min., and step length for the optimal, or most comfortable, walking speed are 0.65-0.95 m/step. Where "most comfortable" is defined as the step rate that requires the least amount of oxygen consumption per unit distance. These values result in walking speeds of approximately 50-95 m/min. (1.9-3.5 mi/hr). Studies of a large sample of males and females have shown an average speed of 83.4 m/min (3.11 mi/hr) [113] [60] [115].

3.3 Biped Balancing Terminology

Stationary balancing and steady-state locomotion both require control of foot placement at touchdown to obtain or maintain stability. One of the primary balance indicators is the zero moment point (ZMP) [134]. The ZMP is an equilibrium point where no moment is required to maintain position. In most cases, this is the same as the projected center of mass position. The neural point (NP) [111] is another stability indicator that is used during walking. The NP is the foot placement position where the cycle average velocity of the composite center of mass remains the same. Placement of the foot ahead of the NP tends to decrease average velocity, while placing the foot behind the NP will increase velocity, as shown in Figure 3.4.

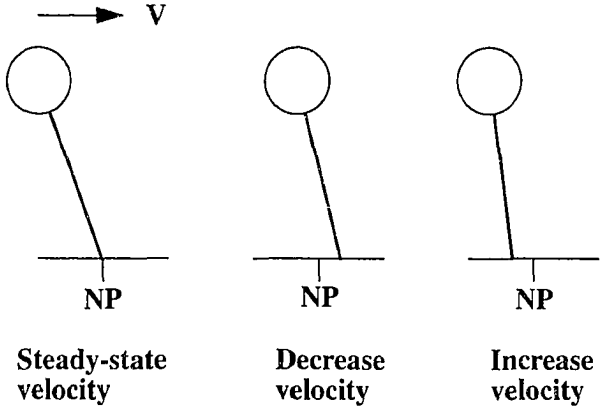

Figure 3.4 Foot placement relative to the neutral point

3.3.1 Static Balance

The statically stable gait (passive balance) requires the ZMP to remain inside the support polygon, as shown in Figure 3.5. During the single support phase, the ZMP must stay within the support polygon of one foot. A double support phase is required to transfer the ZMP from one foot to the other. This type of locomotion must be relatively slow to keep the accelerations small so that the ZMP can be located and controlled kinematically (i.e., no calculations of system dynamics are necessary).

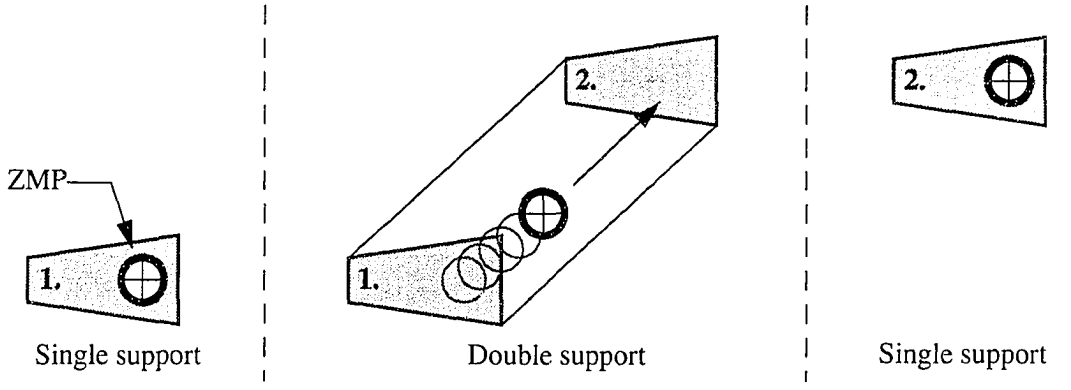

Figure 3.5 Statically balanced gait cycle

3.3.2 Dynamic Balance

In dynamically balanced locomotion (active balance), the ZMP is not required to stay within the support polygon, as shown in Figure 3.6. Predicting system positions, velocities, and accelerations using dynamics equations is essential for this type of locomotion control.

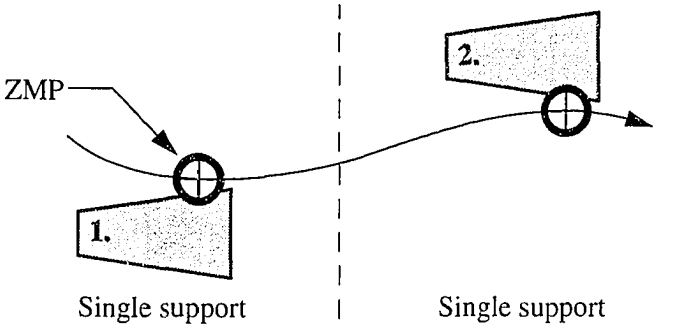

Figure 3.6 Dynamically balanced gait cycle

4. PHYSICALLY BASED MODELING

Modeling of physically based systems is based on the concept that mathematical equations can be used to predict the motion of objects acted on by forces and moments. The goal of these mathematical calculations is to find the system states (position, velocity, and acceleration) as functions of time. System response to external forces and moments is defined by the objects physical properties of mass and inertia and by the systems geometrical configuration. The configuration or arrangement of a series of interconnected objects forms a multibody system. Several methods exist for determining the mathematical equations that will predict motion for multibody systems. Formulation of the equations of motion for several types of monoped and biped models will be the focus of this chapter.

The first topic will be a discussion of the multibody techniques used for development of planar and spatial system models. Next, model descriptions as well as symbolic equations of motion and derivation for some of the systems will be presented. Finally, techniques for solving these equations will be discussed.

4.1 Generating Equations of Motion for Multibody Systems

Two different types of multibody dynamics were used to develop the equations of motion for the models that will be described in this chapter. Both methods produce equations in generalized coordinates. The Lagrange method will be used for planar (2D) mechanisms and the Newton-Euler method will be used for spatial (3D) mechanisms. Although several other methods exist for obtaining multibody equations of motion, the Lagrange and the Newton-Euler methods were chosen due to the simplicity and efficiency, for their respective uses.

4.1.1 Planar Dynamics

The relative simplicity of planar dynamics allows the use of scalar multibody dynamics methods. One of the most common methods for obtaining planar dynamics equations of motion is through the use of Lagrange's equations.

Lagrange equations

Lagrangian dynamics methods are based on the exchange of energy between kinetic and potential forms, with the external forces and torques represented by the virtual work terms. The efficiency of Lagrange's method is due to the representation of system variables in terms of generalized coordinates. The advantage of using generalized coordinates is that they represent the minimum number of equations necessary and do not require solving for joint constraint forces. The symbolic representation of the multibody systems in generalized coordinates were derived using (4.1).

$$\frac{d}{dt}\left(\frac{\partial T}{\partial \dot{q}_i}\right) - \frac{\partial T}{\partial q_i} + \frac{\partial V}{\partial q_i} = Q_i \tag{4.1}$$

Where T is the scalar kinetic energy equation, V is the scalar potential energy equation, and Q is the virtual work. The nonlinear equations of motion are then setup in matrix form (4.2) and solved for the acceleration terms (4.3).

$$A\ddot{X} = B \tag{4.2}$$

$$\ddot{X} = A^{-1}B \tag{4.3}$$

Where A is an $n \times n$ matrix (n = # DOF), and B is a function of the generalized velocities, positions, control torques, and ground reaction forces. These equations can then be linearized about operating points for the control system design. For a more in-depth review of Lagrangian dynamics see [121] and [140].

Jacobian velocity transformations

The cartesian positions and velocities of the distal end of the last link in the mechanism chain will be needed for ground contact reactions. The cartesian positions can be found using forward kinematics, and the velocities can be found using the Jacobian matrix. The Jacobian matrix is a multidimensional derivative transformation between the joint space velocities and the cartesian velocities. For simple planar mechanisms, the cartesian velocities can be sometimes be derived by inspection, but for spatial mechanisms, a matrix based approach will be needed.

4.1.2 Spatial Dynamics

The relative complexity of spatial or 3D dynamics makes the use of the scalar form of the Lagrange's equations very difficult. A matrix formulation of the Lagrange equations has been developed by Hollerbach [58], but it has been shown to be less efficient than the Newton-Euler formulation, which will be the method used here. In order to develop spatial systems, it is necessary to have a standardized method for developing the kinematic relationships between bodies, specifically, matrix based coordinate system definitions. After the spatial reference frames have been defined, the kinetic system equations can be developed.

Coordinate systems

The coordinate system used here is based on Denavit-Hartenberg (D-H) notation [29] for lower-pair mechanisms. This method identifies link parameters that describe the position of each link relative to an adjacent link. Each link is described by two angles (α_i and θ_i) and two linear offsets (a_i and d_i). For any lower pair joint (revolute or translational) three of the four D-H parameters are fixed and one is variable. For a revolute joint the variable parameter is θ_i, for translational joints it is the link offset d_i. Figure 4.1 (a) and (b) show these parameters as specified for rotational and translational joints respectively.

The parameters D-H are specified as follows:

- a_{i-1} = distance from z_{i-1} to z_i relative to axis x_{i-1}
- α_{i-1} = angle from z_{i-1} to z_i relative to axis x_{i-1}
- d_i = distance from x_{i-1} to x_i relative to axis z_i
- θ_i = angle from x_{i-1} to x_i relative to axis z_i

For some arrangements, an initial angular offset (90°) may be needed for the angular position, θ, in order to achieve the desired orientation for the next reference frame in the series.

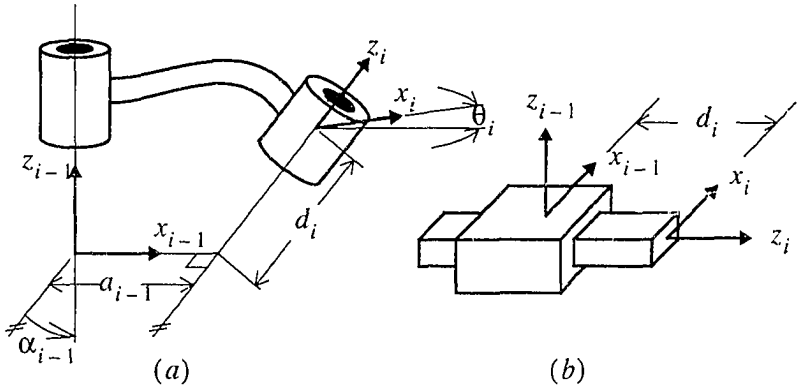

Figure 4.1 Frame definitions for a rotational joint (a) and translational joint (b)

When assigning the D-H parameters that define a mechanism's coordinate frames, it is useful to make a table listing the four values for each link. The table provides a consistent way of describing the robot and will be used later in the link transformation calculation procedure. Note that it is possible to have different parameter values depending on how the local coordinate frames of each link are assigned. However, any rotation or translation of the variable parameter takes place about or along the local z-axis.

Once the D-H parameters have been assigned, they are used to determine the link transformations using 4X4 transformation matrices. The general equation for a transformation matrix is given by:

$$
{}^{i-1}_{i}T = \begin{bmatrix} \cos\theta_i & -\sin\theta_i & 0 & a_{i-1} \\ \sin\theta_i\cos\alpha_{i-1} & \cos\theta_i\cos\alpha_{i-1} & -\sin\alpha_{i-1} & -\sin\alpha_{i-1}d_i \\ \sin\theta_i\sin\alpha_{i-1} & \cos\theta_i\sin\alpha_{i-1} & \cos\alpha_{i-1} & \cos\alpha_{i-1}d_i \\ 0 & 0 & 0 & 1 \end{bmatrix} \tag{4.4}
$$

After the transformation matrices have been defined for each link, they can be multiplied together to get the matrix relating the coordinate system of any one link to any other link in the system. In general, the transformation matrix of reference frame M relative to frame N is

$$
{}^{N}_{M}T = {}^{N}_{N+1}T\,{}^{N+1}_{N+2}T \cdots {}^{M-2}_{M-1}T\,{}^{M-1}_{M}T \tag{4.5}
$$

Transformations of each link must be calculated relative to a stationary coordinate system. This involves premultiplying the transformations described in the base coordinate system by the base frame relative to the stationary frame transformation. For example, to find the absolute position of reference frame 3,

$$
{}^{0}_{3}T = {}^{0}_{1}T\,{}^{1}_{2}T\,{}^{2}_{3}T \tag{4.6}
$$

where reference frame 0 is the stationary frame, as shown by the frame diagram in Figure 4.2.

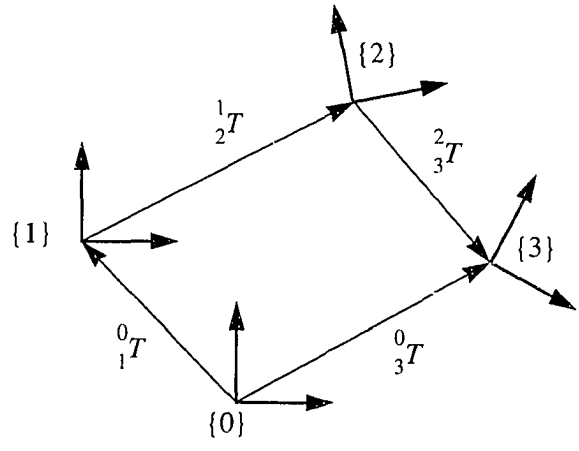

Figure 4.2 Generalized frame diagram

Newton-Euler equations

The Newton-Euler multibody dynamics method offers straight forward approach for spatial (3D) mechanism analysis, and is also one of the most efficient computational methods [58]. This type on multibody dynamics formulation is mainly used for single open chain systems, but can be modified to include multiple branches.

The Newton-Euler equations are based on Newton's equation (4.7) for translations forces and Euler's equation (4.8) for rotational moments. The development of equations of motion using the Newton-Euler approach involves an outward propagation (or iteration) to calculate velocities and accelerations, and then an inward iteration to calculate forces and torques. For a numerical solution these iterations must be executed every time step. A symbolic solution requires that this procedure be performed only once, but for larger systems, the symbolic equations can become large to handle — even for symbolic math programs.

$$F = m\dot{v}_c \tag{4.7}$$

$$N = {}^{C}I\dot{\omega} + \omega \times {}^{C}I\omega \tag{4.8}$$

Where the 3×3 inertia tensor, I, is defined relative to the center of mass of reference frame i, and F, N, v, and ω are 3×1 vectors.

Outward iterations:

$${}^{i+1}\omega_{i+1} = {}^{i+1}_{i}R\,{}^{i}\omega_i + \dot{\theta}_{i+1}\,{}^{i+1}\hat{Z}_{i+1} \tag{4.9}$$

$${}^{i+1}\dot{\omega}_{i+1} = {}^{i+1}_{i}R\,{}^{i}\dot{\omega}_i + {}^{i+1}_{i}R\,{}^{i}\omega_i \times \dot{\theta}_{i+1}\,{}^{i+1}\hat{Z}_{i+1} + \ddot{\theta}_{i+1}\,{}^{i+1}\hat{Z}_{i+1} \tag{4.10}$$

$${}^{i+1}\dot{v}_{i+1} = {}^{i+1}_{i}R\,({}^{i}\dot{\omega}_i \times {}^{i}P_{i+1} + {}^{i}\omega_i \times ({}^{i}\omega_i \times {}^{i}P_{i+1}) + {}^{i}\dot{v}_i) \tag{4.11}$$

$$^{i+1}\dot{v}_{C_{i+1}} = {}^{i+1}\dot{\omega}_{i+1} \times {}^{i}P_{C_i} + {}^{i+1}\omega_{i+1} \times ({}^{i+1}\omega_{i+1} \times {}^{i}P_{C_i}) + {}^{i+1}\dot{v}_{i+1} \tag{4.12}$$

$$^{i+1}F_{i+1} = m_{i+1}\,{}^{i+1}\dot{v}_{C_{i+1}} \tag{4.13}$$

$$^{i+1}N_{i+1} = {}^{C_{i+1}}I_{i+1}\,{}^{i+1}\dot{\omega}_{i+1} + {}^{i+1}\omega_{i+1} \times {}^{C_{i+1}}I_{i+1}\,{}^{i+1}\omega_{i+1} \tag{4.14}$$

Inward iterations:

$$^{i}f_i = {}_{i+1}^{i}R\,{}^{i+1}f_{i+1} + {}^{i}F_i \tag{4.15}$$

$$^{i}n_i = {}^{i}N_i + {}_{i+1}^{i}R\,{}^{i+1}n_{i+1} + P_{C_i} \times {}^{i}F_i + {}^{i}P_{i+1} \times {}_{i+1}^{i}R\,{}^{i+1}f_{i+1} \tag{4.16}$$

$$\tau_i = {}^{i}n_i^{Ti}\hat{Z}_i \tag{4.17}$$

For prismatic joints, (4.17) becomes:

$$\tau_i = {}^{i}f_i^{Ti}\hat{Z}_i \tag{4.18}$$

where f_i and n_i are the force and torque exerted on link i by link i-1, respectively. And the inertial forces and torques are F_i and N_i, respectively. The 3×3 rotation matrix, R, and the 3×1 position vector, P, are obtained from the 4×4 transformation matrices as defined in the previous section.

These equations as stated are formulated for serial chain mechanisms. When several branched chains are specified, as is the case with biped mechanisms, a modified version of the Newton-Euler formulations is needed. The method proceeds as given above until a branching link is encountered. (A branching link is a link with three or more attachment points, instead of the usual two for a non-branched chain.) For this situation, outward iterations require that

special attention be paid to the indexing so the i terms point to the branching link, and not to links on other branches. In addition to special indexing requirements, inward iterations for branching systems require that the forces and moments from all the branches be included in the formulations.

The sequence of equations given above is used for calculating actuator torques as a function of the position, velocity, and acceleration variables. This procedure is referred to as an inverse dynamics or computed torque method. In order to simulate a system, the dynamics problem needs to be solved for joint accelerations. If (4.17) and (4.18) are developed symbolically and represented in the form of (4.19), the joint acceleration variables can be solved for algebraically. Solutions for the positions and velocities can then be obtained using numerical integration techniques. Unfortunately, more complex systems usually require numerical solution of the Newton-Euler equations, in which case the final result is a number which does not relay any direct information about the joint accelerations contained within it. For numerically derived systems like this, an additional procedure is needed that will provide the joint acceleration terms.

$$\tau = H(q)\ddot{q} + C(q, \dot{q})\dot{q} + G(q) + K(q)^T k \tag{4.19}$$

One method for obtaining the acceleration terms explicitly is presented by Walker and Orin [141]. This method first solves for the acceleration and coefficient matrix terms by representing all terms other than the acceleration terms on the right side of (4.19) as the single bias vector term, b, in (4.20). This bias vector can be solved for by using the same Newton-Euler sequence as before, but with the acceleration terms set to zero. The left side term of (4.21) is solved for by subtracting the bias vector solution from the initial torque solution.

$$b = C(q, \dot{q})\dot{q} + G(q) + K(q)^T k \tag{4.20}$$

$$H(q)\ddot{q} = (\tau - b) \tag{4.21}$$

Next, the inertia matrix, $H(q)$, will need to be found to decouple the acceleration terms for numerical integration. To find the inertia matrix elements, a simplified version of the Newton-Euler equations can be developed that does not include velocity, gravitational, or external moments and forces. This sequence of equations is solved n times for the columns of $H(q)$, by setting q equal to the current state and setting $\ddot{q} = e_j$, where e_j is an n×1 vector with the jth element set to 1 and all other elements set to 0. The coefficient matrix, $H(q)$, can then be inverted and premultiplies the right side of (4.21), leaving equations defined for the acceleration terms. This set of differential equations can then be solved using numerical integration.

4.1.3 Linearization

Once the nonlinear equations have been developed, they will need to be linearized for control system design. Linearization of nonlinear equations of motion involves using the first order terms of the Taylor series:

$$f_{q^*} + \left.\frac{\partial f}{\partial q}\right|_{q^*} \Delta q + \left.\frac{\partial f}{\partial \dot{q}}\right|_{q^*} \Delta \dot{q} + \left.\frac{\partial f}{\partial \ddot{q}}\right|_{q^*} \Delta \ddot{q} = 0 \tag{4.22}$$

The linearization point q^* is selected by setting acceleration and velocity terms of the nonlinear system to zero and solving the resulting set of equilibrium state equations.

Developing an analytical set of linearized equations for each model used for control system design allows the on-line calculation of new feedback control gains, which results in a more autonomous mechanism. Symbolic forms of the linearized system equations will be presented when needed.

4.2 Models

Several types of physically based multibody models will be discussed, these include: planar monoped and bipeds, and spatial monoped and bipeds. In addition, several relatively simple preliminary systems were modeled and used to assemble portions of the final model as

well as for testing purposes, these include various planar and spatial forms of single, double, and triple pendulums (details given in Appendix A). Table 4.1 lists the monoped and biped models developed here. The purpose of presenting an entire collection of models, from the simplest planar monoped to the most complex spatial biped, is to show the method of design progression. This type of evolution shows the tradeoffs between speed of interactive simulation and realism for each degree of complexity. Model designs based on the components of previous designs, with all models having the single link inverted pendulum as the starting point. The addition of another degree of freedom and controlled input from one model to the next allows for a logical progression, with new problems to be solved for each modeling iteration.

Table 4.1 Multibody monoped and biped models

Monopeds				Bipeds					
Planar		Spatial		Sagittal Plane		Frontal Plane		Spatial	
Links	DOF	Links	DOF	Links	DOF	Links	DOF	Links	DOF
2[a]	2	2	7	3[a]	3	3[a]	3	3	8
2	4	3	8	3	5	3	5	3	10
3[a]	3	4	9	5[a]	5			5	12
4	6			5	7			7	14
				7	9			8	15
								8	17

a. models with one foot constrained to stationary reference frame

Equations of motion for planar systems will be developed symbolically using Lagrangian dynamics methods. Two separate models will be developed for each planar system: one constrained to a stationary reference frame, and one unconstrained model. The unconstrained model will be linearized and used in the control system design.

Development of spatial systems will be accomplished using the Newton-Euler multibody dynamics methods, which is better suited to 3D systems than the standard form of Lagrange's equations. Equations of motion will not be developed symbolically for all of the spatial mod-

els as was done for the planar systems. For the higher order systems, only numerical solutions of the recursive Newton-Euler equations will be used.

An important design decision was made to not include additional human-like features to the models, like head and arm links. These systems are not intended to be exact models of humans. The head and arms could easily be modeled as separate systems that are uncoupled from the rest of the model, but would offer little benefit in the design of either the manual or automatic control system. Adding realistic (i.e. correct) head and arm components requires mathematical coupling to the body link. For the planar case, this would add five additional degrees of freedom to the system (one for the head and two for each arm) and further reduce the possibility of real-time operation. Due to these facts, the head and arm segments will not be modeled.

4.2.1 Planar Monopeds

Much of the initial mathematical modeling that will be presented here is based on one legged (monoped) balancing. Several planar single leg models were used in the early stages of the control system development. These models include two, three, and four link models with four, five, and six-DOF, respectively. The two link model has a body segment and a leg segment; the three link model adds an articulated knee joint; and the four link model adds a foot. These models where helpful in designing balancing and foot placement algorithms that will be used in the biped control systems. A color image of the three planar monoped models developed here is shown in Figure D.1(a) of Appendix D.

Planar 2-link monoped

The simplest monoped model discussed here is a 2-link system with 4 degrees-of-freedom, shown in Figure 4.3 and Figure 4.4. Note the larger CG marker in this figure is the composite center of mass for the system, which is also projected onto the floor. This model consists of a body segment, a leg segment, and a single element spring-damper foot pad. This type of ground reaction force model will be discussed in more detail in a subsequent section.

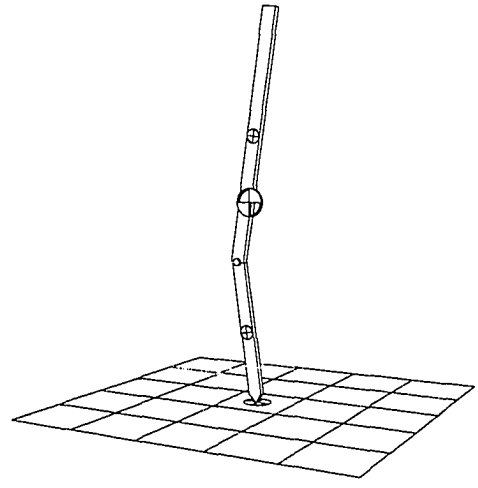

Figure 4.3 2-link, 4-DOF planar monoped model

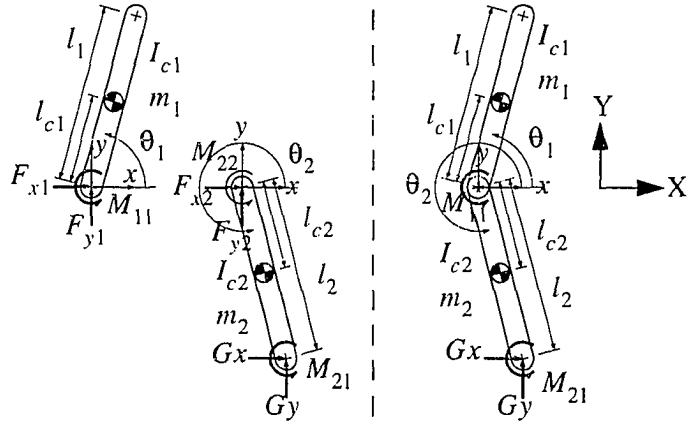

Figure 4.4 2-link planar monoped variable definitions

Using the two single link components, which were derived using Lagrange's equations (see Appendix A for additional details), the 2-link planar monoped equations of motion for the generalized system variables defined in Figure 4.4 are derived below.

The generalized coordinates used here are: $X = [x, y, \theta_1, \theta_2]^T$

$$(I_{c1} + m_1 l_{c1}^2)\,\ddot{\theta}_1 - (m_1 l_{c1} \sin\theta_1)\,\ddot{x} + (m_1 l_{c1} \cos\theta_1)\,\ddot{y} + m_1 g l_{c1} \cos\theta_1 = M_{11} \qquad (4.23)$$

$$m_1\ddot{x} - (m_1 l_{c1}\sin\theta_1)\ddot{\theta}_1 - (m_1 l_{c1}\cos\theta_1)\dot{\theta}_1^2 = F_{x1} \tag{4.24}$$

$$m_1\ddot{y} + (m_1 l_{c1}\cos\theta_1)\ddot{\theta}_1 - (m_1 l_{c1}\sin\theta_1)\dot{\theta}_1^2 + m_1 g = F_{y1} \tag{4.25}$$

$$\begin{aligned}&(I_{c2} + m_2 l_{c2}^2)\ddot{\theta}_2 - (m_2 l_{c2}\sin\theta_2)\ddot{x} + (m_2 l_{c2}\cos\theta_2)\ddot{y} + m_2 g l_{c2}\cos\theta_2 \\ &= M_{21} + M_{22} - G_{x2} l_2 \sin\theta_2 + G_{y2} l_2 \cos\theta_2\end{aligned} \tag{4.26}$$

$$m_2\ddot{x} - (m_2 l_{c2}\sin\theta_2)\ddot{\theta}_2 - (m_2 l_{c2}\cos\theta_2)\dot{\theta}_2^2 = F_{x2} + G_{x2} \tag{4.27}$$

$$m_2\ddot{y} + (m_2 l_{c2}\cos\theta_2)\ddot{\theta}_2 - (m_2 l_{c2}\sin\theta_2)\dot{\theta}_2^2 + m_2 g = F_{y2} + G_{y2} \tag{4.28}$$

System is coupled at the hip (branching link) by:

$$F_{x1} = -F_{x2} \tag{4.29}$$

$$F_{y1} = -F_{y2} \tag{4.30}$$

$$M_{11} = -M_{22} \tag{4.31}$$

And, viscous damping at the joints can be added by replacing M_{11} with $M_{11} - \rho(\dot{\theta}_1 - \dot{\theta}_2)$, where ρ is the viscous damping coefficient.

Substitution of (4.29) to (4.31) into (4.23) to (4.28), and combining (4.24) with (4.27), and (4.25) with (4.28) reduces the system into the four, second order nonlinear ordinary differential equations shown below:

$$\begin{aligned}&(m_1 + m_2)\ddot{x} - (m_1 l_{c1}\sin\theta_1)\ddot{\theta}_1 - (m_2 l_{c2}\sin\theta_2)\ddot{\theta}_2 \\ &= m_1\dot{\theta}_1^2 l_{c1}\cos\theta_1 + m_2\dot{\theta}_2^2 l_{c2}\cos\theta_2 + G_x\end{aligned} \tag{4.32}$$

$$(m_1 + m_2)\,\ddot{y} + (m_1 l_{c1}\cos\theta_1)\,\ddot{\theta}_1 + (m_2 l_{c2}\cos\theta_2)\,\ddot{\theta}_2 \\ = m_1\dot{\theta}_1^2 l_{c1}\sin\theta_1 + m_2\dot{\theta}_2^2 l_{c2}\sin\theta_2 + G_y - (m_1 + m_2)\,g \tag{4.33}$$

$$(-m_1 l_{c1}\sin\theta_1)\,\ddot{x} + (m_1 l_{c1}\cos\theta_1)\,\ddot{y} + (I_{c1} + m_1 l_{c1}^2)\,\ddot{\theta}_1 \\ = -m_1 g l_{c1}\cos\theta_1 + M_{11} - \rho\,(\dot{\theta}_1 - \dot{\theta}_2) \tag{4.34}$$

$$(-m_2 l_{c2}\sin\theta_2)\,\ddot{x} + (m_2 l_{c2}\cos\theta_2)\,\ddot{y} + (I_{c2} + m_2 l_{c2}^2)\,\ddot{\theta}_2 \\ = -m_2 g l_{c2}\cos\theta_2 - M_{11} + M_{21} + \rho\,(\dot{\theta}_1 - \dot{\theta}_2) - G_x l_2\sin\theta_2 + G_y l_2\cos\theta_2 \tag{4.35}$$

These equations can be represented in matrix form given by (4.36), and will be solved by numerical integration after transforming into the acceleration form of (4.37). Where A is the 5×5 coefficient matrix for the acceleration terms and B is a vector of the right side elements (all the non-acceleration terms).

$$A\ddot{X} = B \tag{4.36}$$

$$\ddot{X} = A^{-1}B \tag{4.37}$$

The linearized equations of motion for the 2-link monoped are derived for a system with the foot attached to the ground by a single DOF (revolute) joint. This system is the same as the inverted double pendulum system derived in Appendix A.

The first step is to pick points about which to linearize the system. Setting the acceleration and velocity terms of the nonlinear system to zero results in a set of equilibrium state equations. For the inverted double pendulum system the equilibrium equations are:

$$m_1 g l_{c1}\cos\theta_1 + M_1 = 0 \tag{4.38}$$

$$(m_2 l_{c2} + m_1 l_1)\,g\cos\theta_2 + M_2 - M_1 = 0 \tag{4.39}$$

This set of equations has four unknowns, which requires picking two and solving for the other two variables. The stable equilibrium points exist where the external torques are chosen to be zero, resulting in a finite number of solutions (four in this case) for q^*. Unstable equilibrium points occur when the external torques are non-zero, resulting in an infinite number of solutions. This requires the selection of q^*, instead of torques M. Selection of q^* will be discussed later. Eliminating M_1 from (4.38) and (4.39) results in (4.40).

$$m_1 g l_{c1} \cos\theta_1 + (m_2 l_{c2} + m_1 l_1)\, g \cos\theta_2 + M_2 = 0 \tag{4.40}$$

The linearized system equations of motion, using the nonlinear variable definitions at equilibrium point X, are given below:

$$X = [\theta_1, \ddot{\theta}_1, \theta_2, \ddot{\theta}_2] = [\frac{\pi}{2}, 0, -\frac{\pi}{2}, 0]$$

$$(I_{c1} + m_1 l_{c1}^2)\, \ddot{\theta}_1 = -m_1 g l_{c1} \Delta\theta_1 + M_1 \tag{4.41}$$

$$(I_{c2} + m_2 l_{c2}^2 + m_1 l_2^2)\, \ddot{\theta}_2 = (m_2 l_{c2} + m_1 l_2)\, g \Delta\theta_2 + M_2 - M_1 \tag{4.42}$$

where $\Delta\theta_i = \theta_i - \theta_i^*$.

For any desired equilibrium point, the linearized system equations of motion are:

$$X = [\theta_1, \ddot{\theta}_1, \theta_2, \ddot{\theta}_2] = [\theta_1^*, 0, \theta_2^*, 0]$$

$$(I_{c1} + m_1 l_{c1}^2)\, \ddot{\theta}_1 + m_1 l_2 l_{c1} \sin(\theta_2^* - \theta_1^*)\, \ddot{\theta}_2 = -m_1 g l_{c1} \sin(\theta_1^*)\, \Delta\theta_1 + M_1 \tag{4.43}$$

$$\begin{aligned} &m_1 l_2 l_{c1} \sin(\theta_2^* - \theta_1^*)\, \ddot{\theta}_1 + (I_{c2} + m_2 l_{c2}^2 + m_1 l_2^2)\, \ddot{\theta}_2 \\ &= (m_2 l_{c2} + m_1 l_2)\, g \sin(\theta_2^*)\, \Delta\theta_2 + M_2 - M_1 \end{aligned} \tag{4.44}$$

Composite body properties

The composite center of mass (or center of gravity, CG) position and velocity that will be used in subsequent control system design are calculated by summing the weighted individual link contributions in the x and y directions relative to the origin of the branching link and dividing by the total mass. Additional properties that will be needed in the control system including: ZMP, projected CG, composite inertia, virtual leg length and angular velocity are calculated in a similar manner.

Cartesian velocity of foot pads

In order to determine the ground reaction forces the cartesian velocity at the distal end of the final segment of the leg (i.e. foot pads) will need to be determined in terms of the joint velocities. The Jacobian matrix can be used to do this, but for simpler systems the velocities can be found by inspection. The cartesian foot position and velocity equation for this 2-link system are given below.

$$x_{foot} = x + l_2 \cos\theta_2 \tag{4.45}$$

$$y_{foot} = y + l_2 \sin\theta_2 \tag{4.46}$$

$$\dot{x}_{foot} = \dot{x} - l_2 \dot{\theta}_2 \sin\theta_2 \tag{4.47}$$

$$\dot{y}_{foot} = \dot{y} + l_2 \dot{\theta}_2 \cos\theta_2 \tag{4.48}$$

Planar 3-link monoped

A more complex monoped model is the 3-link system with 5-DOF, shown in Figure 4.5. This system consists of a body segment, a two part articulated leg, and a single element spring-damper foot pad.

Using a single link component and double link components, which were derived using the Lagrange method (see Appendix A for additional details), the 3-link planar monoped equations of motion for the generalized system variables defined in Figure 4.6 are given below, and the linearized equations of motion for the triple pendulum are given in Appendix A. From here on, only the final equations of motion for each system will be presented.

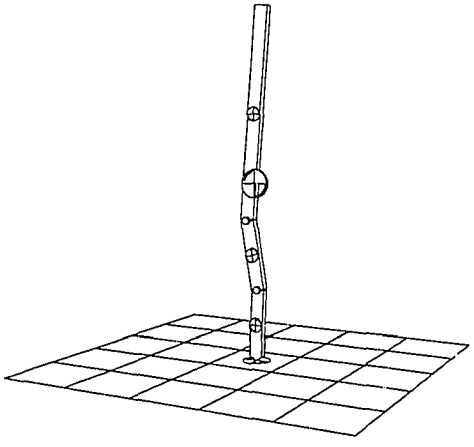

Figure 4.5 3-link, 5-DOF planar monoped model

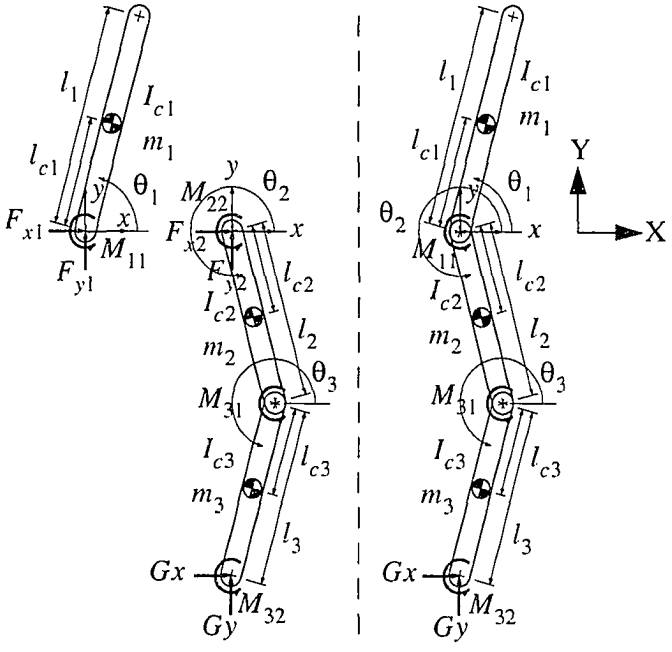

Figure 4.6 3-link planar monoped variable definitions

The generalized coordinates used here are: $X = [x, y, \theta_1, \theta_2, \theta_3]^T$

$$(m_1 + m_2 + m_3)\ddot{x} - m_1 l_{c1}\sin(\theta_1)\ddot{\theta}_1 - (m_2 l_{c2} + m_3 l_2)\sin(\theta_2)\ddot{\theta}_2 - m_2 l_{c3}\sin(\theta_3)\ddot{\theta}_3 \quad (4.49)$$
$$= m_1 l_{c1}\cos(\theta_1)\dot{\theta}_1^2 + (m_2 l_{c2} + m_3 l_2)\cos(\theta_2)\dot{\theta}_2^2 + m_2 l_{c3}\cos(\theta_3)\dot{\theta}_3^2 + G_{x3}$$

$$(m_1 + m_2 + m_3)\ddot{y} + m_1 l_{c1}\cos(\theta_1)\ddot{\theta}_1 + (m_2 l_{c2} + m_3 l_2)\cos(\theta_2)\ddot{\theta}_2 \quad (4.50)$$
$$+ m_2 l_{c3}\cos(\theta_3)\ddot{\theta}_3 = m_1 l_{c1}\sin(\theta_1)\dot{\theta}_1^2 + (m_2 l_{c2} + m_3 l_2)\sin(\theta_2)\dot{\theta}_2^2$$
$$+ m_3 l_{c3}\sin(\theta_3)\dot{\theta}_3^2 - (m_1 + m_2 + m_3)g + G_{y3}$$

$$-m_1 l_{c1}\sin(\theta_1)\ddot{x} + m_1 l_{c1}\cos(\theta_1)\ddot{y} + (I_{c1} + m_1 l_{c1}^2)\ddot{\theta}_1 \quad (4.51)$$
$$= -m_1 l_{c1} g\cos(\theta_1) - M_{21}$$

$$-(m_2 l_{c2} + m_3 l_2)\sin(\theta_2)\ddot{x} + (m_2 l_{c2} + m_3 l_2)\cos(\theta_2)\ddot{y} + (I_{c2} + m_2 l_{c2}^2 + m_3 l_2^2)\ddot{\theta}_2 \quad (4.52)$$
$$+ m_3 l_{c3} l_2\cos(\theta_3 - \theta_2)\ddot{\theta}_3 = m_3 l_{c3} l_2\sin(\theta_3 - \theta_2)\dot{\theta}_3^2 - (m_2 l_{c2} + m_3 l_2)\cos(\theta_2)g$$
$$- G_{x3} l_2\sin(\theta_2) + G_{y3} l_2\cos(\theta_2) + M_{21} - M_{31}$$

$$-m_3 l_{c3}\sin(\theta_3)\ddot{x} + m_3 l_{c3}\cos(\theta_3)\ddot{y} + m_3 l_{c3} l_2\cos(\theta_3 - \theta_2)\ddot{\theta}_2 + (I_{c3} + m_3 l_{c3}^2)\ddot{\theta}_3 \quad (4.53)$$
$$= -m_3 l_{c3} l_2\sin(\theta_3 - \theta_2)\dot{\theta}_2^2 - G_{x3} l_3\sin(\theta_3) + G_{y3} l_3\cos(\theta_3) + M_{31} + M_{32}$$

Planar 4-link monoped

The most complex monoped model discussed here is a 4-link system with 6 DOF, shown in Figure 4.7 and Figure 4.8. This system consists of a body segment, a two part articulated leg, and a foot with two spring-damper elements.

The 4-link planar monoped equations of motion use the same system as the 3-link planar monoped with the addition of a decoupled single link for the foot. The decoupling of the foot from the other links of the system was done for two reasons. First, this link spends much of

the time in contact with the surface, which essentially reduces it to a 3-link system. Second, the mass and inertia of the foot are small when compared to the other links. The moments due to input torques and the ground reaction forces are still transmitted to the other links, but inertia moments and forces due to the movement of the foot itself are not.

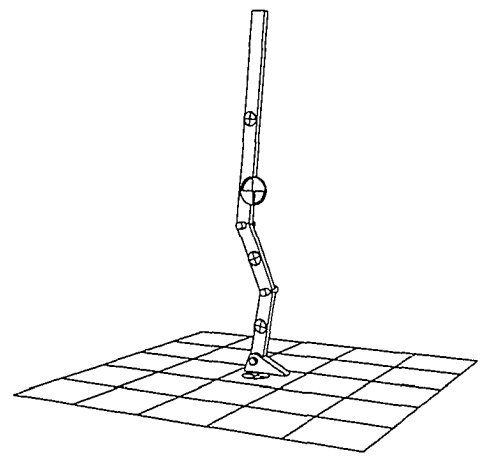

Figure 4.7 4-link, 6-DOF planar monoped model

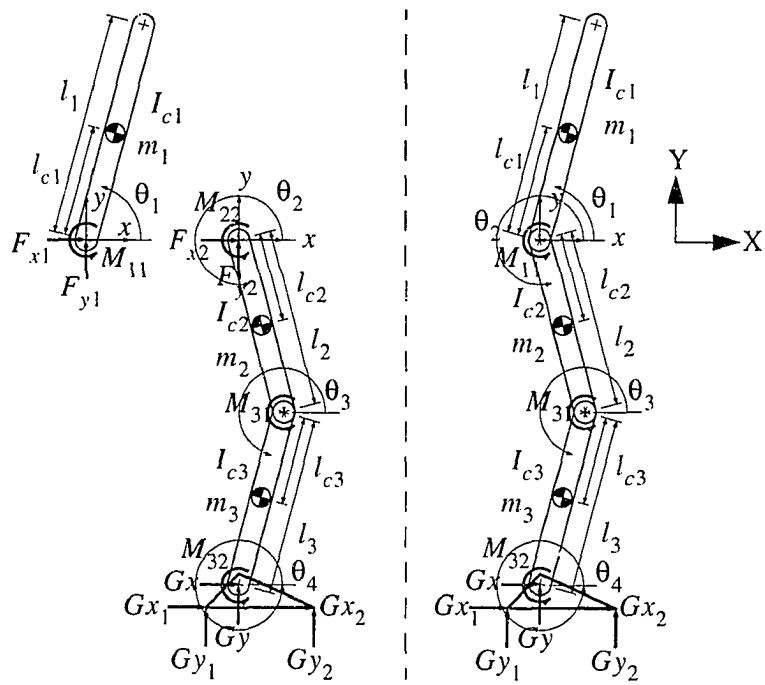

Figure 4.8 4-link planar monoped variable definitions

The equations of motion for the upper links of the generalized system variables defined in Figure 4.8 are the same as those of the planar 3-link monoped system, and will not be repeated here. The equations for the decoupled foot are given below.

The generalized coordinates used here are: $X = [x, y, \theta_1, \theta_2, \theta_3, \theta_4]^T$

$$\ddot{x}_{ankle} = \ddot{x} - l_2\ddot{\theta}_2\sin\theta_2 - l_2\dot{\theta}_2^2\cos\theta_2 - l_3\ddot{\theta}_3\sin\theta_3 - l_3\dot{\theta}_3^2\cos\theta_3 \tag{4.54}$$

$$\ddot{y}_{ankle} = \ddot{y} + l_2\ddot{\theta}_2\cos\theta_2 - l_2\dot{\theta}_2^2\sin\theta_2 + l_3\ddot{\theta}_3\cos\theta_3 - l_3\dot{\theta}_3^2\sin\theta_3 \tag{4.55}$$

$$\ddot{\theta}_4 = \frac{m_4 l_{c4}(\ddot{x}_{ankle}\sin\theta_4 - (\ddot{y}_{ankle} - g)\cos\theta_4) - M_{32} - M_f}{I_{c4} + m_4 l_{c4}^2} \tag{4.56}$$

where M_f is calculated from the moment balance due to the foot pads contacting the surface.

4.2.2 Planar Biped Models

Two distinct types of planar biped models were designed: sagittal and frontal plane models. The initial sagittal biped mechanism that will be presented is a planar 3-link (5-DOF) model. This model consists of a body link (an inverted pendulum) and two legs, each with a massless translational joint section. The next model is a 5-link (7-DOF) sagittal plane model with articulated revolute jointed legs. The articulated lower leg segments will replace the massless translational joints used in the previous model. The lower leg segments can no longer just be kinematically positioned during the swing portion of the gait cycle. This adds two additional torque inputs to the model. This system will then be modified into a 7-link (9-DOF) model, similar to the 5-link, but with articulated feet. A color image of the three sagittal plane biped models developed here is shown in Figure D.1(b) of Appendix D.

One type of frontal plane model will also be presented, a 3-link (5-DOF) model, with two controlled inputs.

3-link sagittal plane biped

The initial biped mechanism that will be discussed here is a planar 3-link (5-DOF) model, shown in Figure 4.9 and Figure 4.10. It consists of a body link and two legs. Both legs also include massless translational joint segments which are not considered to be additional degrees of freedom. These kinematic leg extensions are actuated in a manner similar to the 2-link planar monoped system by retracting the lower leg segments to avoid stubbing the foot during the return stroke. The two main controlled inputs are the torques acting on the hip joint.

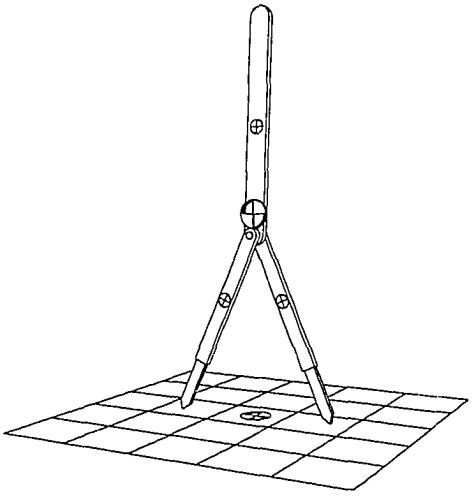

Figure 4.9 3-link, 5-DOF sagittal plane biped model

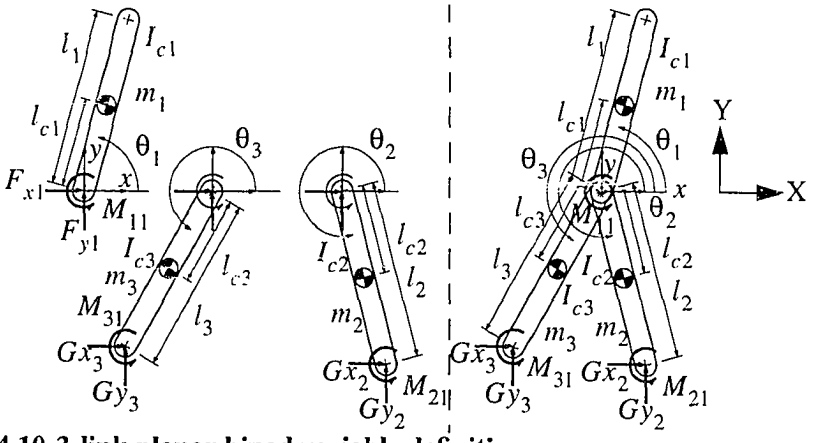

Figure 4.10 3-link planar biped variable definitions

As in the simplest monoped case, a complete derivation of the system equations is given for this 3-link system. Only the final results will be given for additional planar bipeds. The 3-link equations of motion are developed as follows:

$$(I_{c1} + m_1 l_{c1}^2)\,\ddot{\theta}_1 - (m_1 l_{c1}\sin\theta_1)\,\ddot{x} + (m_1 l_{c1}\cos\theta_1)\,\ddot{y} + m_1 g l_{c1}\cos\theta_1 = M_{11} \tag{4.57}$$

$$m_1\ddot{x} - (m_1 l_{c1}\sin\theta_1)\,\ddot{\theta}_1 - (m_1 l_{c1}\cos\theta_1)\,\dot{\theta}_1^2 = {}^{A}F_{x1} \tag{4.58}$$

$$m_1\ddot{y} + (m_1 l_{c1}\cos\theta_1)\,\ddot{\theta}_1 - (m_1 l_{c1}\sin\theta_1)\,\dot{\theta}_1^2 + m_1 g = {}^{A}F_{y1} \tag{4.59}$$

$$\begin{aligned}&(I_{c2} + m_2 l_{c2}^2)\,\ddot{\theta}_2 - (m_2 l_{c2}\sin\theta_2)\,\ddot{x} + (m_2 l_{c2}\cos\theta_2)\,\ddot{y} + m_2 g l_{c2}\cos\theta_2 \\ &= M_{21} + M_{22} - G_{x2} l_2\sin\theta_2 + G_{y2} l_2\cos\theta_2\end{aligned} \tag{4.60}$$

$$m_2\ddot{x} - (m_2 l_{c2}\sin\theta_2)\,\ddot{\theta}_2 - (m_2 l_{c2}\cos\theta_2)\,\dot{\theta}_2^2 = {}^{A}F_{x2} + G_{y2} \tag{4.61}$$

$$m_2\ddot{y} + (m_2 l_{c2}\cos\theta_2)\,\ddot{\theta}_2 - (m_2 l_{c2}\sin\theta_2)\,\dot{\theta}_2^2 + m_2 g = {}^{A}F_{y2} + G_{y2} \tag{4.62}$$

$$\begin{aligned}&(I_{c3} + m_3 l_{c3}^2)\,\ddot{\theta}_3 - (m_3 l_{c3}\sin\theta_3)\,\ddot{x} + (m_3 l_{c3}\cos\theta_3)\,\ddot{y} + m_3 g l_{c3}\cos\theta_3 \\ &= M_{31} + M_{33} - G_{x3} l_3\sin\theta_3 + G_{y3} l_3\cos\theta_3\end{aligned} \tag{4.63}$$

$$m_3\ddot{x} - (m_3 l_{c3}\sin\theta_3)\,\ddot{\theta}_3 - (m_3 l_{c3}\cos\theta_3)\,\dot{\theta}_3^2 = {}^{A}F_{x3} + G_{y3} \tag{4.64}$$

$$m_3\ddot{y} + (m_3 l_{c3}\cos\theta_3)\,\ddot{\theta}_3 - (m_3 l_{c3}\sin\theta_3)\,\dot{\theta}_3^2 + m_3 g = {}^{A}F_{y3} + G_{y3} \tag{4.65}$$

System is coupled at the hip (i.e. branching link) by:

$$F_{x1} = -F_{x2} - F_{x3} \tag{4.66}$$

$$F_{y1} = -F_{y2} - F_{y3} \tag{4.67}$$

$$M_{11} = -M_{22} - M_{32} \tag{4.68}$$

Substitution of these three equations into (4.57) to (4.65) reduces the system into the five, second order nonlinear ordinary differential equation below:

$$(m_1+m_2+m_3)\ddot{x}-(m_1l_{c1}\sin\theta_1)\ddot{\theta}_1-(m_2l_{c2}\sin\theta_2)\ddot{\theta}_2-(m_3l_{c3}\sin\theta_3)\ddot{\theta}_3 \quad (4.69)$$
$$=m_1l_{c1}\dot{\theta}_1^2\cos\theta_1+m_2l_{c2}\dot{\theta}_2^2\cos\theta_2+m_3l_{c3}\dot{\theta}_3^2\cos\theta_3+Gx_2+Gx_3$$

$$(m_1+m_2+m_3)\ddot{y}+(m_1l_{c1}\cos\theta_1)\ddot{\theta}_1+(m_2l_{c2}\cos\theta_2)\ddot{\theta}_2+(m_3l_{c3}\cos\theta_3)\ddot{\theta}_3 \quad (4.70)$$
$$=m_1l_{c1}\dot{\theta}_1^2\sin\theta_1+m_2l_{c2}\dot{\theta}_2^2\cos\theta_2+m_3l_{c3}\dot{\theta}_3^2\cos\theta_3+Gy_2+Gy_3-(m_1+m_2+m_3)g$$

$$-(m_1l_{c1}\sin\theta_1)\ddot{x}+(m_1l_{c1}\cos\theta_1)\ddot{y}+(I_{c1}+m_1l_{c1}^2)\ddot{\theta}_1=-m_1gl_{c1}\cos\theta_1-M_{22}-M_{32} \quad (4.71)$$

$$-(m_2l_{c2}\sin\theta_2)\ddot{x}+(m_2l_{c2}\cos\theta_2)\ddot{y}+(I_{c2}+m_2l_{c2}^2)\ddot{\theta}_2=(Gy_2l_2+m_2gl_{c2})\cos\theta_2 \quad (4.72)$$
$$-Gx_2l_{c2}\sin\theta_2+M_{22}+M_{21}$$

$$-(m_3l_{c3}\sin\theta_3)\ddot{x}+(m_3l_{c3}\cos\theta_3)\ddot{y}+(I_{c3}+m_3l_{c3}^2)\ddot{\theta}_3=(Gy_3l_3+m_3gl_{c3})\cos\theta_3 \quad (4.73)$$
$$-Gx_3l_{c3}\sin\theta_3+M_{32}+M_{31}$$

In matrix form:

$$\begin{bmatrix} a & 0 & b & c & d \\ 0 & a & e & f & h \\ b & e & i & 0 & 0 \\ c & f & 0 & j & 0 \\ d & h & 0 & 0 & k \end{bmatrix} \begin{bmatrix} \ddot{x} \\ \ddot{y} \\ \ddot{\theta}_1 \\ \ddot{\theta}_2 \\ \ddot{\theta}_3 \end{bmatrix} = \begin{bmatrix} R_1 \\ R_2 \\ R_3 \\ R_4 \\ R_5 \end{bmatrix} \quad (4.74)$$

The linearized equations of motion for the 3-link monoped are derived for a system with the foot attached to the ground by a single DOF (revolute) joint. The resulting linearized 3-DOF system equations of motion are given in Appendix A.

5-link sagittal plane biped

The 5-link (7-DOF) planar model with articulated revolute jointed legs is shown in Figure 4.11, with the coordinate system and variables in Figure 4.12. These lower leg segments will replace the massless translational joints used in the previous model. Due to this

modification, the lower leg segments can no longer be kinematically positioned during the swing portion of the gait cycle. The addition of the lower leg segments adds two additional torque inputs to the model. To save space, the nonlinear system equations of motion will be presented in matrix form only.

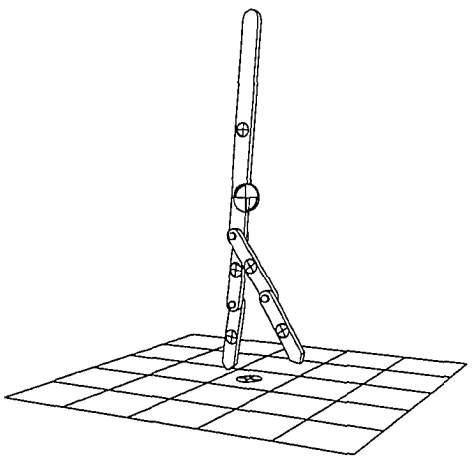

Figure 4.11 5-link, 7-DOF sagittal plane biped model

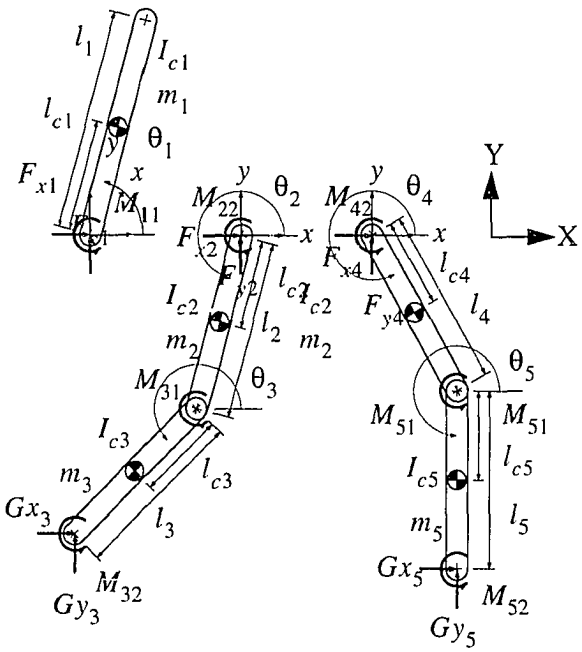

Figure 4.12 5-link planar biped variable definitions

$$\begin{bmatrix} a & 0 & b & c & d & e & f \\ 0 & a & h & i & j & k & l \\ b & h & m & 0 & 0 & 0 & 0 \\ c & i & 0 & n & p & 0 & 0 \\ d & j & 0 & p & q & 0 & 0 \\ e & k & 0 & 0 & 0 & r & s \\ f & l & 0 & 0 & 0 & d & t \end{bmatrix} \begin{bmatrix} \ddot{X} \\ \ddot{Y} \\ \ddot{\theta}_1 \\ \ddot{\theta}_2 \\ \ddot{\theta}_3 \\ \ddot{\theta}_4 \\ \ddot{\theta}_5 \end{bmatrix} = \begin{bmatrix} R_1 \\ R_2 \\ R_3 \\ R_4 \\ R_5 \\ R_6 \\ R_7 \end{bmatrix} \tag{4.75}$$

where the mass/inertia matrix coefficients and the right hand side vector values are:

$$a = m_1 + m_2 + m_3 + m_4 + m_5 \tag{4.76}$$

$$b = -m_1 l_{c1} \sin\theta_1 \tag{4.77}$$

$$c = -(m_2 l_{c2} + m_3 l_2) \sin\theta_2 \tag{4.78}$$

$$d = -m_2 l_{c3} \sin\theta_3 \tag{4.79}$$

$$e = -(m_4 l_{c4} + m_5 l_4) \sin\theta_4 \tag{4.80}$$

$$f = -m_4 l_{c5} \sin\theta_5 \tag{4.81}$$

$$h = m_1 l_{c1} \cos\theta_1 \tag{4.82}$$

$$i = (m_2 l_{c2} + m_3 l_2) \cos\theta_2 \tag{4.83}$$

$$j = m_3 l_{c3} \cos\theta_3 \tag{4.84}$$

$$k = (m_4 l_{c4} + m_5 l_4) \cos\theta_4 \tag{4.85}$$

$$l = m_5 l_{c5} \cos\theta_5 \tag{4.86}$$

$$m = I_{c1} + m_1 l_{c1}^2 \tag{4.87}$$

$$n = I_{c2} + m_2 l_{c2}^2 + m_3 l_3^2 \tag{4.88}$$

$$p = m_3 l_{c3} l_2 \cos(\theta_3 - \theta_2) \tag{4.89}$$

$$q = I_{c3} + m_3 l_{c3}^2 \tag{4.90}$$

$$r = I_{c4} + m_4 l_{c4}^2 + m_5 l_5^2 \tag{4.91}$$

$$s = m_5 l_{c5} l_4 \cos(\theta_4 - \theta_5) \tag{4.92}$$

$$t = I_{c5} + m_5 l_{c5}^2 \tag{4.93}$$

$$R_1 = m_4 l_{c5} \dot{\theta}_5^2 \cos\theta_5 + m_1 l_{c1} \dot{\theta}_1^2 \cos\theta_1 + m_2 l_{c3} \dot{\theta}_3^2 \cos\theta_3 + (m_2 l_{c2} + m_3 l_2) \dot{\theta}_2^2 \cos\theta_2 + (m_4 l_{c4} + m_5 l_4) \dot{\theta}_4^2 \cos\theta_4 + Gx_3 + Gx_5 \tag{4.94}$$

$$R_2 = (m_4 l_{c4} + m_5 l_4) \dot{\theta}_4^2 \sin\theta_4 + m_1 l_{c1} \dot{\theta}_1^2 \sin\theta_1 + m_3 l_{c3} \dot{\theta}_3^2 \sin\theta_3 + m_5 l_{c5} \dot{\theta}_5^2 \sin\theta_5 + (m_2 l_{c2} + m_3 l_2) \dot{\theta}_2^2 \sin\theta_2 - (m_1 + m_2 + m_3 + m_4 + m_5) g + Gy_3 + Gy_5 \tag{4.95}$$

$$R_3 = -(m_1 l_{c1} g \cos\theta_1 + M_{21} + M_{41}) \tag{4.96}$$

$$R_4 = m_3 l_{c3} l_2 \dot{\theta}_3^2 \sin(\theta_3 - \theta_2) - ((m_2 l_{c2} + m_3 l_2) g + Gy_3 l_2) \cos\theta_2 - Gx_3 l_2 \sin\theta_2 - M_{31} + M_{21} \tag{4.97}$$

$$R_5 = -(m_3 l_{c3} g + Gy_3 l_3) \cos\theta_3 - m_3 l_{c3} l_2 \dot{\theta}_2^2 \sin(\theta_3 - \theta_2) - Gx_3 l_3 \sin\theta_3 + M_{32} + M_{31} \tag{4.98}$$

$$R_6 = -m_5 l_{c5} l_4 \dot{\theta}_5^2 \sin(\theta_4 - \theta_5) - ((m_4 l_{c4} + m_5 l_4) g + Gy_5 l_4) \cos\theta_4 - Gx_5 l_4 + M_{41} - M_{51} \tag{4.99}$$

$$R_7 = -(m_5 l_{c5} g + Gy_5 l_5)\cos\theta_5 - m_5 l_{c5} l_4 \dot{\theta}_4^2 \sin(\theta_5 - \theta_4) - Gx_5 l_5 \sin\theta_5 + M_{51} + M_{52} \quad (4.100)$$

7-link sagittal plane biped

The 7-link (9-DOF) model of Figure 4.13, is similar to the 5-link system, but with articulated feet. The coordinate system is the same as the 5-link system of Figure 4.12 with the addition of the feet variables shown in Figure 4.14. The feet add two more controlled torque inputs bringing the total number of controlled inputs to six. This will be the most complex version of the planar models investigated.

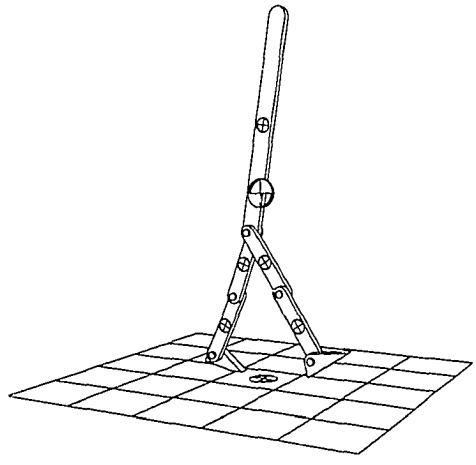

Figure 4.13 7-link, 9-DOF sagittal plane biped model

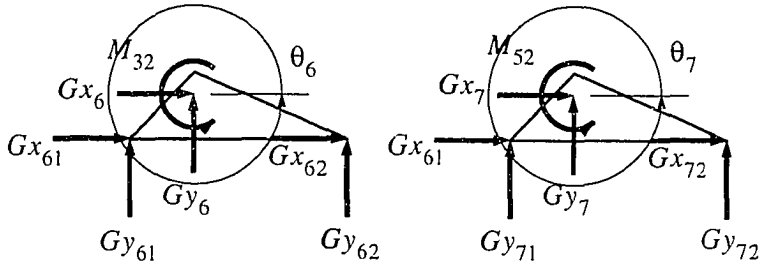

Figure 4.14 Additional 7-link planar biped variable definitions

When the feet are in contact with the ground the stance leg dynamics reduces from a 3-link system to a 2-link system like the legs in the 5-link sagittal plane model. In addition, the feet are relatively light when compared to the rest of the system. Due to these facts, a partially decoupled foot model is added to the 5-link system to make the 7-link system. Moments and forces are still transferred from the foot to the rest of the body, and linear accelerations from the lower leg are transferred to the ankle, but accelerations from the foot are not transferred back to the leg. This simplification reduces the computational requirements significantly, with relatively small impact on the overall system dynamics.

The additional foot dynamics, which are added to the 5-link equations of motion from the previous section to create the 7-link dynamics, are given below.

The generalized coordinates used here are: $X = [x, y, \theta_1, \theta_2, \theta_3, \theta_4, \theta_5, \theta_6, \theta_7]^T$

$$\ddot{x}_{ankle1} = \ddot{x} - l_2\ddot{\theta}_2\sin\theta_2 - l_2\dot{\theta}_2^2\cos\theta_2 - l_3\ddot{\theta}_3\sin\theta_3 - l_3\dot{\theta}_3^2\cos\theta_3 \tag{4.101}$$

$$\ddot{y}_{ankle1} = \ddot{y} + l_2\ddot{\theta}_2\cos\theta_2 - l_2\dot{\theta}_2^2\sin\theta_2 + l_3\ddot{\theta}_3\cos\theta_3 - l_3\dot{\theta}_3^2\sin\theta_3 \tag{4.102}$$

$$\ddot{x}_{ankle2} = \ddot{x} - l_4\ddot{\theta}_4\sin\theta_4 - l_4\dot{\theta}_4^2\cos\theta_4 - l_5\ddot{\theta}_5\sin\theta_5 - l_5\dot{\theta}_5^2\cos\theta_5 \tag{4.103}$$

$$\ddot{y}_{ankle2} = \ddot{y} + l_4\ddot{\theta}_4\cos\theta_4 - l_4\dot{\theta}_4^2\sin\theta_4 + l_5\ddot{\theta}_5\cos\theta_5 - l_5\dot{\theta}_5^2\sin\theta_5 \tag{4.104}$$

$$\ddot{\theta}_6 = \frac{m_f l_{cf}(\ddot{x}_{ankle1}\sin\theta_6 - (\ddot{y}_{ankle1} + g)\cos\theta_6) - M_{32} - M_{f1}}{I_{cf} + m_f l_{cf}^2} \tag{4.105}$$

$$\ddot{\theta}_7 = \frac{m_f l_{cf}(\ddot{x}_{ankle2}\sin\theta_7 - (\ddot{y}_{ankle2} + g)\cos\theta_7) - M_{52} - M_{f2}}{I_{cf} + m_f l_{cf}^2} \tag{4.106}$$

3-link frontal plane biped

The only frontal plane model that will be presented here is a 3-link, 5-DOF system with two controlled input torques, shown in Figure 4.15 and Figure 4.16. Both nonlinear and linearized models will be needed. As with the other systems, the nonlinear equations will be used for simulation and the linearized equations will be used for control system design.

Additional frontal plane models that include articulated knee joints and lower leg segments do not vary significantly from the 3-link model as seen from the frontal plane. Two additional torques could be added to the system if articulated feet were included, but moments generated from those torques would be small compared to the frontal plane hip torques. For these reasons, only one frontal plane model was developed.

The nonlinear 3-link frontal plane model equations of motion are given below, and the linearized equations are given in Appendix A.

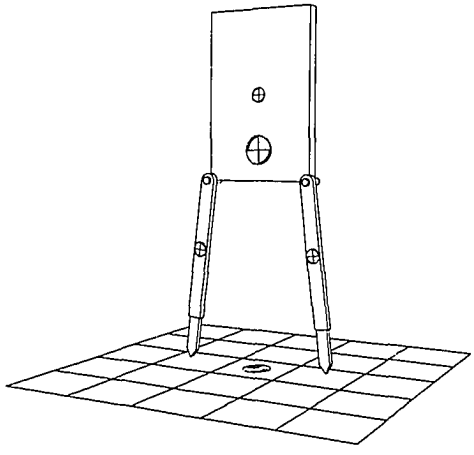

Figure 4.15 3-link, 5-DOF frontal plane biped model

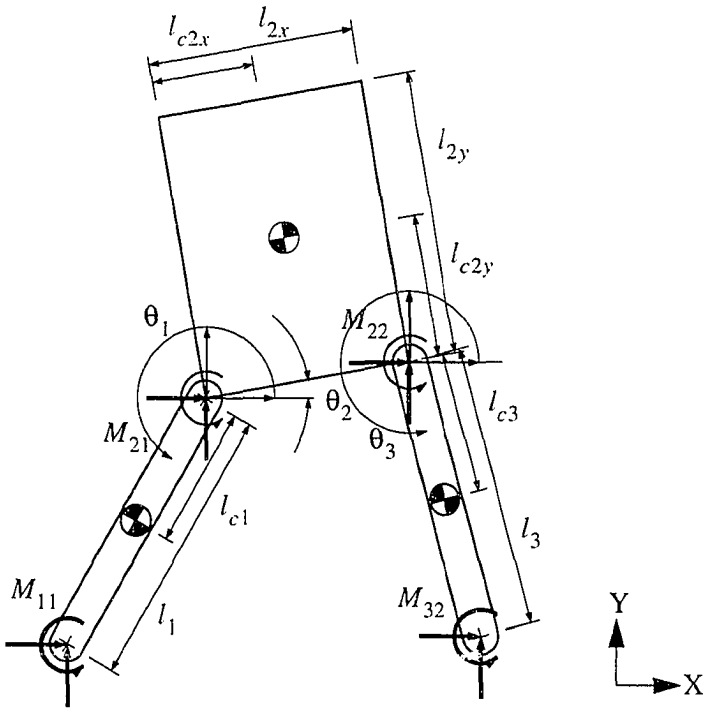

Figure 4.16 3-link frontal plane biped variable definitions

$$(m_1 l_{c1}^2 + (m_2 + m_3) l_1^2 + I_{c1}) \ddot{\theta}_1 + m_3 l_1 l_{c3} \cos(\theta_1 - \theta_3) \ddot{\theta}_3 \tag{4.107}$$
$$+ (m_3 l_1 l_2 \cos(\theta_1 - \theta_2) + m_2 l_1 l_{cy2} \sin(\theta_1 - \theta_2) + m_2 l_1 l_{cx2} \cos(\theta_1 - \theta_2)) \ddot{\theta}_2$$

$$= -(m_2 + m_3) g l_1 \cos\theta_1 - m_2 l_1 l_{cx2} \dot{\theta}_2^2 \sin(\theta_1 - \theta_2) - m_3 l_1 l_{c3} \dot{\theta}_3^2 \sin(\theta_1 - \theta_3)$$
$$- m_3 l_1 l_2 \dot{\theta}_2^2 \sin(\theta_1 - \theta_3) + m_2 l_1 l_{cy2} \dot{\theta}_2^2 \cos(\theta_1 - \theta_2) - m_1 g l_{c1} \cos\theta_1 + M_{11} - M_{21}$$

$$(m_3 l_2^2 + m_2 (l_{cx2}^2 + l_{cx2}^2) + I_{c2}) \ddot{\theta}_2 + m_3 l_2 l_{c3} \cos(\theta_1 - \theta_3) \ddot{\theta}_3 \tag{4.108}$$
$$+ (m_3 l_1 l_2 \cos(\theta_1 - \theta_2) + m_2 l_1 l_{cy2} \sin(\theta_1 - \theta_2) + m_2 l_1 l_{cx2} \cos(\theta_1 - \theta_2)) \ddot{\theta}_1$$

$$= -m_3 g l_2 \cos\theta_2 - m_2 g l_{c2} \cos(\theta_2 + \phi) + m_3 l_1 l_2 \dot{\theta}_1^2 \sin(\theta_1 - \theta_2)$$
$$- m_3 l_2 l_{c3} \dot{\theta}_3^2 \sin(\theta_2 - \theta_3) - m_3 l_1 l_2 \dot{\theta}_2^2 \sin(\theta_1 - \theta_3) + m_2 l_1 l_{cy2} \dot{\theta}_1^2 \cos(\theta_1 - \theta_2)$$
$$- m_1 g l_{c1} \cos\theta_1 + M_{21} - M_{22}$$

$$m_3 l_1 l_{c3} \cos(\theta_1 - \theta_2)\,\ddot{\theta}_1 + m_3 l_2 l_{c3} \cos(\theta_3 - \theta_2)\,\ddot{\theta}_2 + (m_3 l_{c3}^2 + I_{c3})\,\ddot{\theta}_3 \qquad (4.109)$$
$$= -m_3 l_c l_{c3} \dot{\theta}_2^2 \sin(\theta_3 - \theta_2) + m_3 l_c l_{c3} \dot{\theta}_1^2 \sin(\theta_1 - \theta_3) - m_3 g l_{c3} \cos\theta_3 + M_{22}$$

4.2.3 Spatial Monopeds

The first spatial (3D) model investigated will be a 2-link, 8-DOF monoped model with a single point support foot pad. Two separate modifications will be made to this model. The first addition will be to include an articulated knee the system to make an 3-link, 9-DOF model with three controlled joint torques. An additional modification will be to add a single degree of freedom foot with two contact pads, resulting in a 4-link, 10-DOF model with four controlled inputs. A color image of these systems is shown in Figure D.3(a) of Appendix D.

2-link spatial monoped

The 2-link model, shown in Figure 4.17 and Figure 4.18, consists of a 6-DOF body link, and one 2-DOF leg, for a total of 8-DOF. This model is similar to the 2-link planar monoped with the addition of an extra rotational joint between the body and leg links. The lower leg segment is massless and is provided to allow for return clearance of the foot. Extension is controlled kinematically and is not considered to be additional degree of freedom. This 2-link system has two controlled inputs, in addition to the kinematically controlled leg extension. Ground contact forces are generated by a 3D version of the spring-damper foot pad described in Figure 4.31. The D-H parameter table for this system is shown in Table 4.2. An additional transformation will be required to convert the ground reaction forces into the reference frame of the foot

3-link spatial monoped

The 3-link model, shown in Figure 4.19, consists of a 6-DOF body link, and one 3-DOF leg, for a total of 9-DOF. This 3-link system has three controlled inputs. Ground contact forces are generated by a 3D version of the spring-damper foot pad described in Figure 4.31. The D-H parameter table for this system is shown in Table 4.3.

4-link spatial monoped

The 4-link model, shown in Figure 4.20, consists of a 6-DOF body link, and one 4-DOF leg, for a total of 10-DOF. This 4-link system has four controlled inputs. Ground contact forces are generated by two 3D spring-damper foot pads described in Figure 4.31. The D-H parameter table for this system is shown in Table 4.4.

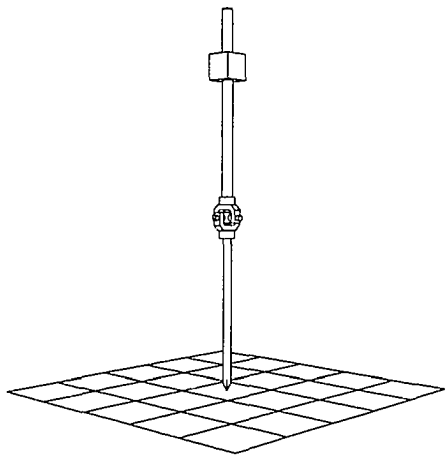

Figure 4.17 2-link, 8-DOF spatial monoped

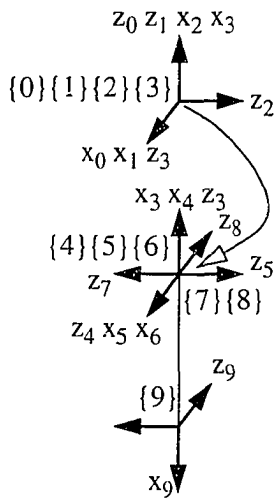

Figure 4.18 2-link, 8-DOF spatial monoped frame diagram

Table 4.2 D-H parameters for a 2-link, 8-DOF spatial monoped

i	α_{i-1}	a_{i-1}	d_i	θ_i
1	0°	0	z	0°
2	-90°	0	y	-90°
3	-90°	0	x	0°
4	0°	0	0	θ_1
5	90°	0	0	$\theta_2 + 90°$
6	90°	0	0	θ_3
7	90°	0	0	$\theta_4 - 90°$
8	90°	0	0	θ_5
9	0	L_2	0	0

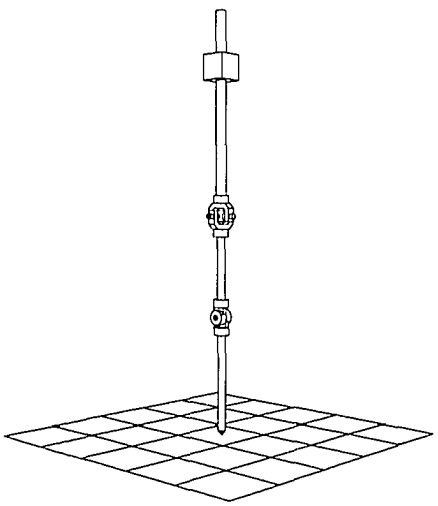

Figure 4.19 3-link, 9-DOF spatial monoped

Table 4.3 D-H parameters for a 3-link, 9-DOF spatial monoped

i	α_{i-1}	a_{i-1}	d_i	θ_i
1	0°	0	z	0°
2	-90°	0	y	-90°
3	-90°	0	x	0°
4	0°	0	0	θ_1
5	90°	0	0	$\theta_2 + 90°$
6	90°	0	0	θ_3
7	90°	0	0	$\theta_4 - 90°$
8	90°	0	0	θ_5
9	90°	L_2	0	θ_6
10	0	L_3	0	0

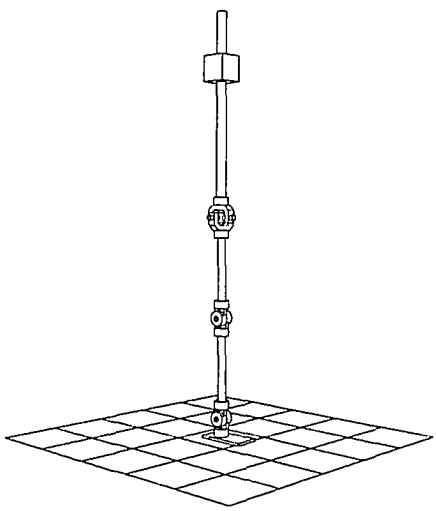

Figure 4.20 4-link, 10-DOF spatial monoped

Table 4.4 D-H parameters for a 4-link, 10-DOF spatial monoped

i	α_{i-1}	a_{i-1}	d_i	θ_i
1	0°	0	z	0°
2	-90°	0	y	-90°
3	-90°	0	x	0°
4	0°	0	0	θ_1
5	90°	0	0	$\theta_2 + 90°$
6	90°	0	0	θ_3
7	90°	0	0	$\theta_4 - 90°$
8	90°	0	0	θ_5
9	90°	L_2	0	θ_6
10	0°	L_3	0	θ_7

Notice that no additional reference frames were added for the 4-link monoped over the system without an articulated foot. The ankle position relative to the surface is handled independently by the foot model algorithm.

4.2.4 Spatial biped models

The spatial biped models are also developed by Newton-Euler numerical formulations of the equations of motion. Four types of spatial biped models will be presented: 3-link, 10-DOF; 3-link, 10-DOF; 5-link, 12-DOF; 7-link, 14-DOF; and two version of an 8-link model, one with 15-DOF and the other with 17-DOF. Denavit-Hartenberg (D-H) parameter tables are given for each model. Some of these systems are shown in Figure D.3(b) of Appendix D.

3-link, 8-DOF spatial biped

The 3-link, 8-DOF spatial biped, shown in Figure 4.21, consists of a 6-DOF body link, and two 1-DOF legs, for a total of 8-DOF. This model has point support feet and is similar to

the 3-link planar model. As in the planar model, the lower leg segments are massless. Leg extension is provided to allow for clearance of the foot during the swing (return) portion of the gait cycle. Extension is controlled kinematically and is not considered as an additional degree of freedom. This 3-link system has two controlled inputs, in addition to the two kinematically controlled leg extensions. Ground contact forces are generated by a 3D version of the spring-damper foot pad described in Figure 4.31, with one pad per foot. The frame diagram and D-H parameter table for this system are shown in Figure 4.22 and Table 4.5, respectively.

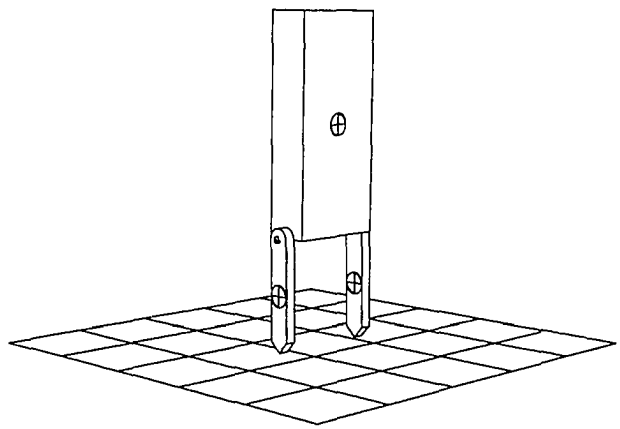

Figure 4.21 3-link, 8-DOF spatial biped

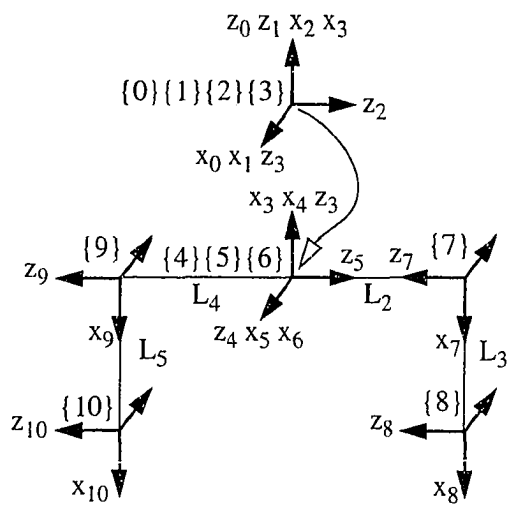

Figure 4.22 3-link, 8-DOF spatial biped frame diagram

Table 4.5 D-H parameters for a 3-link, 8-DOF spatial biped

i	α_{i-1}	a_{i-1}	d_i	θ_i
1	0°	0	z	0°
2	-90°	0	y	-90°
3	-90°	0	x	0°
4	0°	0	0	θ_1
5	90°	0	0	$\theta_2 + 90°$
6	90°	0	0	θ_3
7	90°	0	$-L_2$	$\theta_4 - 90°$
8	0	L_3	0	0
9[a]	90°	0	L_4	$\theta_5 - 90°$
10	0	L_5	0	0

a. for i=9, i-1=6

Note that an additional transformation will be required to convert the ground reaction forces given in the stationary reference frame into the reference frame of the foot.

3-link, 10-DOF spatial biped

The 3-link, 10-DOF spatial biped, shown in Figure 4.23 and Figure 4.24, consists of a 6-DOF body link, and two 2-DOF legs, for a total of 10-DOF. From here on, system models will be represented by cylindrical links instead of the block-like links used in previous models. This allows better visualization of the link joints. This model is similar to the 3-link, 8-DOF spatial model with the addition of frontal plane leg joints. This 3-link system has four controlled inputs, in addition to the two kinematically controlled leg extensions. The 3D version of the spring-damper foot pad is used to generate ground contact forces. The D-H parameter table for this system is shown in Table 4.6.

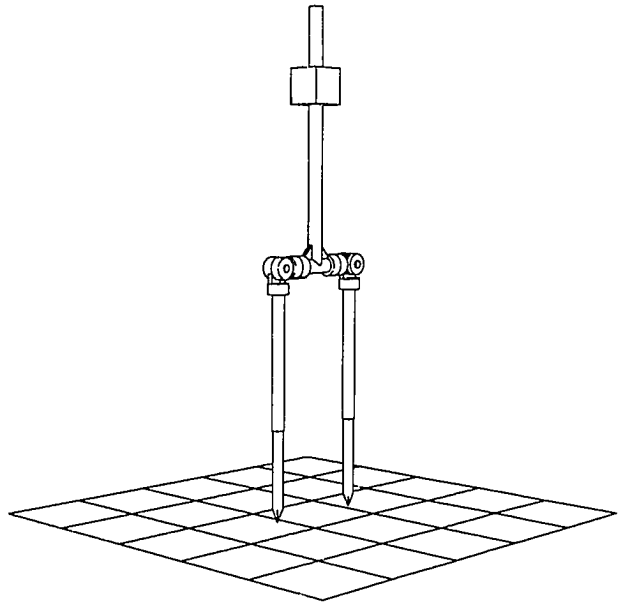

Figure 4.23 3-link, 10-DOF spatial biped

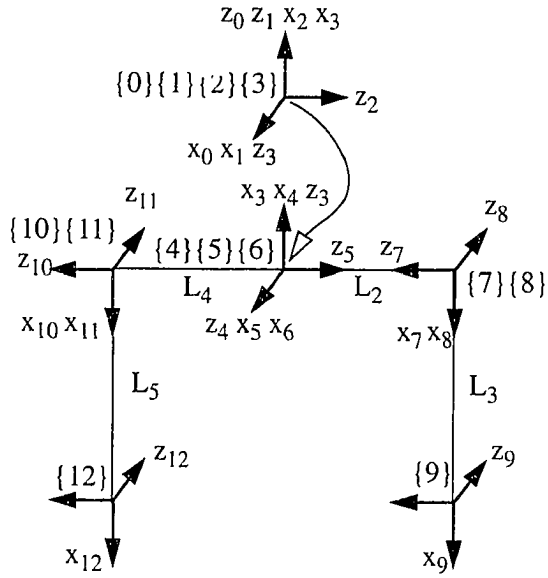

Figure 4.24 3-link, 10-DOF spatial biped frame diagram

Table 4.6 D-H parameters for a 3-link, 10-DOF spatial biped

i	α_{i-1}	a_{i-1}	d_i	θ_i
1	0°	0	z	0°
2	-90°	0	y	-90°
3	-90°	0	x	0°
4	0°	0	0	θ_1
5	90°	0	0	$\theta_2 + 90°$
6	90°	0	0	θ_3
7	90°	0	$-L_2$	$\theta_4 - 90°$
8	90°	0	0	θ_5
9	0	L_3	0	0
10[a]	90°	0	L_4	$\theta_6 - 90°$
11	90°	0	0	θ_7
12	0	L_5	0	0

a. for i=10, i-1=6

5-link spatial biped

The 5-link spatial biped, shown in Figure 4.25 and Figure 4.26, consists of a 6-DOF body link, and two 3-DOF articulated legs, for a total of 12-DOF. This model has point support feet and is similar to the 5-link planar model with the addition of frontal plane hip joints. This system has six controlled torque inputs. Ground contact forces are generated by a 3D version of the spring-damper foot pad described in Figure 4.31, with one 3D pad per foot. The D-H parameter table for this system is shown in Table 4.7.

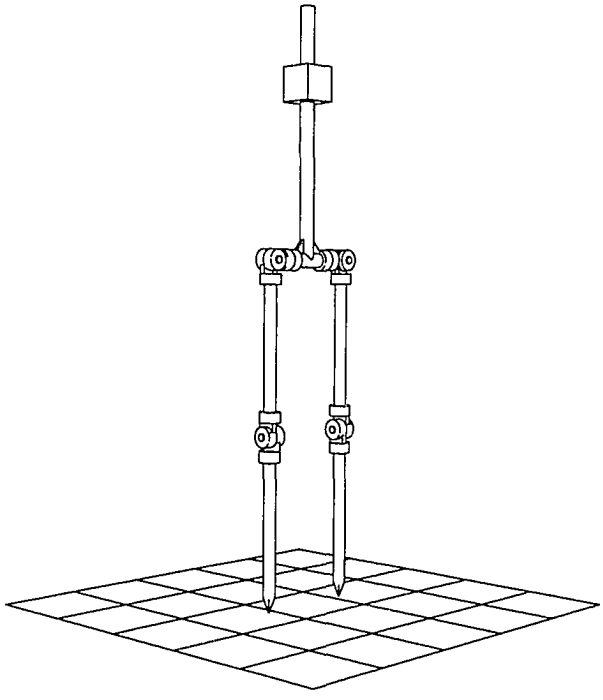

Figure 4.25 5-link, 12-DOF spatial biped

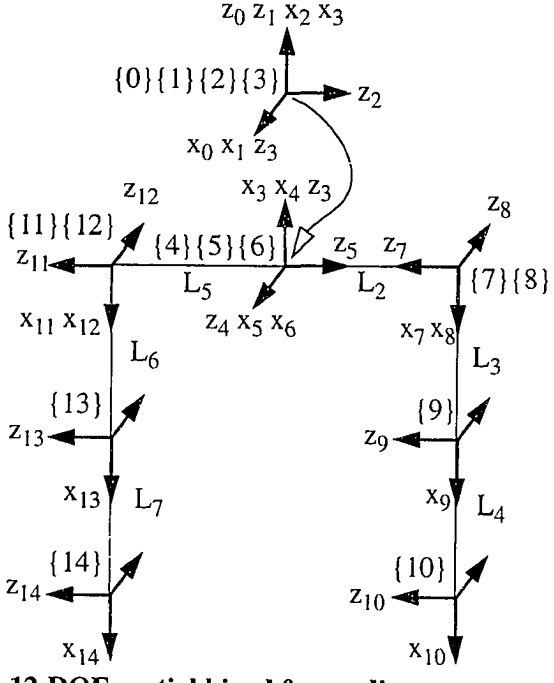

Figure 4.26 5-link, 12-DOF spatial biped frame diagram

Table 4.7 D-H parameter table for the 5-link, 12-DOF spatial biped

i	α_{i-1}	a_{i-1}	d_i	θ_i
1	0°	0	z	0
2	-90°	0	y	-90°
3	-90°	0	x	0°
4	0°	0	0	θ_1
5	90°	0	0	$\theta_2 + 90°$
6	90°	0	0	θ_3
7	90°	0	$-L_2$	$\theta_4 - 90°$
8	90°	0	0	θ_5
9	-90°	L_3	0	θ_6
10	0	L_4	0	0
11[a]	90°	0	L_5	$\theta_7 - 90°$
12	90°	0	0	θ_8
13	-90°	L_6	0	θ_9
14	0	L_7	0	0

a. for i=11, i-1=6

7-link spatial biped

The 7-link spatial biped, shown in Figure 4.27 and Figure 4.28, consists of a 6-DOF body link, and two 4-DOF articulated legs, for a total of 14-DOF. This system has eight controlled inputs. Ground contact forces are generated by a 3D version of the spring-damper foot pad described in Figure 4.31, with two 3D pads per foot. The D-H parameter table for this system is shown in Table 4.8. As in the 4-link monoped system, the ankle height for biped systems with articulated feet (i.e. the 7 and 8-link models) is handled by the foot model instead of with additional reference frames.

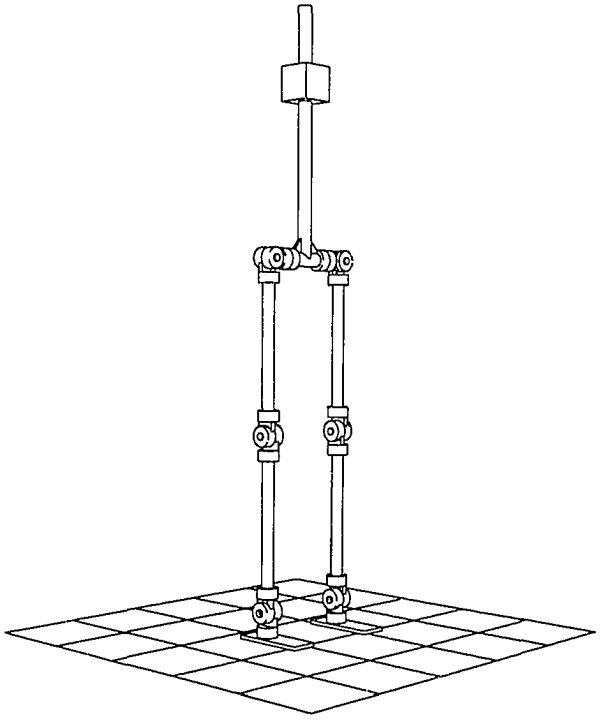

Figure 4.27 7-link, 14-DOF spatial biped

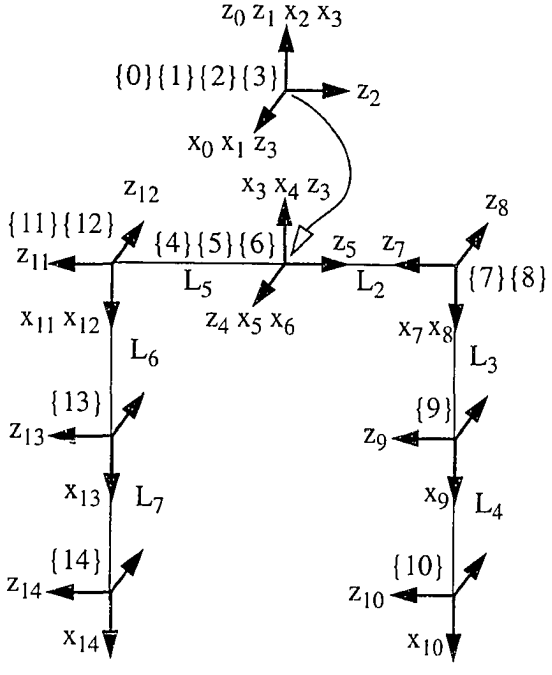

Figure 4.28 7-link, 14-DOF spatial biped frame diagram

Table 4.8 D-H parameter table for a 7-link, 14-DOF spatial biped

i	α_{i-1}	a_{i-1}	d_i	θ_i
1	0°	0	z	0
2	-90°	0	y	-90°
3	-90°	0	x	0°
4	0°	0	0	θ_1
5	90°	0	0	$\theta_2 + 90°$
6	90°	0	0	θ_3
7	90°	0	$-L_2$	$\theta_4 - 90°$
8	90°	0	0	θ_5
9	-90°	L_3	0	θ_6
10	0	L_4	0	θ_7
11[a]	90°	0	L_5	$\theta_8 - 90°$
12	90°	0	0	θ_9
13	-90°	L_6	0	θ_{10}
14	0	L_7	0	θ_{11}

a. for i=11, i-1=6

8-link, 15-DOF spatial biped

The 8-link spatial biped, shown in Figure 4.29, consists of a 6-DOF body link with a 1-DOF body segment attachment joint, and two 4-DOF articulated legs, for a total of 15-DOF. This system has nine controlled inputs. Ground contact forces are generated by a 3D version of the spring-damper foot pad described in Figure 4.31, with two 3D pads per foot. The D-H parameter table for this system is shown in Table 4.9. Notice that the initial cartesian space translations are in a different order than in the previous systems.

Here the hip link is used as the initial link and the branching link. Another option would be to use the body (torso) link as the initial link and the hip link as the branching link. This brings up an important issue — which segment of the model should be considered the "base" link?

In the previous biped models, the torso and hip segments were considered as one component. In the 8-link model presented here, the hip segment was chosen as the base link to allow for the three open chains to be separated after the initial link, instead of having two chains attached to a branch in the middle of the system. This seems to offer a simpler procedure for the dynamics calculations.

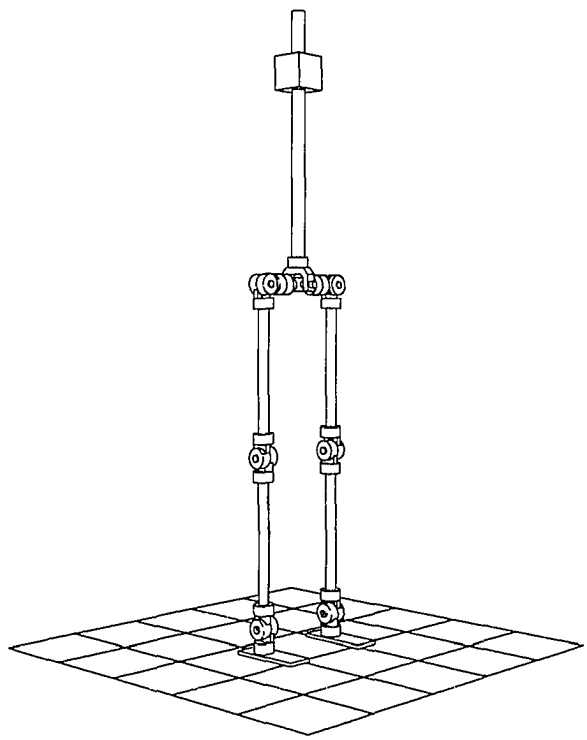

Figure 4.29 8-link, 15-DOF spatial biped

Table 4.9 D-H parameter table for a 8-link, 15-DOF spatial biped

i	α_{i-1}	a_{i-1}	d_i	θ_i
1	-90°	0	y	90°
2	90°	0	x	90°
3	-90°	0	z	-90°
4	0°	0	0	θ_1
5	-90°	0	0	$\theta_2 - 90°$
6	-90°	0	0	θ_3
7	0°	0	0	θ_4
8[a]	-90°	0	L_2	θ_5
9	90°	0	0	θ_6
10	-90°	$-L_3$	0	θ_7
11	0°	$-L_4$	0	θ_8
12[a]	-90°	0	$-L_5$	θ_9
13	90°	0	0	θ_{10}
14	-90°	$-L_6$	0	θ_{11}
15	0°	$-L_7$	0	θ_{12}

a. for i=8 and i=12, i-1=6

8-link, 17-DOF spatial biped

The 8-link spatial biped, shown in Figure 4.30, consists of a 6-DOF body link with a 1-DOF body attachment joint, and two 5-DOF articulated legs, for a total of 17-DOF. This system has eleven controlled inputs. Feet are attached to the lower leg segments with 2-DOF universal joints. Ground contact forces are generated by a 3D version of the spring-damper foot pad described in Figure 4.31, with four 3D pads per foot. The D-H parameter table for this system is shown in Table 4.10.

An additional concern with this model is the control of the 2-DOF ankle joints. Since the foot is allowed to move relative to the lower leg in the frontal plane as well as the sagittal plane, frontal plane ankle control torque will need to be defined. Due to the small region of contact of each foot in the frontal plane, only small frontal plane torques can be generated. A modified version of the frontal plane model could be used, but since the torque transmitted through this joint is small when compared to all other input torques, a separate frontal plane model was not developed.

The primary use for frontal plane ankle torque is for foot placement prior to foot touch-down. Therefore, independent passive (spring-damper) control elements will be prescribed for this joint.

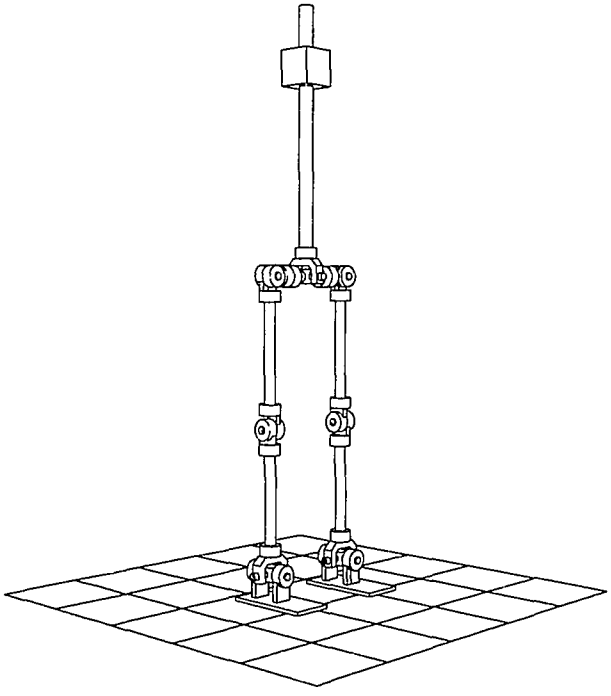

Figure 4.30 8-link, 17-DOF spatial biped

Table 4.10 D-H parameter table for a 8-link, 17-DOF spatial biped

i	α_{i-1}	a_{i-1}	d_i	θ_i
1	-90°	0	y	90°
2	90°	0	x	90°
3	-90°	0	z	-90°
4	0°	0	0	θ_1
5	-90°	0	0	$\theta_2 - 90°$
6	-90°	0	0	θ_3
7	0°	0	0	θ_4
8[a]	-90°	0	L_2	θ_5
9	90°	0	0	θ_6
10	-90°	$-L_3$	0	θ_7
11	0°	$-L_4$	0	θ_8
12	90°	0	0	θ_9
13[a]	-90°	0	$-L_5$	θ_{10}
14	90°	0	0	θ_{11}
15	-90°	$-L_6$	0	θ_{12}
16	0	$-L_7$	0	θ_{13}
17	90°	0	0	θ_{14}

a. for i=8 and i=13, i-1=6

Jacobian velocity transformations

As mentioned earlier, the Jacobian matrix can be used to find the cartesian velocities of any coordinate frame of the mechanism from a given set of joint space values. For planar mechanisms the mapping equations can sometimes be found be inspection, but for spatial

mechanisms a more formal approach is needed. A method using velocity propagation method [24] will be described here.

The cartesian velocities that make up the elements of the Jacobian matrix can be found in a sequential manner similar to the outward iterations of the Newton-Euler dynamics formulation. For revolute joints the velocity equations are:

$$^{i+1}\omega_{i+1} = {}^{i+1}_{i}R\,{}^{i}\omega_i + \dot{\theta}_{i+1}\,{}^{i+1}\hat{Z}_{i+1} \tag{4.110}$$

$$^{i+1}v_{i+1} = {}^{i+1}_{i}R\,({}^{i}v_i + {}^{i}\dot{\omega}_i \times {}^{i}P_{i+1}) \tag{4.111}$$

For prismatic joints the velocity equations are:

$$^{i+1}\omega_{i+1} = {}^{i+1}_{i}R\,{}^{i}\omega_i \tag{4.112}$$

$$^{i+1}v_{i+1} = {}^{i+1}_{i}R\,({}^{i}v_i + {}^{i}\dot{\omega}_i \times {}^{i}P_{i+1}) + \dot{d}_{i+1}\,{}^{i+1}\hat{Z}_{i+1} \tag{4.113}$$

The Jacobian can then be written as the coefficient matrix premultiplying the joint angular velocity vector as shown below.

$$^{0}V = {}^{0}J(\Theta)\,\dot{\Theta} \tag{4.114}$$

where the leading superscript denotes the reference frame in which the value is defined.

4.3 Ground Reaction Forces

In creating the multibody dynamics biped models one of the most important choices to make deals with how to handle the foot-ground interface. Two main options exist: mathematically constraining the feet to the floor, or using spring-damper elements as constraints. The mathematical joint constraint method requires a momentum transfer step to calculate the

velocity changes due to the impulsive forces generated by contact. In addition, the system equations must be reconfigured at the point of contact and add or remove joints that attach the foot to the floor [52]. Adding spring-damper elements (sometimes referred to as a soft constraint or penalty method) to the foot allows for the modeling of the elastic effects of collision, but at the expense of a stiffer set of system equations.

The foot constraint method used here makes use of spring-damper components along with an error term to control the reaction of the system with a surface. This type of ground contact modeling is essentially the same as a proportional-integral-derivative (PID) controller. The one and two pad feet are shown in Figure 4.31.

The choice of the spring-damper foot model, was selected for this project over the joint constraint model in order to simulate compliance between the foot and ground. Although this type of system adds two more degrees-of-freedom to the system (over a joint constraint) and requires a smaller time step for numerical integration of the equations of motion, it results in a more realistic model. This type of model does not require system reconfiguration for different support situations. One unified system model can handle all single support, double support, and flight modes. This method also avoids the impulse momentum transfer calculations required at change of support transitions.

During system operation, the spring-damper elements attach themselves to the surface at the moment of contact with multi-directional elements parallel to the surface and a single direction element perpendicular to the surface. Error terms are continually summed up between the current position and the initial contact position. Each summation terms behaves like the integral term in a PID controller to compensate for steady-state error. The touchdown position is maintained by the foot pad(s) unless the forces become larger than can be supported by friction. In this case, the foot is allowed to slide along the surface until a new holding position can be established.

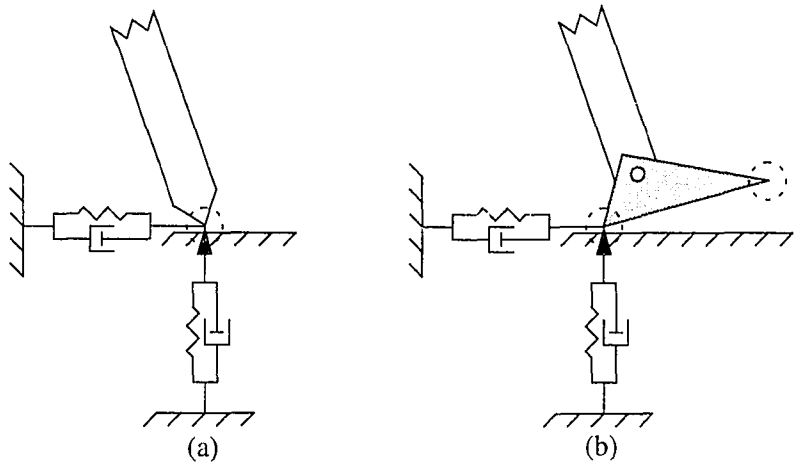

Figure 4.31 2D Foot-ground constraint models: (a) single pad foot, (b) two pad foot

4.4 Numerical Integration

Once the system equations of motion have been developed a method of finding a solution is needed. The type of equations that have been formulated in this chapter are referred to as initial value problems for ordinary differential equations (ODEs), which usually require numerical integration solution techniques. Both Taylor polynomial approximation methods and multistep methods will be discussed, as well as the procedure for setting up a system of second order differential equations. A brief introduction to numerical integration is summarized in Appendix B. Appendix B also gives an example of setting up uncoupled and coupled second order systems for numerical integration.

4.4.1 Euler Integration

The simplest form of numerical integration is the Euler method. Euler methods involve solving the linear form, or an approximation to the linear form, of a Taylor series polynomial. Euler integration methods are relatively inefficient especially if an accurate solution is desired, but they are conceptually simple and easy to program. Equation (4.115) is the simplest form of Euler's method, which uses an approximation to the first derivative of the Taylor series.

$$y_{n+1} = y_n + hf(x_n, y_n) \tag{4.115}$$

4.4.2 Runga-Kutta Integration

Using higher order terms of a Taylor polynomial leads to additional formulations like Runga-Kutta (RK) methods, which have improved convergence speed over the Euler method. The fourth order Runga-Kutta procedure in Equations (4.116) to (4.120) uses approximate derivatives for the first four derivatives of the Taylor series polynomial.

$$v_1 = f(x_n, y_n) \tag{4.116}$$

$$v_2 = f(x_n + h, y_n + h) \tag{4.117}$$

$$v_3 = f(x_n + \frac{h}{2}, y_n + \frac{h}{2}) \tag{4.118}$$

$$v_4 = f(x_n + h, y_n + hv_3) \tag{4.119}$$

$$y_{n+1} = y_n + \frac{h}{6}(v_1 + 2v_2 + 2v_3 + v_4) \tag{4.120}$$

RK methods can operate with either a constant step size or be modified to allow for an adaptive step size.

4.4.3 Adams-Bashforth-Moulton Integration

Another family of numerical integration methods, called multistep methods, are based on finding an approximate solution to the integral in (4.121). The types that will be discussed here are the Adams-Bashforth (AB) and Adams-Moulton methods (AM). A second order version of an Adams-Bashforth method is given by (4.122). An Adams-Moulton method is given by (4.123).

$$Y(x_{n+1}) = Y(x_n) + \int_{x_n}^{x_{n+1}} f(x, Y(x))\, dx \tag{4.121}$$

$$y_{n+1} = y_n + \frac{h}{2}[3f(x_n, y_n) - f(x_{n-1}, y_{n-1})] \tag{4.122}$$

$$y_{n+1} = y_n + \frac{h}{2}[f(x_n, y_n) + f(x_{n+1}, y_{n+1})] \tag{4.123}$$

Since the values of x_{n-1} and x_n are needed to find x_{n+1} these methods require another method to get started (like an Euler or RK method).

4.4.4 Setting Up a System of ODEs

Setting up a system to be solved by numerical integration involves reducing equations to a system of several first order equations. To convert coupled second order systems like the kind developed in this chapter into first order equations, the second order system must be uncoupled, as shown in (4.2) and (4.3). The uncoupled system is then transformed into $2n$ first order systems. Detailed examples of this procedure are given in Appendix B.

The main issues in programming an initial value ODE for numerical solution are, integration step size and the degree of stiffness of the system. A system of ODEs is considered to be a stiff system if it has some eigenvalues that are much larger or much smaller than the others. Stiff systems require a smaller step size in order to obtain a desired degree of accuracy. One method of dealing with this type of system is to use a relatively simple algorithm and take a large number of steps. Another is to use an adaptive step size driver that automatically selects a smaller step size when the accuracy is not meeting the desired tolerance.

In an interactive simulation environment it is usually not desirable to have the simulation speeding up and slowing down, so for this reason, a constant step size driver was chosen for solving most of the systems presented here. Based on run-time performance testing, the fourth order Runga-Kutta method was chosen for integration.

5. MOTION CONTROL

The next step after the biped system models have been defined, is to apply the necessary joint torques to produce the desired motion. There are several ways to calculate these torques, they can be separated into two main types: open-loop and closed-loop control. Open-loop techniques, like inverse dynamics methods, are sometimes used in biped simulation, but lack the ability to deal with changing environments and disturbances. Closed-loop techniques, on the other hand, use feedback of state variables to handle changing environments, modeling and sensing errors, and unexpected disturbances.

The main goal of this project is to develop feedback control methods to balance on one or both feet, and to initiate and sustain a steady-state walking gait cycle. In addition, the control system should be able to transition between balancing and walking, change velocity, and react appropriately to varying terrain.

Several types of feedback control will be discussed, these include conventional single-input single-output (SISO) control techniques, like proportional-derivative (PD) and proportional-integral-derivative (PID) controllers, as well as state-space, multi-input multi-output (MIMO) methods, like the linear-quadratic regulator (LQR). In addition to the different methods of control, three distinct control applications for achieving the desired locomotion tasks will be presented: manual joint position control, automatic control for balancing modes, and state machines for automatic walking control. Both the conventional and state space methods are used for controlling the biped models.

5.1 Conventional Control Techniques

Closed-loop feedback control uses information about the current state of the system as input to the system. This differs from open-loop control, which uses a command signal that is

not influenced by current state. This section briefly discusses closed-loop single-input single output (SISO) control systems, specifically PD and PID control, but is not meant to be a complete review control systems. See [102], [27], or [7] for more detailed information.

5.1.1 Standard Problem Statement

Most problems can be cast (or recast) into the standard form shown in Figure 5.1, which contains a plant, controller, feedback, and disturbances. For multibody dynamics systems, the plant, *G(s)*, is the system equation(s) of motion which can not be modified. For control system design the plant is a linearized system, while in the application or simulation form, it is nonlinear. The input command (or reference) signal, *r(s)*, is chosen by the user or some other higher level control algorithm. The controller is made up of an optional pre-filter, *P(s)*, and a vector of feedback gains, *K(s)*. The pre-filter and feedback gains make up the control law which produces the control signal, *u(s)*, the direct input to the plant. The plant output states, *y(s)*, are then fed back to the controller. Disturbances and measurement errors are represented by *d(s)* and *m(s)*, respectively.

5.1.2 PD Controllers

The first type of conventional (or classical) controller that will be discussed is the proportional-derivative (PD) controller, which fits into the category of single-input single-output (SISO) controllers. These control systems can be designed by using classical SISO design techniques like root locus. In an interactive simulation environment it is sometime easier (and faster) to design PD controllers by interactively varying the gains and simulating the system response. The PD controller of Figure 5.2, uses the output variable state and its derivative, along with the reference signal to define the control signal sent to the plant. The two feedback gains are, the proportional gain, K_p, and the derivative gain, K_d. This controller will be used for independent joint control as part of a higher level walking control algorithm called a state machine, which will be discussed later.

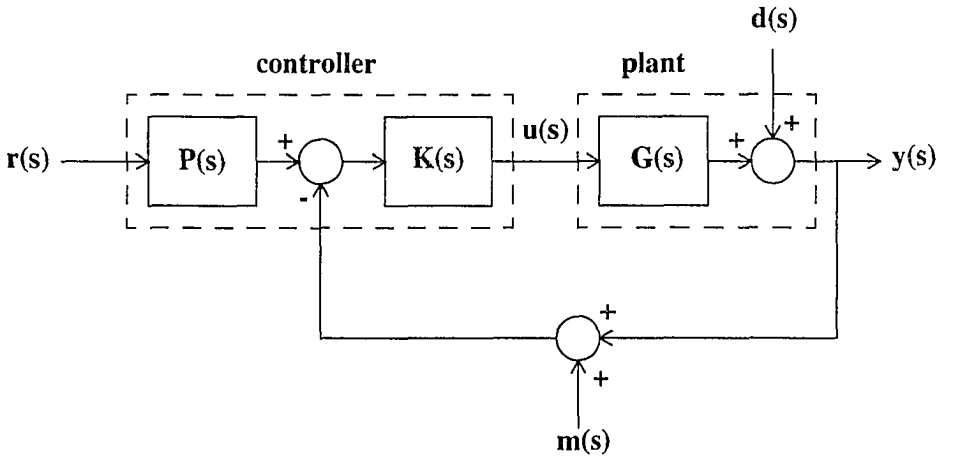

Figure 5.1 Standard feedback control configuration

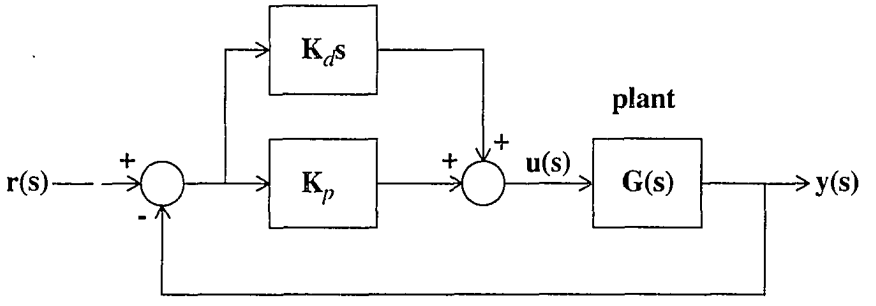

Figure 5.2 PD controller block diagram

5.1.3 PID Controllers

Another SISO method that will be used in this research is proportional-integral-derivative (PID) control, as shown in Figure 5.3. This type of controller consists of three feedback gains, the same two from the PD controller, plus an additional integral gain, K_i. PID controllers are normally used to eliminate the steady-state error of a PD controlled system.

The integral term essentially generates a continuous sum of the error between the reference term(s) and the plant output. This sum is scaled by the integral gain, K_i, and added to the control law. In practice, the integral term is usually kept small to minimized effect on the system characteristics. This allows an independently calculated sum to be generated, and does not require an additional state if the system is second order. If a larger integral term is needed

to obtain desired system response, it may become necessary to design the controller by increasing the order of the system characteristic equation.

One of the applications of a PID controller in this research will be to generate the reaction forces between the foot and the ground surface.

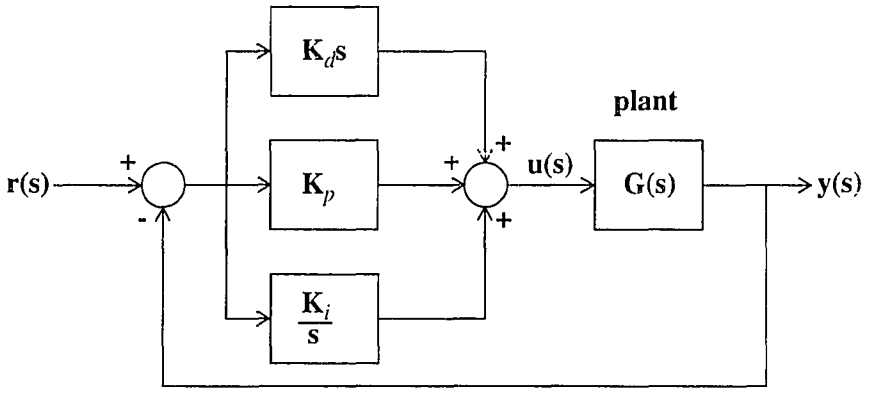

Figure 5.3 PID controller block diagram

5.2 State-Space Control

State-space control methods (also called modern control) offer better techniques for handling multi-input multi-output (MIMO) control system design. These methods are based on time domain representation of the system instead of the Laplace or frequency domain procedures of conventional control system design. Although conventional SISO design techniques can be used to design controllers for MIMO systems by simplifying or decoupling the system, modern MIMO design offers better techniques for reshaping the controller/plant system to get a desired response.

5.2.1 Optimal Controllers

The main type of optimal control that will be discussed here is the linear-quadratic regulator (LQR). This type of control system design is based on minimizing a specified performance index to arrive at a set of feedback gains. Different procedures exist to produce gains that are functions of time or that are linear time-invariant (LTI).

Linear-quadratic regulator

The linear-quadratic regulator (LQR) design method calculates gains for a given set of weighting matrices, which can be time varying. Several variations of the LQR problem definition can be formulated depending on which boundary conditions and time constraints are specified.

The method that will be used here is the LTI steady-state linear-quadratic regulator. This type of LQR does not put any restrictions on final end time and is a better choice for use in an interactive simulation environment than the time varying versions of the LQR. The LQR control system design involves linearizing the second order system equations of motion (5.1), and reformulating the system in terms of first order equations in the form of (5.2).

$$A\ddot{X} = B \tag{5.1}$$

$$\dot{X} = AX + BU \tag{5.2}$$

$$U = -KX \tag{5.3}$$

where X is the state and U is the feedback control. The problem then is to find the set of gain matrices, K, to minimize the performance index

$$J = \int_t^{t_f} (x^T Q x + u^T R u)\, dt \tag{5.4}$$

Where Q and R are the state and control weighting matrices, respectively. The associated steady-state algebraic Riccati equation is

$$0 = A^T S + SA - SBR^{-1}B^T S + Q \tag{5.5}$$

(where $\dot{S}$ is set to 0 at t_f=∞). Solving for the unique positive-definite solution, S_∞, the full state gain matrix can then be found

$$K = R^{-1}B^{T}S_{\infty} \tag{5.6}$$

The linear-quadratic regulator is not the only type of design procedure that could have been used here. Another useful method is pole-placement control system design, in which the designer decides what the system eigenvalues should be to achieve a desired system response. Other methods include: dynamic programming, neural networks, QFT, LQG, and H_{∞}, but will not be discussed here.

5.3 Open-Loop Methods

5.3.1 Inverse Plant Control

One type of open-loop control is the inverse plant or computed torque method. For robotic systems inverse kinematics are used to get the joint variables, then the torque necessary to obtain those joint variables is computed. This involves solving the system equations of motion for the torque values and plugging in the desired angular position, angular velocity, and angular acceleration values.

One of the problems that goes along with this type of control is determining valid angular velocities and angular accelerations. The Jacobian matrix can be found and used to transform cartesian velocities and accelerations to angular velocities and angular accelerations. But then the question becomes "what should the cartesian velocities and accelerations be?" Another problem to be solved with the inverse plant method is that of disturbances. As with all open-loop systems, any unpredicted disturbance will cause an error to arise in the state variables that is not self-correcting. A realistic inverse plant system requires that some form of error feedback control be used to compensate for disturbances.

5.4 Manual Control

Manual control of the types of physically based models presented here requires the user to perform the low level link movement tasks by simultaneous manipulation of several input

devices. Interacting with these types of models is similar to playing a video game. And many of the coordination skills required for successfully mastering video games also apply here.

The first required element of user interaction with these systems is high frequency visual feedback control (i.e. efficient hand-eye coordination). The user must be able to process the visual information and relay a measured change to the computers input devices at a rate fast enough to avoid destabilization. The second requirement is a sense of balance. Since the only type of information that the user receives is visual, he/she must develop a "visual sense of balance." In order to help achieve this, several visual cues are added to the virtual environment: CG position, CG projection, and zero moment point (ZMP) markers. The final requirement is for the user to figure out the series of movements necessary to initiate and sustain a gait cycle (or any other type of motion).

Several levels of manual control have been developed. The control methods used in this project progressed from simple direct joint torque input, to several semi-automatic schemes which include, linking multiple variables to functions of a few user inputs, specifying angular positions instead of joint torques, and specifying leg touchdown positions.

Some of the input devices that are used for manual input are: a dial box, a button box, foot pedals, and 6-DOF magnetic sensors. The need for multi-input or simultaneous input devices precludes the use of the single input slider type graphical device controlled by a mouse. Although a mouse can be used to control two degrees of freedom at once (with x and y movements), this type of input is not intuitive for the simultaneous rotational position control required of the biped systems.

The control sequences produced by user inputs can also be saved and fed back into the system later in an open-loop control manner. The user can then provide additional corrective or touch-up adjustments on-line. This iterative procedure can be repeated until a satisfactory motion sequence is obtained. The flexibility of this type of motion control allows generation of almost any motion that is physically possible. In addition to walking and running, other specific movement sequences, like jumping and backflips, can be generated and stored for

playback at a later time. Other manual control issues include human input sampling, interpretation, and response capabilities.

5.5 Automatic Control

A complete automatic balancing and walking control system for biped mechanisms involves several layers arranged in a hierarchical structure. The overall control structure used in this project is described by the decision tree shown in Figure 5.4.

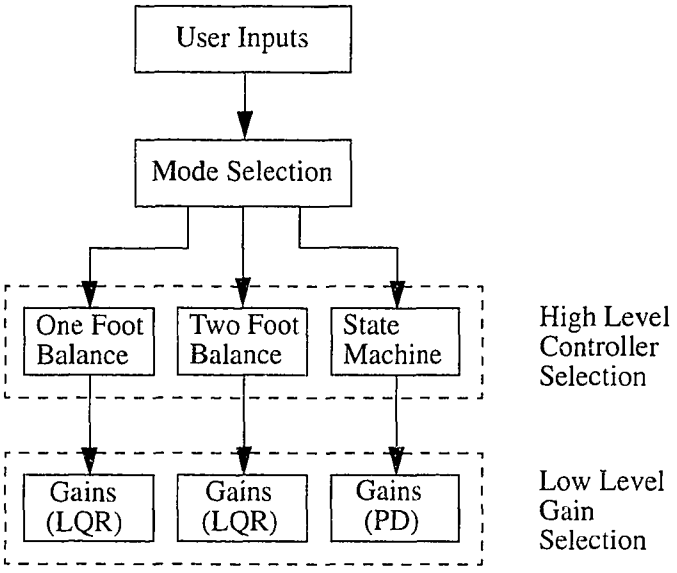

Figure 5.4 Control decision tree

At the lowest level of the hierarchy are the feedback gains. These gains are the most basic elements of the control system that define how the system reacts in a certain configuration. Above this level are the higher level controllers for balance and walking. These consist of sets of instructions used to pick the low level feedback gains based on the current state of the mechanism and the current mode selection. Finally, at the top of the control hierarchy are the user inputs, which consist of desired actions: direction, velocity, step length, and/or step frequency. The individual balancing and walking control components of this system will be discussed in the next two sections.

5.6 Balancing Control

Controlling the balancing modes of monoped and biped systems involves finding a set of feedback gains that can stabilize these unstable systems. In addition, algorithms for initial foot placement will be needed.

5.6.1 Balancing

Two separate types of balancing control systems will be needed for each biped model. The first case exists when both legs are touching the surface, usually referred to as double support. The second case, single support, exists when only one leg is in contact with the surface. Since the linearized system will be different for each mode, the different balancing modes will require separate sets of gains. Both types balancing will use the LQR design method to obtain full state feedback gains.

Obtaining a good set of gains depends on the choice of LQR weighting matrices Q and R. A "good" set of feedback gains for biped balancing should allow the system to achieve balance quickly, with a fast response time, and be able to handle many types of input conditions and disturbances. This set should also be able to transition effectively to other balancing modes as well as to walking modes.

Picking the Q and R matrices to achieve this type of performance is in some ways dependent on the designers intuition. When computing full state feedback gains using LQR design techniques, the ability to quickly simulate and visualize the response of the nonlinear system for many different sets of gains is a useful tool that can compliment (and even help develop) the designer's intuition. An interactive graphical simulation environment used in conjunction with the LQR method was the main design technique used for this project.

One way in which this type of iterative "design by simulation" is utilized, is by allowing the designer to quickly discover which elements of the weighting matrices have the most effect on certain aspects of the system performance. Once these elements have been identified, tuning system performance becomes a much simpler task.

5.6.2 Balance foot placement

Placement of the foot on touchdown is an important issue for obtaining and maintaining balance. Achieving balance after a system is dropped onto a surface with an initial horizontal velocity involves predicting a touchdown position that will convert the kinetic energy to potential energy so that the projected CG and the zero moment point (ZMP) are in the same location. Two of the possible ways to predict the correct landing position are, using projectile motion equations along with the energy equation, and using generalized momentum equations with the energy equation. The first method will be discussed here.

Figure 5.5 shows the path of the composite body CG prior to landing. Equations (5.7) through (5.19) calculate the desired body and leg positions that will be required to achieve balance after landing. These equations will need to be solved numerically.

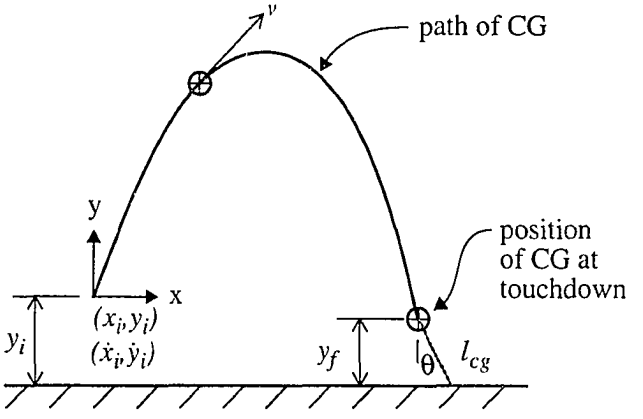

Figure 5.5 Parabolic CG path trace and landing configuration

$$y_f = l_{cg}\cos(\theta) \tag{5.7}$$

$$y_f = y_i + \dot{y}_i t_f - \frac{1}{2} g t_f^2 \tag{5.8}$$

$$\Delta t = \frac{2\dot{y}_i}{g} \tag{5.9}$$

$$t_f = \frac{\dot{y}_i \pm \sqrt{\dot{y}^2 + 2g\,(y_i + y_f)}}{g} \tag{5.10}$$

$$\dot{y}_f = \dot{y}_i - g t_f \tag{5.11}$$

Substituting (5.8) and (5.10) into (5.11) for y_f and t_f respectively, gives the vertical velocity at the touchdown point,

$$\dot{y}_f = -\sqrt{\dot{y}_i^2 + 2g\,(y_i - l_{cg}\cos(\theta))} \tag{5.12}$$

Assume the final horizontal velocity is the same as the initial velocity,

$$\dot{x}_i = \dot{x}_f \tag{5.13}$$

Also assume that energy is conserved during flight. Using the potential-kinetic energy equations results in:

$$\frac{1}{2}mv_i^2 + mgy_i = \frac{1}{2}mv_f^2 + mgy_f \tag{5.14}$$

which reduces to,

$$\dot{y}_i^2 - \dot{y}_f^2 + 2g\,(y_i - y_f) = 0 \tag{5.15}$$

Another application of the energy equation after touchdown is needed to ensure the system reaches the desired equilibrium point (assumed to be the vertical position).

$$\frac{1}{2}I_o\dot{\theta}^2 = mgl_{cg}\,(1 - \cos(\theta)) \tag{5.16}$$

Here, the composite body inertia is used relative to the touchdown point, and is approximated as a point mass,

$$I_o = ml_{cg}^2 \tag{5.17}$$

$$\dot{\theta}^2 = \frac{(\dot{y}\sin(\theta) + \dot{x}\cos(\theta))^2}{l_{cg}^2} \tag{5.18}$$

$$(\dot{y}\sin(\theta) + \dot{x}\cos(\theta))^2 = 2gl_{cg}(1 - \cos(\theta)) \tag{5.19}$$

The three nonlinear, algebraic equations (5.7), (5.15), and (5.19) can be set up to solve for θ numerically. The Newton-Raphson method discussed in Appendix B will be used.

5.7 Walking Cycle Control

The basic walking gait cycle, as described in Chapter 3, consists of several phases that have to occur in sequence for the system to work properly. In addition to leg position control, the overall system balance must be maintained. Several methods exist for programming an automatic gait cycle. One common method is based on using a state machine to evaluate the current position of the links and then decide which set of motion control programs to use. The goal of this part of the control system will be to stabilize the inverted pendulum body, and to establish and maintain a desired horizontal velocity.

5.7.1 State Machines

The state machine, as used here, is an algorithms that selects an appropriate action based on the current state of the system to order to obtain a desired control sequence. State machines are high level control mechanisms that contain or access several low level control systems which may be selected for a particular situation. In addition to choosing control programs, the state machine also selects a set of feedback gains for use within a control program. The individual sets of gains are calculated by the methods described earlier (PD, LQR), and may be calculated on-line or pre-computed and retrieved by table lookup. The general location of a state machine within the control system is shown in Figure 5.6.

The primary inputs to the state machine are, current system states, desired velocity, desired step length, and/or desired step frequency. Other inputs may include, ground reaction

forces, surface information, torque limit constraints, and kinematic customization parameters. State machine outputs are the state feedback gain matrices. In addition, the state machine is in charge of maintaining the phase angle coupling between the two legs to keep the gate cycle synchronized.

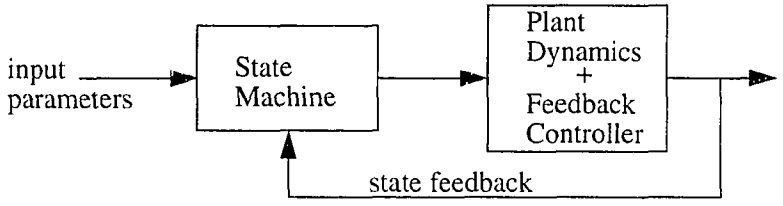

Figure 5.6 General biped control system with state machine

The walking state machine used here is described in Figure 5.7. It has two major regions: single and double support, and five subregions: loading, stance, unloading, swing, and extension. The terminology used here is borrowed from the biomechanics field (see Chapter 3). Each phase of the gait cycle is activated only when certain conditions are met. The most important phase in maintaining stable walking is the stance phase. This portion of the gait cycle is responsible for maintaining posture, and providing most of the input energy for steady-state locomotion.

The stance phase begins after the swing leg is placed on the neutral point, a position where the composite body CG velocity will remain constant [111]. Modifying the touchdown position away from the neutral point and modifying the rate of stance leg sweep allow for changes in velocity. After foot placement, the stance leg is swept backward at a rate that maintains a constant composite CG velocity. The stance phase ends after the leg is unloaded at liftoff. The swing portion of the cycle starts at the liftoff position, retracts and then extends the leg to prepare for the next foot touchdown.

The actual movement of the links can be directed by any of several feedback control methods. These methods range from simple PD servos at each joint to the more complex pole placement and LQR methods.

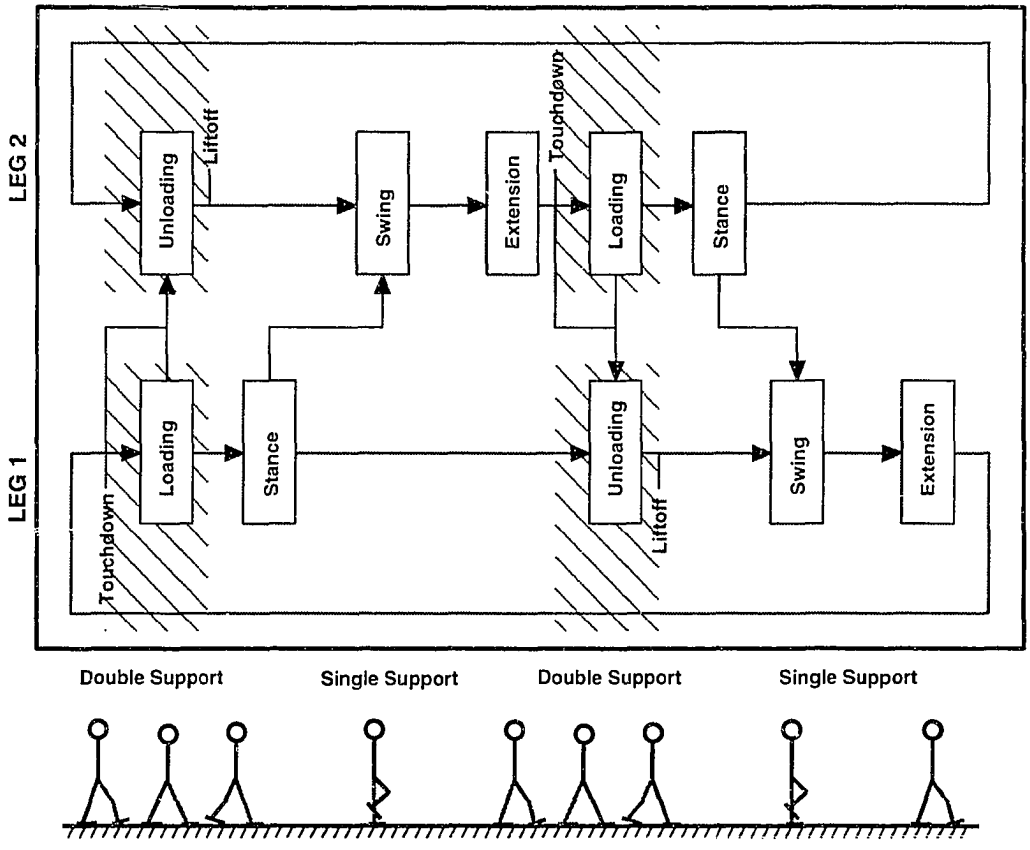

Figure 5.7 Walking state machine

The running state machine, shown in Figure 5.8, differs from the walking state machine in that the double support phase disappears and a flight phase is introduced. As with the walking state machine, the same five subregions are used, but the relative leg positions are shifted in time.

A unified locomotion state machine that can be used for both walking and running can be constructed by considering of the size of the double support or flight regions as a single parameter, with double support at one end and flight at the other. An interactive tool can be built for a graphical environment to vary this parameter and other regions of the walking cycle to give the software user the flexibility to create the desired biped locomotion.

The user supplies the desired velocity, step length, and/or the step frequency which configures the phases of the state machine. The state machine is part of a larger overall feedback control system that can be designed to override desired locomotion parameters to maintain balance.

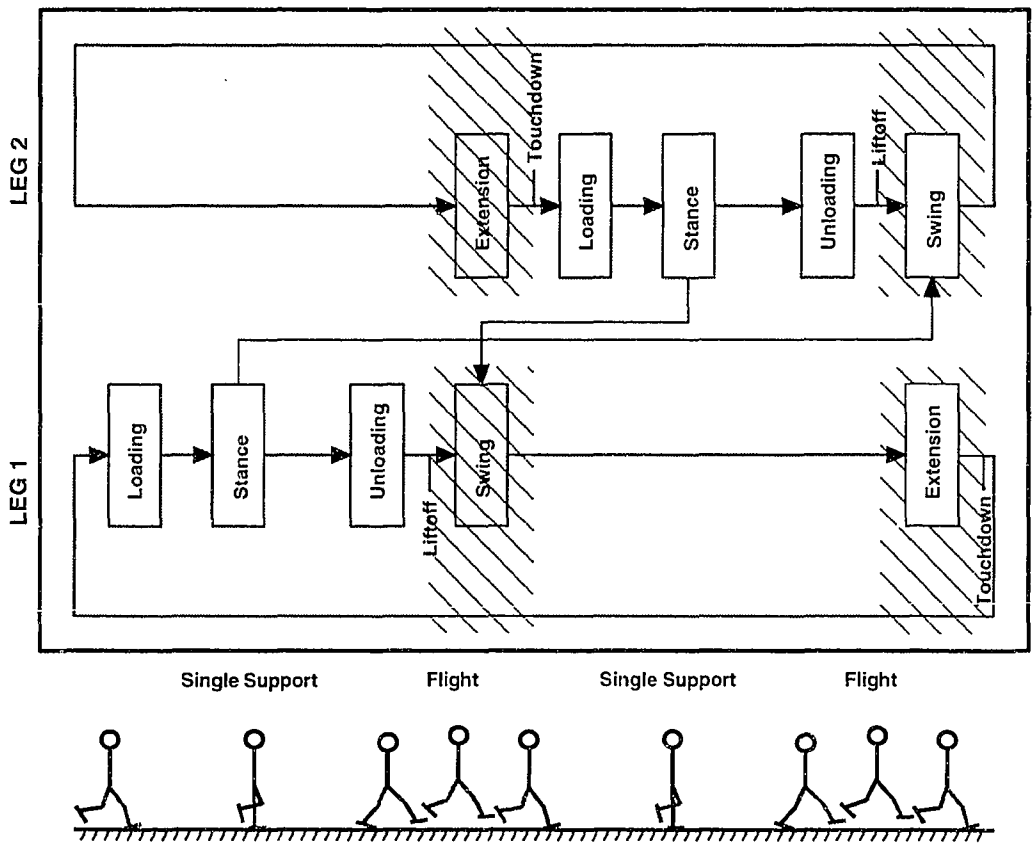

Figure 5.8 Running state machine

5.7.2 Locomotion foot placement

In walking and running, foot placement controls overall linear acceleration of the system for increasing or decreasing speed. As described in Chapter 3, maintaining steady state locomotion either for walking or running depends on the placement of the new stance foot relative to the neutral point [111]. Placing the foot behind the neutral point tends to increase speed, while placing the foot after the neutral point tends to decrease the speed.

Steady-state velocity is determined by the step length and step frequency. In practice, the velocity is specified along with either the step length or frequency. The general steady-state velocity equation is give below.

$$v_{ss} = L_{step} f_{step} \tag{5.20}$$

5.7.3 Cycle Control

Once the foot positions and cycle modes have been selected by the state machine, a lower level control algorithm is needed to cycle the legs through the stance and swing phases. Two types conventional PD controllers will be presented for the low level leg positioning control. The first uses a regulator type approach in which goal points are selected by the state machine. For this method, the path (in joint space) for each leg is defined by the state machine. The second method uses path tracking instead of goal point regulation. This method uses a joint angle function generator to specify the time varying path. Of the two methods, the first is much easier to program into the state machine, but the second offers better position and velocity control.

5.7.4 Handling Terrain Changes

The ability of a system to deal with changing surface environments is an important feature for a complete locomotion control system. Although many different type of surfaces can be expected to be encountered by biped systems, the only two cases (other than a flat surface) that will be developed here are environments involving inclines, and stairs. This surface information is used by the state machine to either modify the body link desired balance position or to pick a different set of feedback gains.

5.8 Planar Monoped Control System Design

Only balancing control will be discussed for the monoped systems. The steady-state LQR design method was used to obtain balancing of all types of monoped systems. Linearized

monoped models with the foot attached to the ground by a revolute joint were used for control system design. The feedback gains developed from the linearized system will then be used to control the nonlinear system in the simulation environment. The only practical mode of monoped locomotion is through the use of a hopping gait cycle, but this type of locomotion was not developed here.

The control system for the 2-link monoped consists of a 2-DOF, linearized, double inverted pendulum (Appendix A) that is attached to the stationary reference frame by a revolute joint. Since the nonlinear model that will be managed by this control system cannot support a moment at the ground contact point, the only controlled input that will be available is the moment between the two links.

With these stipulations in mind, this mechanism can be seen to be a single input multi-output system (SIMO), which is very similar in concept to the standard inverted pendulum-cart problem. One of the main problems here is that of the discontinuous nature of the leg placement. Another is the intersection of the support (foot) with the ground surface.

The control system for the 3-link monoped consists of a 3-DOF, linearized, triple inverted pendulum (Appendix A) that is attached to the stationary reference frame by a revolute joint. As in the 2-link case, no moment at the ground contact point will be allowed. This results in a system with two controlled inputs.

The control system for the 4-link monoped consists of a 3-DOF, linearized, triple inverted pendulum (Appendix A) that is attached to the stationary reference frame through a revolute jointed foot. The foot control is decoupled from the rest of the system. The resulting system has three controlled inputs.

5.9 Sagittal Plane Biped Control System Design

For each sagittal plane biped system presented, two distinct types of controllers will be needed. One controller for balancing, either on one foot or on both feet, and another for walk-

ing. The balancing controllers are designed in the same way as the monoped systems using a revolute joint foot constraining the linearized system to the surface, and the LQR to obtain the feedback gains. This controller then operates a nonlinear, non-revolute joint constrained foot biped system. The balance design procedure outlined in equations (5.1) through (5.6) is used.

The basic walking PD controller design for the 3-link sagittal plane system is given below. Notice that six gains instead of four are given to control the two torques, M_1 and M_2. In addition to cycling the legs through the stance and swing phases, these torques are also used to balance the body segment. The 5-link and 7-link systems include additional PD controllers for the knee and ankle joints.

$$\tau_{body} = Kp_{body}(\theta_1 - \theta_1^*) + Kd_{body}(\dot{\theta}_1 - \dot{\theta}_1^*) \tag{5.21}$$

$$\tau_{stance} = -Kp_{stance}(\theta_2 - \theta_2^*) - Kd_{stance}(\dot{\theta}_2 - \dot{\theta}_2^*) \tag{5.22}$$

$$\tau_{swing} = -Kp_{swing}(\theta_3 - \theta_3^*) - Kd_{swing}(\dot{\theta}_3 - \dot{\theta}_3^*) \tag{5.23}$$

$$M_1 = \tau_{body} + \tau_{stance} \tag{5.24}$$

$$M_2 = \tau_{swing} \tag{5.25}$$

where the * variables are the desired goal positions and velocities selected by the state machine.

Since the overall stability of the gait cycle is the desired goal, the system can be adjusted over several cycles instead of requiring it to be perfectly controlled within each step. This allows for added flexibility when designing a controller. Designing a state machine for walking does not fit into standard SISO control system design techniques. Therefore, an interactive design approach was used within the graphical simulation environment to arrive at the PD feedback gains.

5.10 Frontal Plane Biped Control System Design

The goal of the frontal plane control system is to shift weight from one foot to the other. Since the leg extension and foot movements of the more complex biped models occurs mainly in the sagittal plane, only a 3-link model will be needed in the frontal plane. The LQR method was also used for designing this control system. Unlike the sagittal plane systems, the frontal plane biped does not have a marginally stable equilibrium point to serve as a goal state for stabilization. In this case, an unstable equilibrium point must be chosen. If the body and free leg angular positions are chosen, the resulting stance leg equilibrium position is calculated by (5.26).

$$\theta_2 = \text{acos}\frac{m_1 l_{c1}\cos(\theta_1+\phi) + m_3(l_1\cos(\theta_1) + l_{c3}\cos(\theta_3))}{m_2(l_2 - l_{c2}) + m_1 l_2 + m_3 l_2} \tag{5.26}$$

5.11 Spatial Biped Control System Design

The control systems used for the spatial biped models combine the controllers from the sagittal plane and frontal plane biped models. The basic assumption governing control of nonlinear spatial biped mechanisms, is that the sagittal plane and frontal plane controllers can operate independently on the nonlinear system. This assumption also applies to uncontrolled modes. Uncontrolled modes in one plane will not drastically affect the motion in another plane if the uncontrolled modes are stabilizable and the motions are relatively small.

Although a transverse plane controller was not developed, the same decoupling principle should apply. The addition of this controller to the 3D systems would be used to control turning as well as the body rotation in the transverse plane.

The application of the planar decoupling principle will be applied to the 3-link, 8-DOF model. This model will have the same control system as the sagittal plane 3-link biped system for both balancing and steady-state walking. No frontal plane controller is possible for this

system (since the legs can not move in the frontal plane), but for conditions in which the projected CG position is located between the legs the system is stabilizable.

Although not presented here, the development of controllers for the 3-link, 10-DOF control systems as well as the 5, 7, and 8 link models follow the same decoupling assumptions.

6. RESULTS

Results for monoped and biped balancing, steady-state biped walking, locomotion on inclines and stairs, and transitional sequences are discussed. Simulation results for several types of planar (2D) and spatial (3D) systems are presented. Comparisons are made between data collected from human locomotion and simulated biped mechanisms. Manual control techniques are assessed, and the interactive simulation environment developed for this project is discussed.

Explaining the response of a dynamic system is usually done with plots of state variables, control torques, and reaction forces as functions of time. Unfortunately plots alone fail to give the insight that is found in a visual simulation or animation. So in addition to response plots, results will be supplemented with image sequence and image composite figures.

6.1 Planar Monoped Balancing

Initial model and control system development dealt with monoped balancing. The results obtained from the design and performance analysis of monoped systems helped to direct the design of the biped systems. In fact, monoped balancing can be thought of as a special case of biped balancing when the biped is in the double support mode.

Balancing is the only type of monoped motion that will be discussed in this section. The only realistic form of monoped locomotion is hopping. Although hopping is a valid form of biped locomotion, a state machine for control of continuous monoped hopping locomotion was not developed for this project.

The test cases that were chosen to validate the balancing mode control system responses for all monoped models include: dropping system onto flat surface, dropping onto an inclined surface, and non-zero initial x and y velocities. Within each of these tests, the surface coefficient of friction was also varied from a low to high values (0.1 to 1.0) to test ground reaction response. In addition to the test cases just described, several types of real-time interactive test-

ing sequences were conducted to evaluate the performance with respect to user inputs as well as varying initial conditions and surfaces. As mentioned earlier, interactive simulation is difficult to describe objectively in a static document[1]. Subjective comments dealing with real-time interaction will be discussed later.

6.1.1 Planar 2-link Monoped

The 2-link, 4-DOF, sagittal plane monoped, as described in Section 4.2.1, consists of a body (torso) link and a leg link. Two distinct types of control were investigated for this system: manual control and automatic control.

Manual control

In the initial stages of system design a very simple interactive control system was implemented that consisted of a user sitting at a terminal and using a multi-input dial box for monoped hip torque control and a set of foot pedals for leg extension control. It was discovered that direct torque control by the user was much too demanding for even this simple model. The joint positioning control methods (PD joint control) proved to be much easier and more intuitive to use. But even then, balance could only be maintained for a few seconds.

Automatic control

Automatic balancing control of this monoped system provided much better control than the manual methods. The control system design technique used here to provide balance stabilization was the steady-state form of the linear-quadratic regulator (LQR). Other decoupled joint space control methods like PD and PID controllers were attempted, but were unable to maintain system balance. Figure 6.1(a) shows an image sequence of the LQR controlled monoped system recovering from being dropped onto a surface. Figure 6.1(b) shows the system servoing the leg to achieve a touchdown position from which stable balancing can be achieved. This is the type of non-zero initial condition that would occur during hopping.

---

1. See comments about the interactive version of this document in the Introduction.

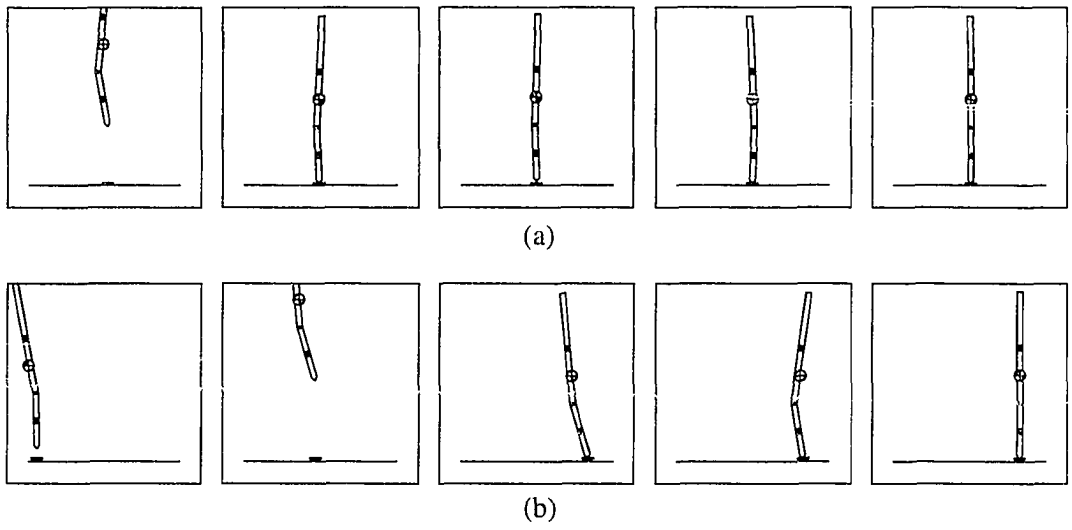

Figure 6.1 Planar 2-link monoped image sequences: (a) zero initial velocity; (b) non-zero initial velocity.

The response for the case of a non-zero initial velocity will be discussed in more detail. The system parameters[2] used in this model are given in Table 6.1, and the initial conditions are given in Table 6.2. Refer back to Figure 4.4 on page 32, for a description of the state variables for this system. It must be noted that the LQR derived gains are only effective for small initial horizontal velocities. An additional algorithm is needed to handle larger initial velocities.

The foot placement algorithm, that was derived in Chapter 5, is required to determine the correct foot touchdown position that will allow balance to be achieved for initial conditions that include large initial horizontal velocities. The system can be seen servoing the leg link in the second frame of Figure 6.1(b) to place the foot to attain an acceptable touchdown position.

Table 6.1 Planar 2-link monoped system parameters

Parameter	link 1	link 2
mass	2.0	1.0
length	2.0	1.0

2. The values selected for the system parameters are somewhat arbitrary, the significant attribute is the relative size.

Table 6.2 Initial conditions for 2-link monoped test case

State Variable	Value	State Variable	Value
x	0.0	θ_1	1.77
$\dot{x}$	2.0	$\dot{\theta}_1$	0.0
y	1.1	θ_2	-1.57
$\dot{y}$	5.0	$\dot{\theta}_2$	0.0

The eight initial conditions listed in Table 6.2 are for the nonlinear system. The control system is based on the linearized form of the double inverted pendulum given in (4.41) and (4.42), and will therefore have four state variables. The LQR control weighting matrices used for the given system parameters are:

$$Q = \begin{bmatrix} 50 & 0 & 0 & 0 \\ 0 & 1 & 0 & 0 \\ 0 & 0 & 50 & 0 \\ 0 & 0 & 0 & 1 \end{bmatrix}$$

$$R = 100$$

Given these parameters, the full state feedback gains are:

$$K = [-294.5143 \ -118.9444 \ -235.6323 \ -118.9479]$$

For these initial conditions and gains, the state response plots are given in Figure 6.2 through Figure 6.4, the control torque in Figure 6.5, and the ground reaction forces in Figure 6.6. Note in the second frame of Figure 6.1(b) that the touchdown position control algorithm positions the leg prior to landing. Also note the spike in the torque figure caused by the impact with the surface. The subsequent balancing control action after touchdown attenuates to zero after approximately 3.5 s.

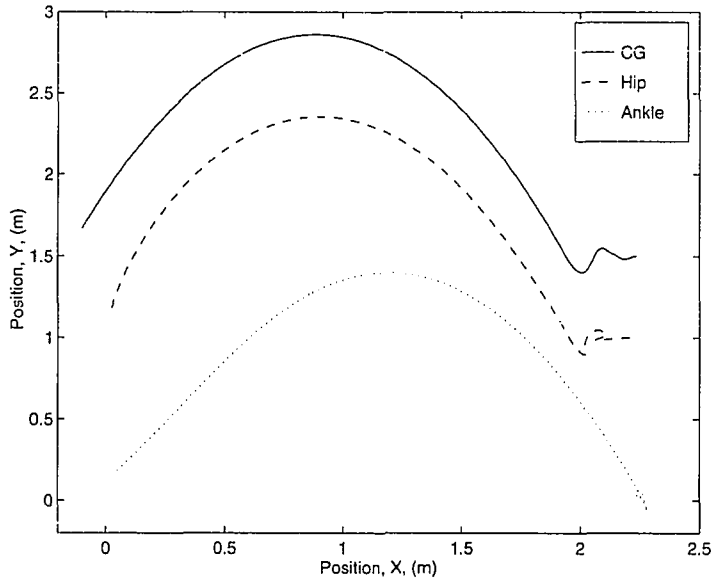

Figure 6.2 Planar 2-link monoped sequence position data

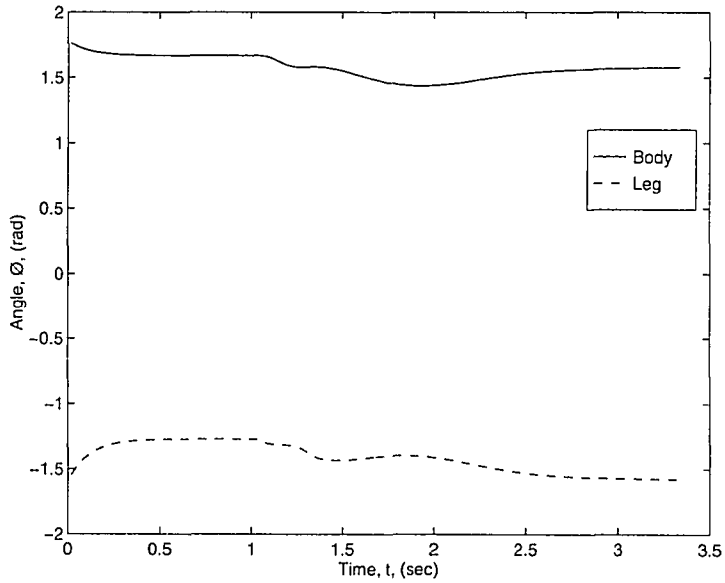

Figure 6.3 Planar 2-link monoped angular positions

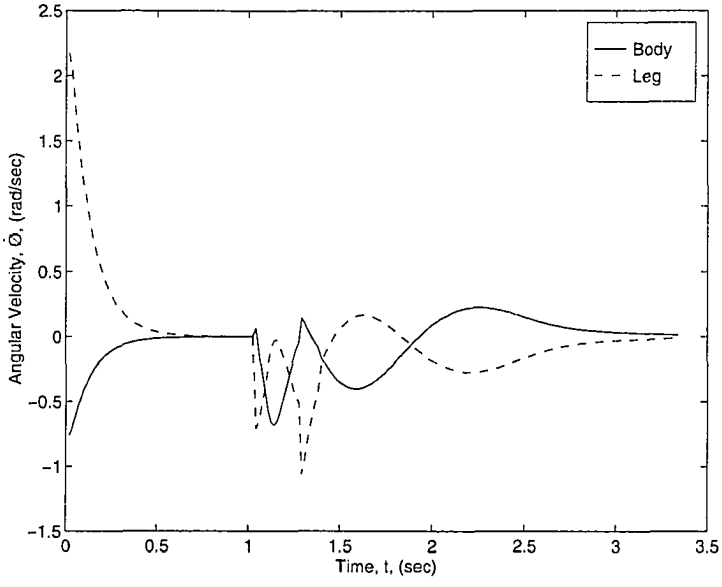

Figure 6.4 Planar 2-link monoped angular velocities

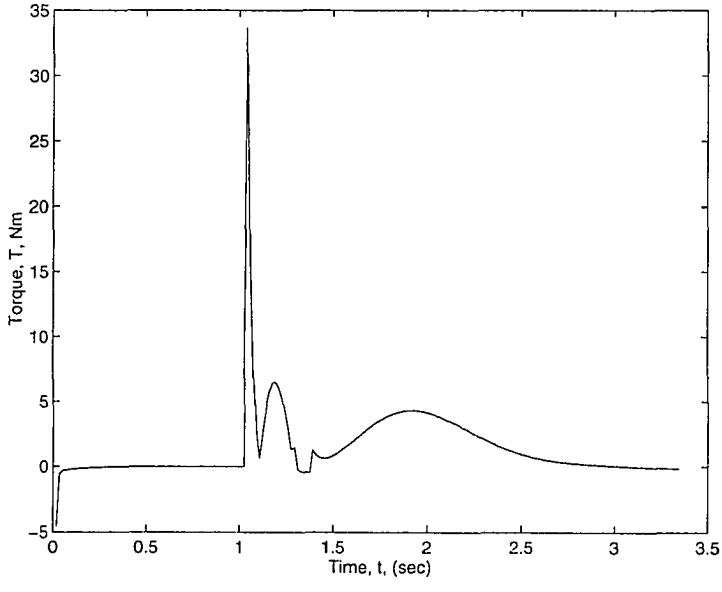

Figure 6.5 Planar 2-link monoped joint torque

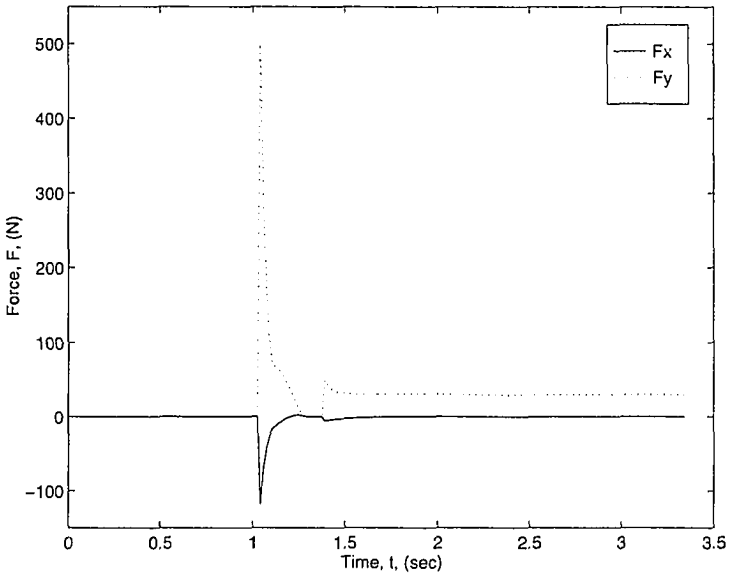

Figure 6.6 Planar 2-link monoped ground reaction forces

6.1.2 Planar 3-link Monoped

The 3-link sagittal plane monoped, as described in Figure 4.6 on page 37, consists of a body (torso) link, upper leg, and lower leg segments[3]. Dropping and jumping onto a flat surface were selected to test the balancing mode response. Note that the knee joint is allowed to bend backwards here. Joint limit constraints where not included here, but can be implemented if necessary.

As in the 2-link case, a more detailed analysis of the non-zero initial condition case will be presented. The variable parameters selected for simulation of this system are listed in Table 6.3, and the initial conditions are given in Table 6.4. The foot placement algorithm of Chapter 5 is used again here to determine an acceptable touchdown position.

3. A version of the 2-link monoped with a foot link was also developed, which would also be considered to be a 3-link system, but will not be discussed here.

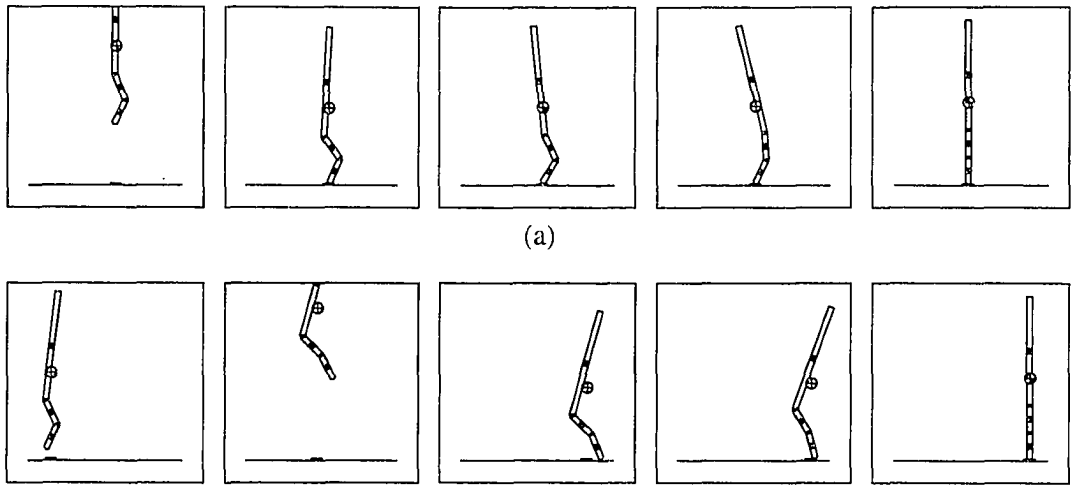

Figure 6.7 **Planar 3-link monoped image sequences: (a) zero initial velocity; (b) non-zero initial velocity.**

Table 6.3 **Planar 3-link monoped system parameters**

Parameter	link 1	link 2	link 3
mass	2.0	0.5	0.5
length	2.0	0.5	0.5

Table 6.4 **Initial conditions for the 3-link monoped test case**

State Variable	Value	State Variable	Value
x	0.0	θ_2	-1.97
$\dot{x}$	2.0	$\dot{\theta}_2$	0.0
y	1.0	θ_3	-2.02
$\dot{y}$	5.0	$\dot{\theta}_3$	0.0
θ_1	1.47		
$\dot{\theta}_1$	0.0		

These ten initial conditions are for the nonlinear, 3-link monoped system. The control system is based on the linearized form of the triple inverted pendulum given in Appendix A, and will therefore have six state variables. The LQR control weighting matrices are:

$$Q = \begin{bmatrix} 5 & 0 & 0 & 0 & 0 & 0 \\ 0 & 50 & 0 & 0 & 0 & 0 \\ 0 & 0 & 5 & 0 & 0 & 0 \\ 0 & 0 & 0 & 50 & 0 & 0 \\ 0 & 0 & 0 & 0 & 50 & 0 \\ 0 & 0 & 0 & 0 & 0 & 50 \end{bmatrix}$$

$$R = \begin{bmatrix} 1 & 0 \\ 0 & 1 \end{bmatrix}$$

Given these parameters, the full state feedback gain matrix is:

$$K = \begin{bmatrix} -168.5296 & -65.8193 & -123.6359 & -52.8219 & -240.3729 & -119.7646 \\ -181.5390 & -70.3867 & -159.4774 & -69.5638 & -269.1284 & -135.0904 \end{bmatrix}$$

For these initial conditions the state response plot are given in Figure 6.8 through Figure 6.10, the control torques in Figure 6.11, and the ground reaction forces in Figure 6.12.

With 3-link systems, it is possible for the knee joint to bend backwards. If this type of motion is considered undesirable (as it would be when simulating human locomotion) a limit constraint must be applied to the joint. As might be expected, performance is better if joint limit constraints are not activated.

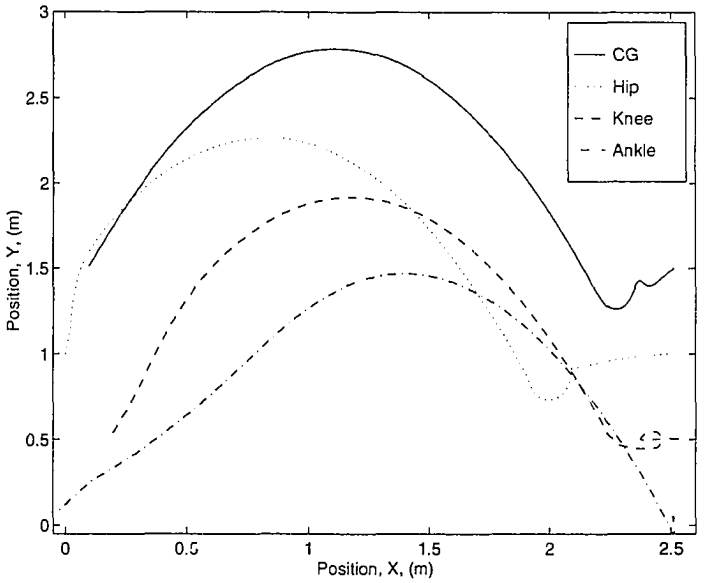

Figure 6.8 Planar 3-link monoped sequence position data

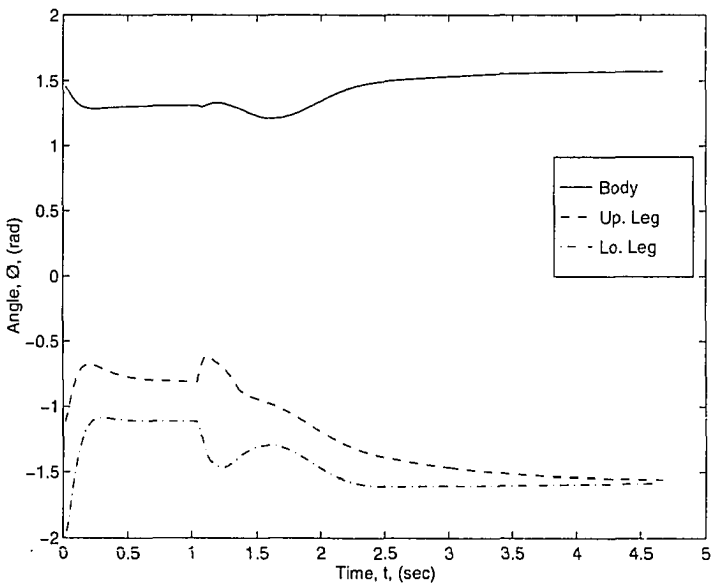

Figure 6.9 Planar 3-link monoped angular positions

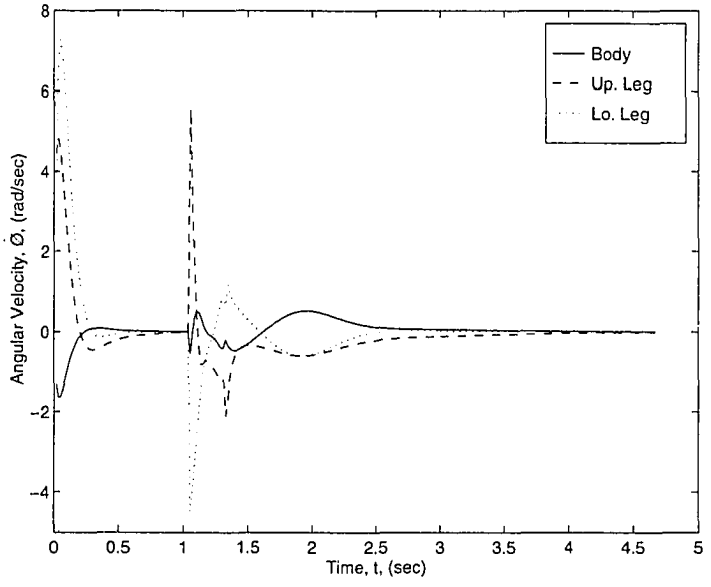

Figure 6.10 Planar 3-link monoped angular velocities

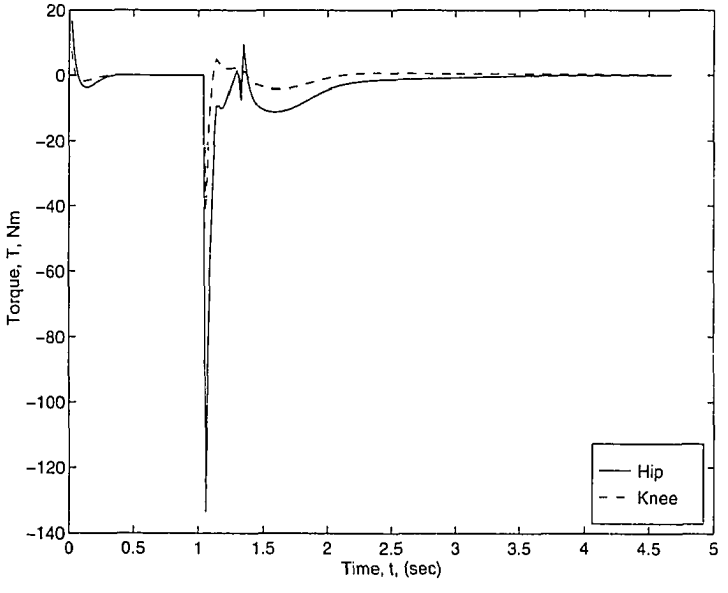

Figure 6.11 Planar 3-link monoped joint torque

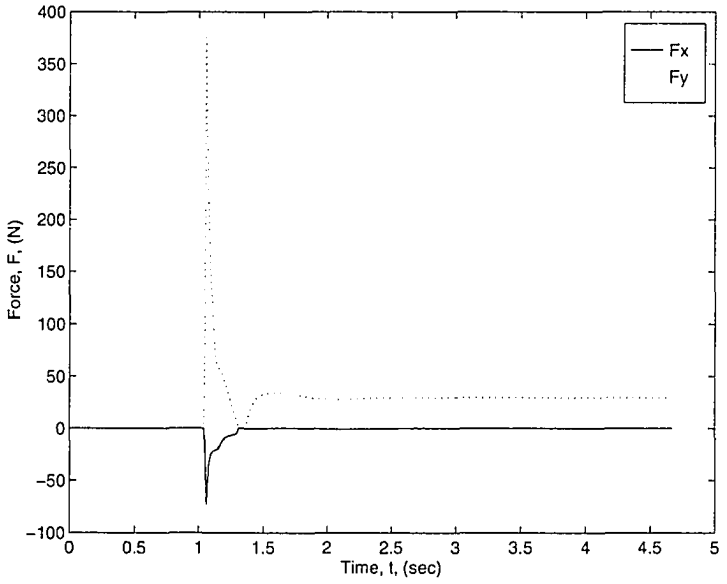

Figure 6.12 Planar 3-link monoped ground reaction forces

6.1.3 Planar 4-link Monoped

The 4-link sagittal plane moped model, as described in Figure 4.8 on page 39, consists of a body segment, upper and lower leg segments, and a two point contact foot. The addition of a another controlled torque at the distal end of the lower leg helps increase balance stability as well as allow for a larger range of flight to touchdown conditions.

As in the previous two monoped balancing cases, the more complex problem of non-zero initial conditions will be analyzed in more detail. The variable parameters selected for simulation of this system are listed in Table 6.5, and the initial conditions are given in Table 6.6. The same foot placement algorithm used in the other monoped balancing examples is used again here.

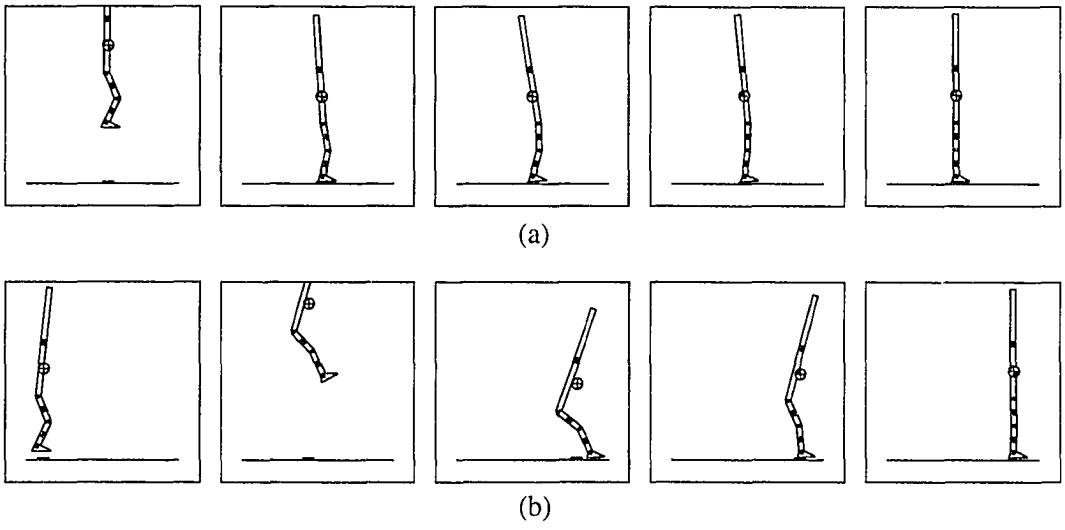

Figure 6.13 Planar 4-link monoped image sequences: (a) zero initial velocity; (b) non-zero initial velocity.

Table 6.5 Planar 4-link monoped system parameters

Parameter	link 1	link 2	link 3	link 4 (foot)
mass	2.0	0.5	0.5	0.2
length	2.0	0.5	0.5	0.3

Table 6.6 Initial conditions for the 4-link monoped test case

State Variable	Value	State Variable	Value
x	0.0	θ_2	-1.97
$\dot{x}$	2.0	$\dot{\theta}_2$	0.0
y	1.0	θ_3	-2.02
$\dot{y}$	5.0	$\dot{\theta}_3$	0.0
θ_1	1.47	θ_4	0.0
$\dot{\theta}_1$	0.0	$\dot{\theta}_4$	0.0

These 12 initial conditions are for the nonlinear, 4-link monoped system. The control system is based on the linearized form of the triple inverted pendulum of Appendix A. The addition of the ankle torque results in a system with three controlled torques and six state variables. The LQR control weighting matrices are:

$$Q = \begin{bmatrix} 5 & 0 & 0 & 0 & 0 & 0 \\ 0 & 50 & 0 & 0 & 0 & 0 \\ 0 & 0 & 5 & 0 & 0 & 0 \\ 0 & 0 & 0 & 50 & 0 & 0 \\ 0 & 0 & 0 & 0 & 50 & 0 \\ 0 & 0 & 0 & 0 & 0 & 50 \end{bmatrix}$$

$$R = \begin{bmatrix} 50 & 0 & 0 \\ 0 & 1 & 0 \\ 0 & 0 & 1 \end{bmatrix}$$

Given these parameters, the full state feedback gains are:

$$K = \begin{bmatrix} 17.8038 & 7.1969 & 15.2621 & 6.6787 & 30.9067 & 15.2596 \\ -56.9720 & -20.9904 & -26.6208 & -10.8044 & -53.9009 & -29.3360 \\ -70.1822 & -25.7101 & -62.4963 & -27.6289 & -83.9374 & -45.5954 \end{bmatrix} \tag{6.1}$$

For the given initial conditions and gains the resulting state response plots are given in Figure 6.14 through Figure 6.16, the control torques in Figure 6.17, and the ground reaction forces in Figure 6.18.

The results of this system along with the other two planar monoped control systems will be applied to the double support, biped balancing control discussed in the next section.

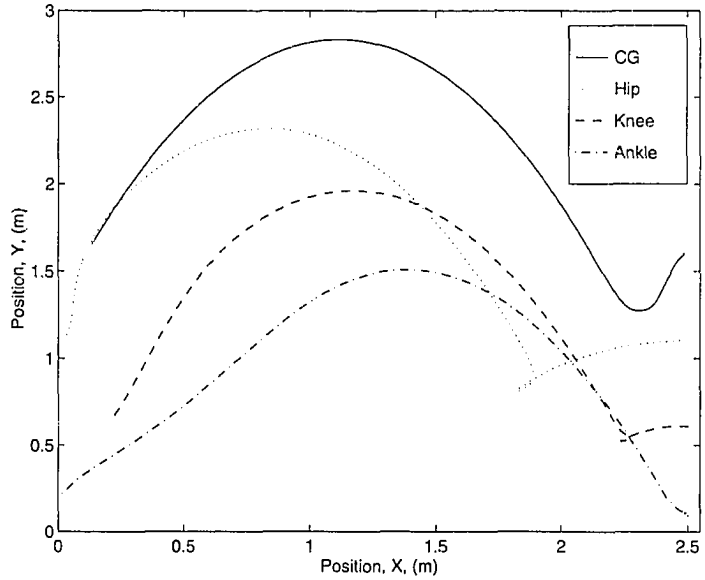

Figure 6.14 Planar 4-iink monoped sequence position data

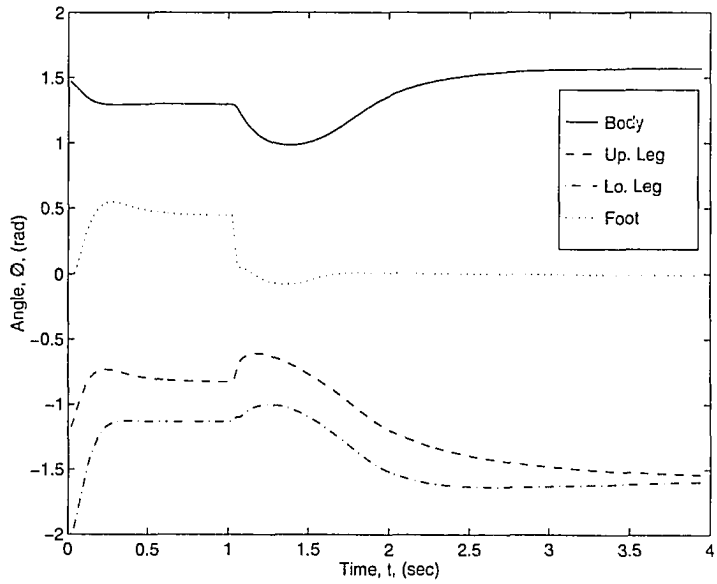

Figure 6.15 Planar 4-link monoped angular positions

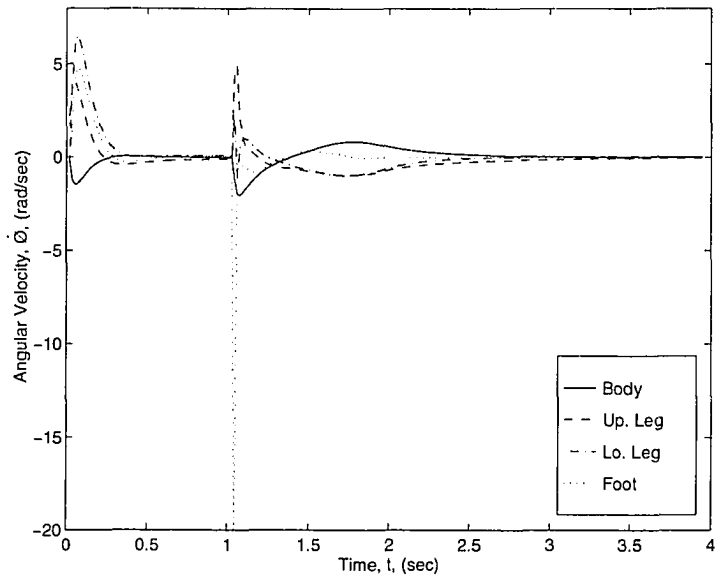

Figure 6.16 Planar 4-link monoped angular velocities

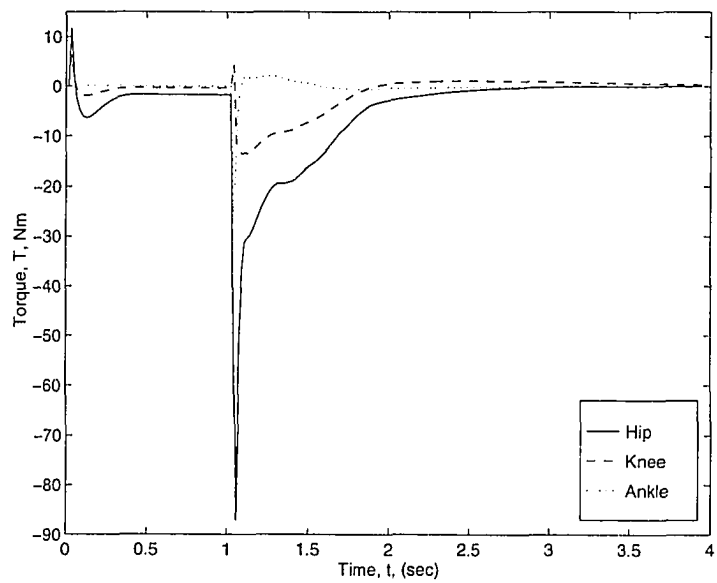

Figure 6.17 Planar 4-link monoped joint torque

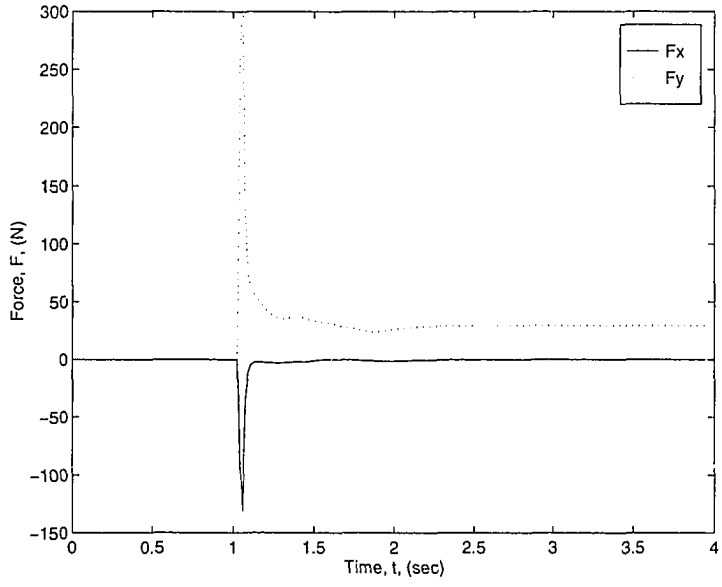

Figure 6.18 Planar 4-link monoped ground reaction forces

6.2 Planar Biped Balancing

Results of control simulation for the planar biped models discussed in Section 4.2.2 on page 40, are presented next. Several modes of biped balancing will be discussed: both feet touching, identical leg angles, different leg angles, and only one foot touching.

Manual balancing control was also tried for these systems. Although the addition of another degree of freedom with the free leg was an advantage for the automatic control system over the monoped case, it did not seem to improve the user's ability to maintain balance manually. As in the monoped balancing case, manual biped balancing suffers from the same human reaction time and interpretation problems.

6.2.1 3-link Sagittal Plane Biped

The test case for the 3-link sagittal plane biped, described in Figure 4.10 on page 41, consists of dropping the system onto a flat surface and establishing balance. The system parameters for this test case are shown in Table 6.7, and the initial conditions in Table 6.8.

Table 6.7 3-link sagittal plane biped system parameters

Parameter	link 1	link 2	link 3
mass	2.0	1.0	1.0
length	2.0	1.2	1.0

Table 6.8 Initial conditions for 3-link sagittal plane test case

State Variable	Value	State Variable	Value
x	0.0	θ_2	-1.3
$\dot{x}$	0.0	$\dot{\theta}_2$	0.0
y	1.65	θ_3	-1.3
$\dot{y}$	0.0	$\dot{\theta}_3$	0.0
θ_1	1.3		
$\dot{\theta}_1$	0.0		

Both feet touching

The control methods developed for monopeds are directly applicable to biped systems when the legs are together and both feet are touching the ground. The planar biped responses for balancing on both feet are nearly identical to the monoped image sequence displayed in Figure 6.1.

Another situation exists when both legs are in contact with the floor, but with a non-zero separation angle. This case would appear to be different than the monoped system, but utilizing a virtual leg model of the system [111], the monoped steady state LQR control and touchdown prediction methods can still be used.

One foot touching

Although conceptually similar to the monoped control system, the biped system with one foot balancing support has additional control inputs that allow the system to maintain balance in more situations than a monoped control system. Because of this, a completely different

model was used for control system design. Several options exist for what to do with the free leg: it can be swung forward, backward, or maintain a stationary position. The degree of activity of the free leg is determined by the weights (Q and R) in the LQR control system design. The LQR weighting matrices and the full state feedback gains used for this system are given below.

$$Q = \begin{bmatrix} 50 & 0 & 0 & 0 & 0 & 0 \\ 0 & 8 & 0 & 0 & 0 & 0 \\ 0 & 0 & 50 & 0 & 0 & 0 \\ 0 & 0 & 0 & 5 & 0 & 0 \\ 0 & 0 & 0 & 0 & 120 & 0 \\ 0 & 0 & 0 & 0 & 0 & 5 \end{bmatrix}$$

$$R = \begin{bmatrix} 1 & 0 \\ 0 & 0.5 \end{bmatrix}$$

$$K = \begin{bmatrix} 142.2384 & 74.2949 & 262.3081 & 93.6629 & -26.2542 & -7.3949 \\ -42.8502 & -17.7686 & -33.3468 & -15.9976 & 15.1722 & 3.7510 \end{bmatrix}$$

Figure 6.19 shows an image sequence of the 3-link sagittal plane biped system balancing on one foot. Figure 6.20 and Figure 6.21 show the 3-link sagittal plane biped joint positions and torques, respectively.

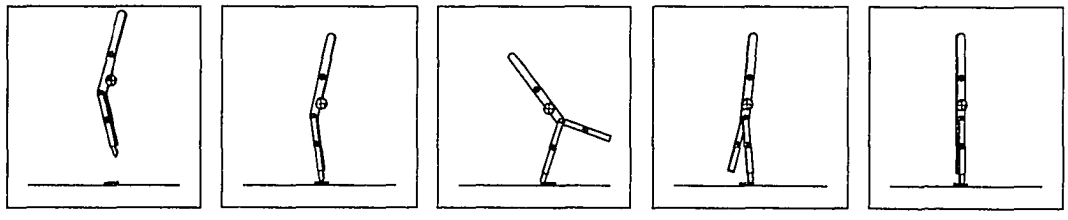

Figure 6.19 3-link sagittal plane biped balancing on one foot

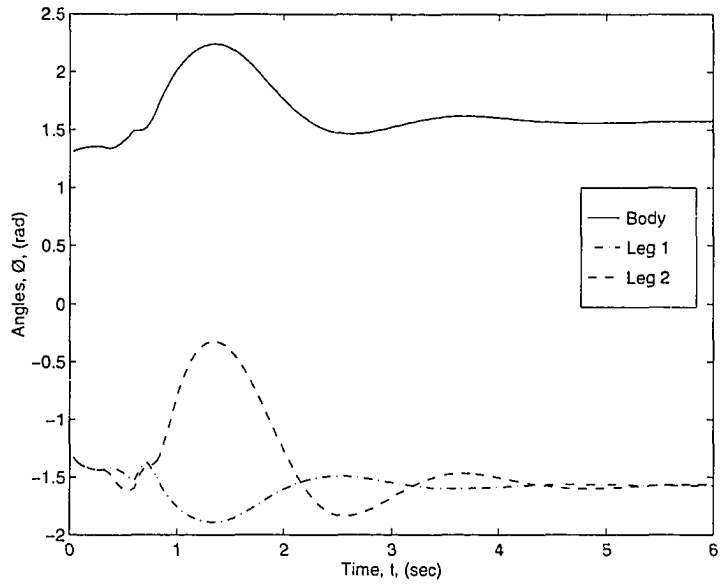

Figure 6.20 3-link sagittal plane biped balancing joint positions

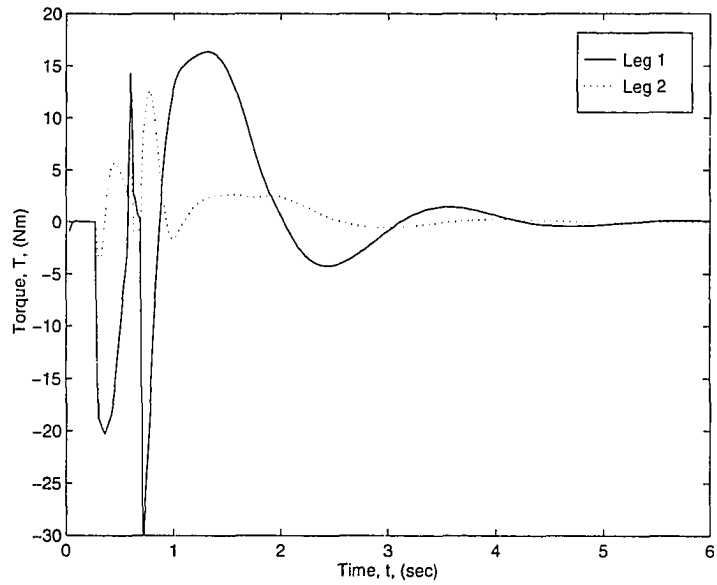

Figure 6.21 3-link sagittal plane biped balancing joint torques

6.2.2 5-link Sagittal Plane Biped

Like the 3-link case, the 5-link sagittal plane biped (Figure 4.12 on page 44) test case consists of dropping the system onto a flat surface and establishing balance. The system parameters for the 5-link sagittal plane biped test case are shown in Table 6.9, and the initial conditions in Table 6.9.

Table 6.9 Planar 5-link biped system parameters

Parameter	link 1	link 2	link 3	link 4	link 5
mass	2.0	0.5	0.5	0.5	0.5
length	2.0	0.5	0.5	0.5	0.5

Table 6.10 Initial conditions for the 5-link sagittal plane biped test case

State Variable	Value	State Variable	Value
x	0.0	θ_3	-1.5
$\dot{x}$	0.0	$\dot{\theta}_3$	0.0
y	1.5	θ_4	-1.5
$\dot{y}$	0.0	$\dot{\theta}_4$	0.0
θ_1	1.45	θ_5	-1.5
$\dot{\theta}_1$	0.0	$\dot{\theta}_5$	0.0
θ_2	-1.5		
$\dot{\theta}_2$	0.0		

Both feet touching

As with the sagittal plane 3-link biped, the 5-link sagittal plane biped response for balancing on both feet is nearly identical to the corresponding monoped image sequence (the 3-link monoped in this case) which is displayed in Figure 6.7.

One foot touching

Figure 6.22 shows an image sequence of the 5-link sagittal plane biped system balancing on one foot. Figure 6.23 and Figure 6.24 show the 5-link sagittal plane biped joint positions and torques, respectively. The LQR weighting matrices and the full state feedback gains used for this system are given below.

$$Q = \begin{bmatrix} 50 & 0 & 0 & 0 & 0 & 0 & 0 & 0 & 0 & 0 \\ 0 & 10 & 0 & 0 & 0 & 0 & 0 & 0 & 0 & 0 \\ 0 & 0 & 50 & 0 & 0 & 0 & 0 & 0 & 0 & 0 \\ 0 & 0 & 0 & 5 & 0 & 0 & 0 & 0 & 0 & 0 \\ 0 & 0 & 0 & 0 & 50 & 0 & 0 & 0 & 0 & 0 \\ 0 & 0 & 0 & 0 & 0 & 5 & 0 & 0 & 0 & 0 \\ 0 & 0 & 0 & 0 & 0 & 0 & 100 & 0 & 0 & 0 \\ 0 & 0 & 0 & 0 & 0 & 0 & 0 & 10 & 0 & 0 \\ 0 & 0 & 0 & 0 & 0 & 0 & 0 & 0 & 50 & 0 \\ 0 & 0 & 0 & 0 & 0 & 0 & 0 & 0 & 0 & 5 \end{bmatrix}$$

$$R = \begin{bmatrix} 1 & 0 & 0 & 0 \\ 0 & 1 & 0 & 0 \\ 0 & 0 & 1 & 0 \\ 0 & 0 & 0 & 1 \end{bmatrix}$$

$$K = \begin{bmatrix} 127.97 & 66.68 & 116.19 & 41.62 & 121.21 & 42.84 & -16.87 & -4.96 & -5.09 & -1.29 \\ 94.28 & 48.83 & 65.48 & 28.54 & 110.13 & 34.14 & -13.52 & -3.92 & -4.20 & -1.06 \\ -57.80 & -26.08 & -33.06 & -13.58 & -32.96 & -13.84 & 12.59 & 4.10 & 3.19 & 1.03 \\ -15.55 & -7.31 & -10.16 & -4.08 & -10.82 & -4.25 & -1.29 & -0.46 & 6.17 & 2.19 \end{bmatrix}$$

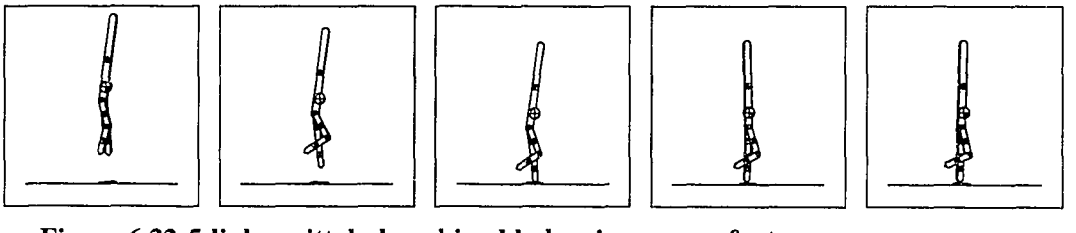

Figure 6.22 5-link sagittal plane biped balancing on one foot

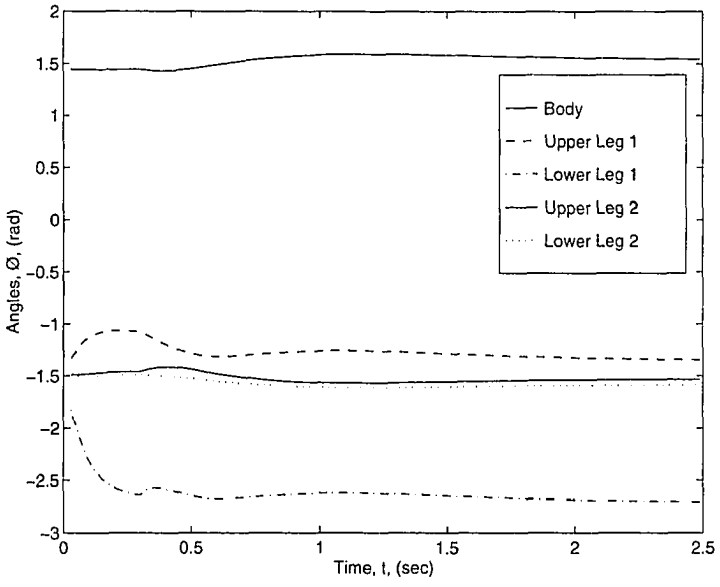

Figure 6.23 5-link sagittal plane balancing joint positions

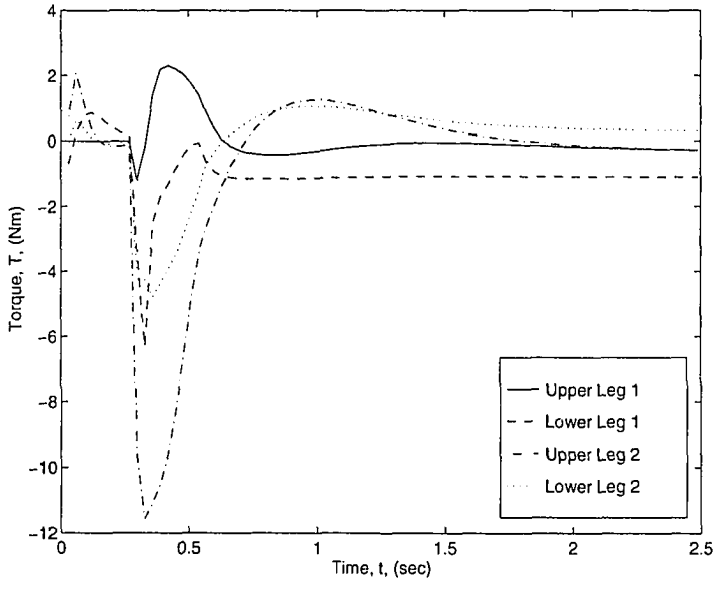

Figure 6.24 5-link sagittal plane balancing joint torques

6.2.3 7-link Sagittal Plane Biped

As in the other two biped balancing cases, the 7-link sagittal plane biped (Figure 4.14 on page 47) balancing test cases consisted of dropping the system onto a flat surface and establishing balance. Control modes for balancing one foot and on both feet were evaluated. The system parameters for the 7-link sagittal plane biped test case are shown in Table 6.11 and the initial conditions in Table 6.12.

Table 6.11 Planar 7-link biped system parameters

Parameter	link 1	link 2	link 3	link4 (foot)	link 5	link 6	link 7 (foot)
mass	2.0	0.5	0.5	0.2	0.5	0.5	0.2
length	2.0	0.5	0.5	0.3	0.5	0.5	0.3

Table 6.12 Initial conditions for the 7-link sagittal plane test case

State Variable	Value	State Variable	Value
x	0.0	θ_4	-1.37
$\dot{x}$	1.0	$\dot{\theta}_4$	0.0
y	1.5	θ_5	-1.77
$\dot{y}$	2.0	$\dot{\theta}_5$	0.0
θ_1	1.47	θ_6	-0.2
$\dot{\theta}_1$	0.0	$\dot{\theta}_6$	0.0
θ_2	-1.37	θ_7	-0.2
$\dot{\theta}_2$	0.0	$\dot{\theta}_7$	0.0
θ_3	-1.77		
$\dot{\theta}_3$	0.0		

Both feet touching

The 7-link sagittal plane biped response for balancing on both feet is nearly identical to the 4-link monoped image sequence of Figure 6.13.

One foot touching

Instead of just dropping the 7-link system onto the surface as in the previous two balancing cases, the initial conditions for this case include positive X and Y velocities to simulate jumping motion. Figure 6.25 shows an image sequence of the 7-link sagittal plane biped system achieving a balanced state on one foot. Figure 6.26 and Figure 6.27 show the 7-link sagittal plane biped joint positions and torques, respectively.

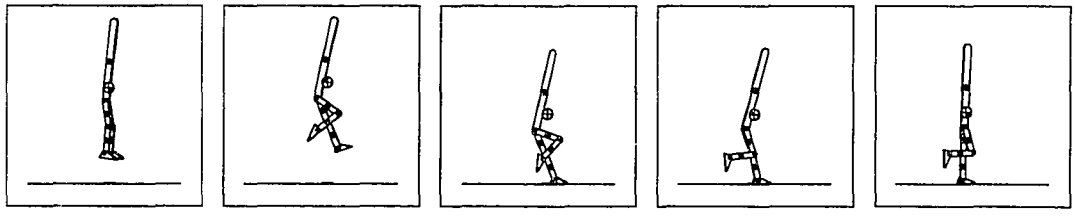

Figure 6.25 7-link sagittal plane biped balancing on one foot

The addition of an articulated foot link allows for better control of situations like this where the additional torque applied to the ankle can be used to help stabilize landing, as well as providing faster response times. The LQR weighting matrices and the full state feedback gains used for this system are given below.

$$Q = \begin{bmatrix} 50 & 0 & 0 & 0 & 0 & 0 & 0 & 0 & 0 & 0 \\ 0 & 10 & 0 & 0 & 0 & 0 & 0 & 0 & 0 & 0 \\ 0 & 0 & 50 & 0 & 0 & 0 & 0 & 0 & 0 & 0 \\ 0 & 0 & 0 & 5 & 0 & 0 & 0 & 0 & 0 & 0 \\ 0 & 0 & 0 & 0 & 50 & 0 & 0 & 0 & 0 & 0 \\ 0 & 0 & 0 & 0 & 0 & 5 & 0 & 0 & 0 & 0 \\ 0 & 0 & 0 & 0 & 0 & 0 & 100 & 0 & 0 & 0 \\ 0 & 0 & 0 & 0 & 0 & 0 & 0 & 10 & 0 & 0 \\ 0 & 0 & 0 & 0 & 0 & 0 & 0 & 0 & 50 & 0 \\ 0 & 0 & 0 & 0 & 0 & 0 & 0 & 0 & 0 & 5 \end{bmatrix}$$

$$R = \begin{bmatrix} 20 & 0 & 0 & 0 & 0 \\ 0 & 1 & 0 & 0 & 0 \\ 0 & 0 & 1 & 0 & 0 \\ 0 & 0 & 0 & 1 & 0 \\ 0 & 0 & 0 & 0 & 1 \end{bmatrix}$$

$$K = \begin{bmatrix} 50.85 & 29.25 & 63.34 & 21.17 & 61.14 & 21.15 & -7.62 & -2.93 & -2.20 & -0.79 \\ 19.59 & 12.55 & 14.20 & 8.69 & 51.68 & 13.06 & -4.56 & -1.95 & -1.40 & -0.58 \\ 23.89 & 11.67 & 16.57 & 6.44 & 19.38 & 6.92 & -2.87 & -0.65 & -0.89 & -0.16 \\ -39.55 & -17.23 & -20.59 & -8.76 & -18.82 & -8.72 & 10.48 & 3.62 & 2.51 & 0.91 \\ -9.27 & -4.27 & -5.87 & -2.41 & -5.95 & -2.48 & -2.04 & -0.62 & 5.93 & 2.15 \end{bmatrix}$$

This same gain matrix can be used for any non-touching position of the free leg, not just the position chosen for this test case. In addition, these gains were chosen to allow smooth transition to the double support and walking controllers. The foot on the free leg is controlled by an independent joint controller and has only minimal effect on the operation of overall system balancing.

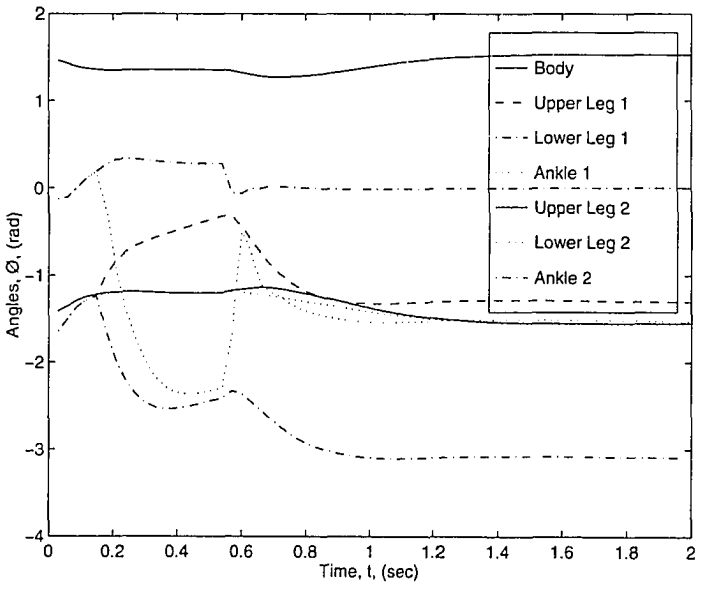

Figure 6.26 7-link sagittal plane balancing joint positions

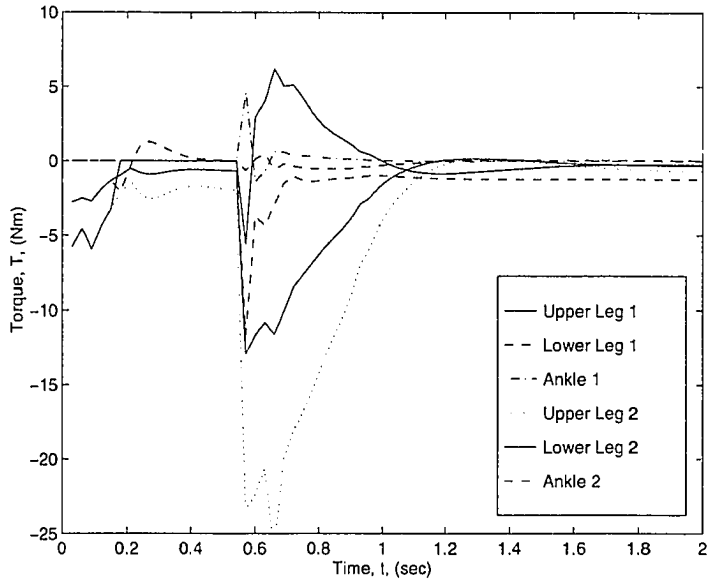

Figure 6.27 7-link sagittal plane balancing joint torques

6.2.4 Frontal Plane Biped

The only frontal plane model that will be analyzed here is the 3-link system shown in Figure 4.16 on page 50. The test case parameters and initial conditions for this system are shown in Table 6.13 and Table 6.14 respectively. For this test case, the frontal plane biped model is initially in an unstable one leg stance, it then establishes steady-state balancing, as shown in the image sequence of Figure 6.28. The image on the far left shows the frontal plane model slightly off balance with the projected CG located to the left of the foot in contact with the surface (i.e. the stance leg). The free leg (swing leg) extension is retracted as would be the case in the swing portion of a walking cycle. The equilibrium position of the far right image has the projected CG located directly over the stance foot. This position has two user defined final joint angles and one selected by the control system.

In contrast to the nonlinear system simulations of all the previous planar monoped and biped simulations, this 3-link frontal plane model was simulated using a linearized system with the stance leg constrained to the surface, instead of using the usual spring-damper foot pad. This simplification was due mainly to development time limitations, and not because of

any additional complexity of the system. Nonlinear simulation results should prove to be very similar to the nonlinear results of the sagittal plane 3-link system described earlier in this chapter.

The state variable plots for this test case are given in Figure 6.29 and Figure 6.30, and a plot of the control torques is given in Figure 6.31. States variables shown in these plots are relative to the linearized position. To match the variable definitions given for this model in Chapter 4, the linearization position will have to be incorporated into the variable definitions. To obtain the actual torque values, the static torque required to hold the desired equilibrium position will also need to be added to the given values.

A few marginally stable equilibrium positions exist for this biped system arrangement that require no joint torque to maintain a static balance, unfortunately, use of these positions is not a practical option for this system. All other equilibrium positions, like the one shown in the last frame of Figure 6.28, are unstable. The equilibrium position chosen here sets the body link position to 0.2 radians and the free leg to $-\pi/2$ radians, the stance leg position is calculated by (5.26).

The LQR weighting matrices and the full state feedback gains used for this system are given below. Note that the large value in the state weighting matrix, Q, was needed to reduce the body segment displacement from the vertical position. This particular element has a large effect on the body segment angular position. For stability purposes, it is desirable for this state to stay relatively close to its vertical linearized position.

$$Q = \begin{bmatrix} 50 & 0 & 0 & 0 & 0 & 0 \\ 0 & 8 & 0 & 0 & 0 & 0 \\ 0 & 0 & 2000 & 0 & 0 & 0 \\ 0 & 0 & 0 & 5 & 0 & 0 \\ 0 & 0 & 0 & 0 & 50 & 0 \\ 0 & 0 & 0 & 0 & 0 & 5 \end{bmatrix}$$

$$R = \begin{bmatrix} 1 & 0 \\ 0 & 0.5 \end{bmatrix}$$

$$K = \begin{bmatrix} 766.7260 & 275.2430 & 311.8407 & 137.4396 & -26.0615 & -7.1074 \\ -551.1454 & -200.6128 & -281.3189 & -106.8580 & 27.2173 & 7.6942 \end{bmatrix}$$

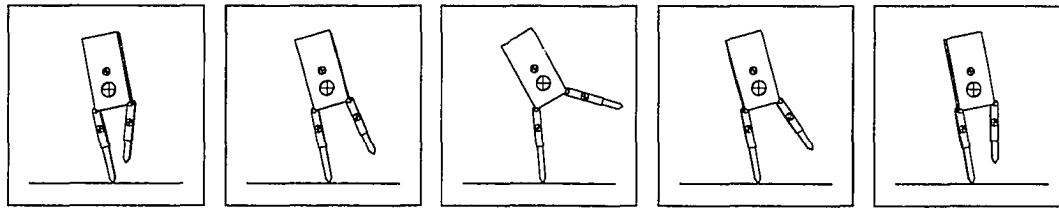

Figure 6.28 3-link frontal plane biped image sequence

Table 6.13 3-link frontal plane biped system parameters

Parameter	link 1	link 2	link 3
mass	2.0	0.5	0.5
length	2.0	1.0	0.5

Table 6.14 Initial conditions for 3-link frontal plane biped test case

State Variable	Value
θ_1	0.05
$\dot{\theta}_1$	0.5
θ_2	0.0
$\dot{\theta}_2$	-1.0
θ_3	-0.1
$\dot{\theta}_3$	0.0

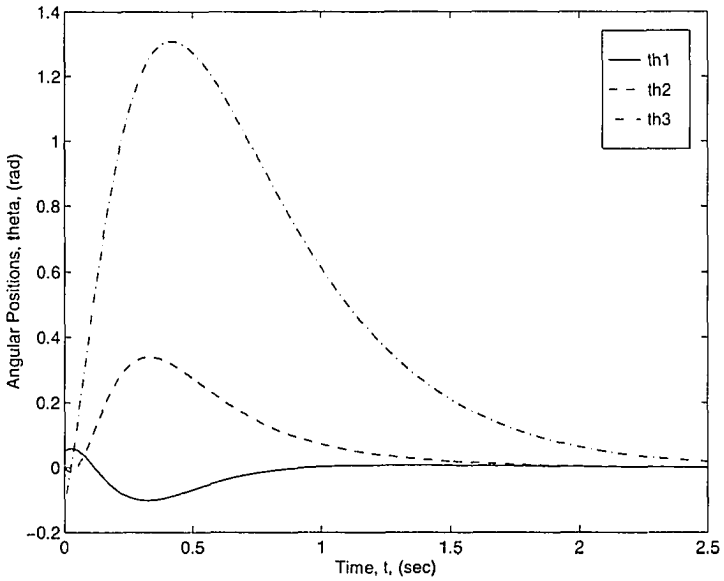

Figure 6.29 Frontal plane 3-link balancing sequence angular positions

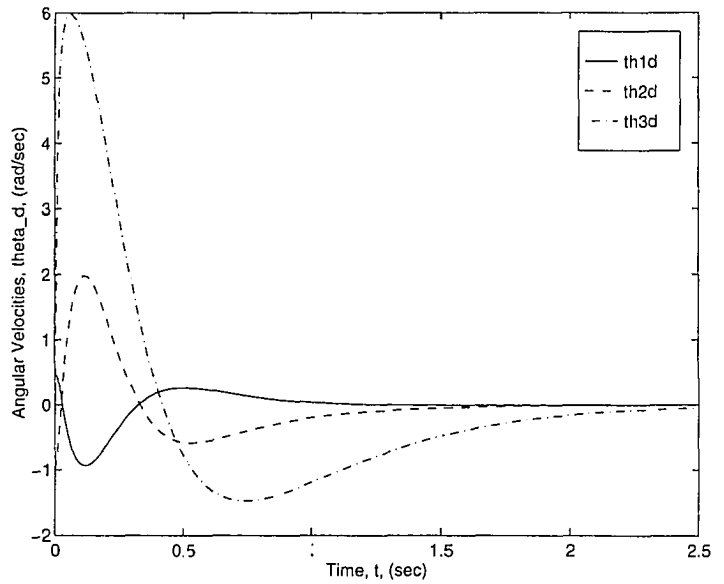

Figure 6.30 Frontal plane 3-link balancing sequence angular velocities

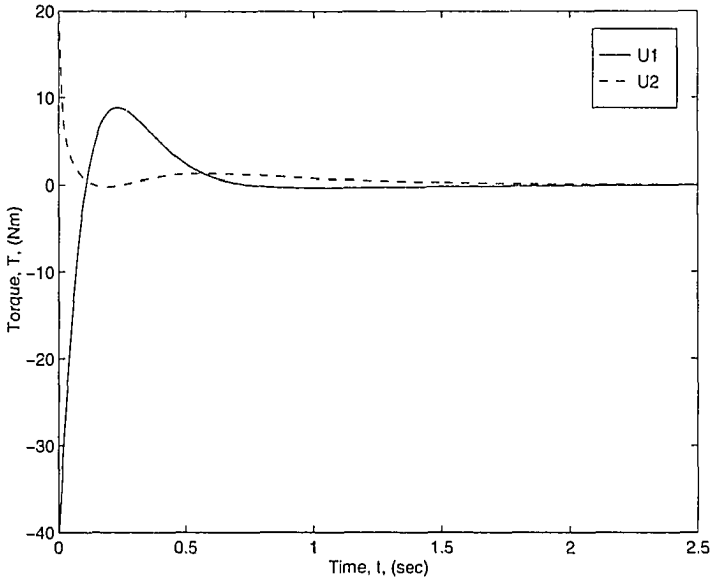

Figure 6.31 Frontal plane 3-link balancing sequence joint torques

6.2.5 Effects of Friction Forces on Balancing

Since the balancing control systems for all planar models presented here are based on linearized models that use a revolute joint to constrain the system to the surface, any modification to the ground contact interface that acts substantially different than a revolute joint can produce unwanted effects. The spring-damper foot constraint model used here acts like a constrained revolute joint in most situations after the transitional effects of surface impact have dissipated. This similarity is one of the main assumptions on which the modeling approach used here is based. But in situations when the lateral reaction forces become larger than the surface coefficient of friction can support, the foot will begin to slide and the revolute joint assumption no longer holds.

Lowering the coefficient of friction (COF, μ) beyond a certain point caused all systems to destabilize. The value of the COF at which destabilization occurs depends on the initial conditions and the state of the system, specifically, the location of the projected center of gravity (PCG) position relative to the foot ground contact point. For example, when any of the systems were dropped so that the contact offset position (the distance between the PCG and the

foot contact point) was small, all systems could balance even with a very low (0.1) COF. At the other extreme, recovering balance from a conditions where the contact offset position was large, required COF which exceeded 1.0.

6.3 Planar Biped Walking

The control systems for both manual and automatic biped walking are much different from balancing mode control. The difference here is that the goal is not to balance the system on one point, but to initiate and maintain a steady state gait cycle. All three of the planar biped systems that will be discussed here use the same basic type of state machine, with slight modifications for additional degrees of freedom. In addition to steady-state walking, transitional phases between balancing and walking will be discussed.

6.3.1 3-Link Sagittal Plane Biped

As with the balancing monoped case, manual and automatic control methods were attempted. Both have the ability to establish a steady state gait cycle and provide similar looking motion, but with a different amount of user interaction. In addition to automatic steady-state walking, transition to walking from balancing was also successfully implemented.

Manual control

Interactive manual walking control is much more attainable than manual balancing due to the users ability to perceive additional visual feedback cues. Instead of LQR controllers for the automatic control system, state machines with PD feedback are used.

Although manual control tended to be a little sloppy, with a little practice, most users could establish some type of steady state walking gait. Unfortunately, maintaining this type of gait cycle is very tedious. Other types of motion were attempted with manual control (like jumps and backflips) that show that manual control does have practical uses, but it is not the best choice for walking control.

Automatic control

As might be expected, automatic walking control of this biped system provided better control than the manual methods. An automatically generated walking sequence for the planar 3-link biped defined in Figure 4.10 on page 41, is shown in the composite image of Figure 6.32. The model starts from a balancing state and transitioning to a steady-state gait cycle. A detailed plot of the link path traces is shown in Figure 6.33. Figure 6.34 through Figure 6.37 show plots of the state variables, joint torques, and ground reaction forces.

Two types of proportional-derivative (PD) controllers were tested for controlling this system. The simpler of the two is a goal point regulation method in which end-of-cycle leg positions were selected by the state machine. The second method uses path tracking instead of goal point regulation. Both types of PD controllers can establish and maintain a stable gait cycle, the results of the first method will be discussed below.

The gains selected for the body posture, stance, and swing phases of the walking cycle for the regulator method are given in Table 6.15. The variable parameters selected for simulation of this system are listed in Table 6.16.

Table 6.15 3-link sagittal plane biped walking gains

Parameter	Kp	Kd
body	60.0	8.0
stance leg	30.0	8.0
swing leg	30.0	8.0

Table 6.16 Planar 3-link biped system parameters

Parameter	link 1	link 2	link 3
mass	2.0	0.5	0.5
length	2.0	0.5	0.5

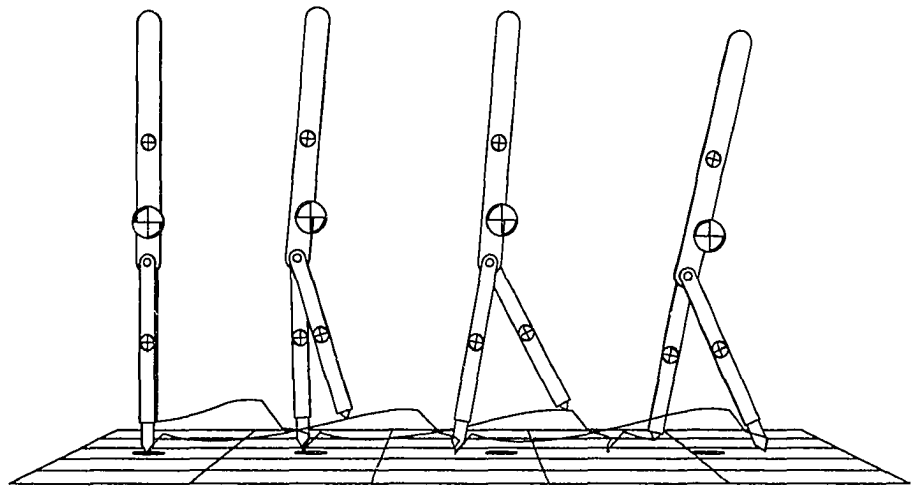

Figure 6.32 Planar 3-link biped walking sequence composite

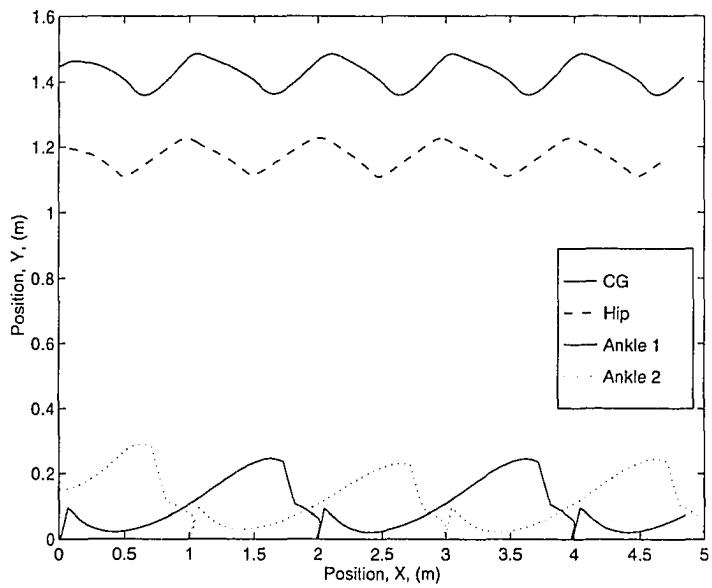

Figure 6.33 Planar 3-link biped walking sequence position data

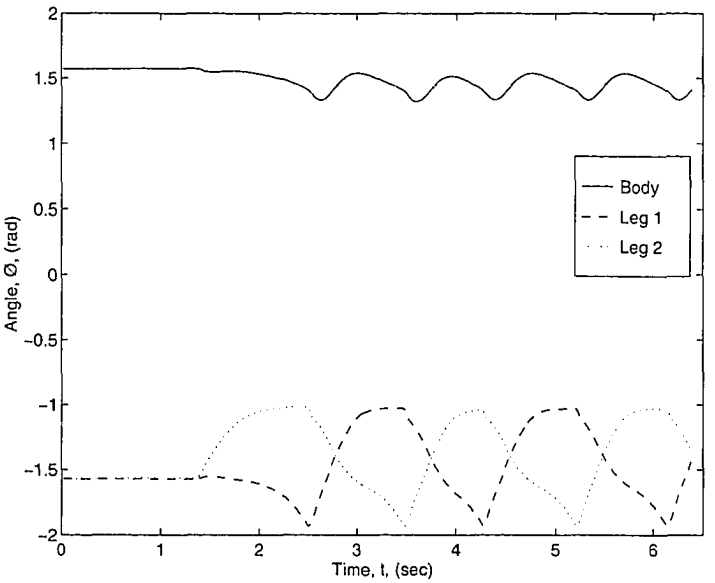

Figure 6.34 Planar 3-link biped angular positions

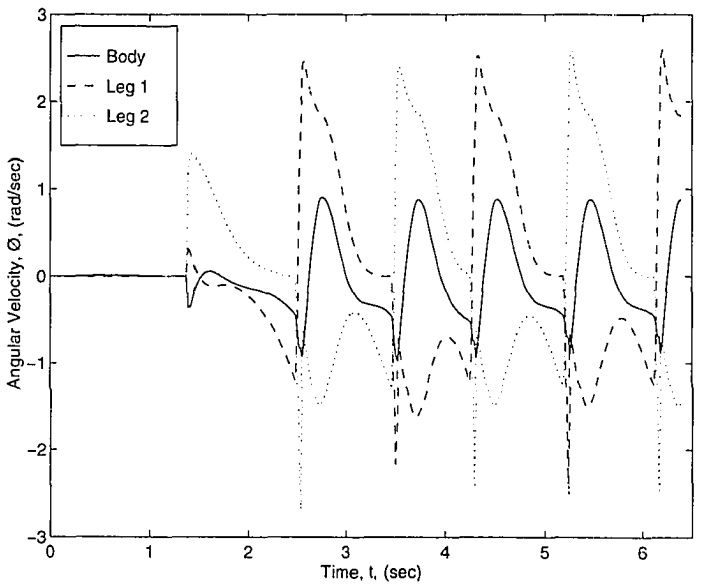

Figure 6.35 Planar 3-link biped angular velocities

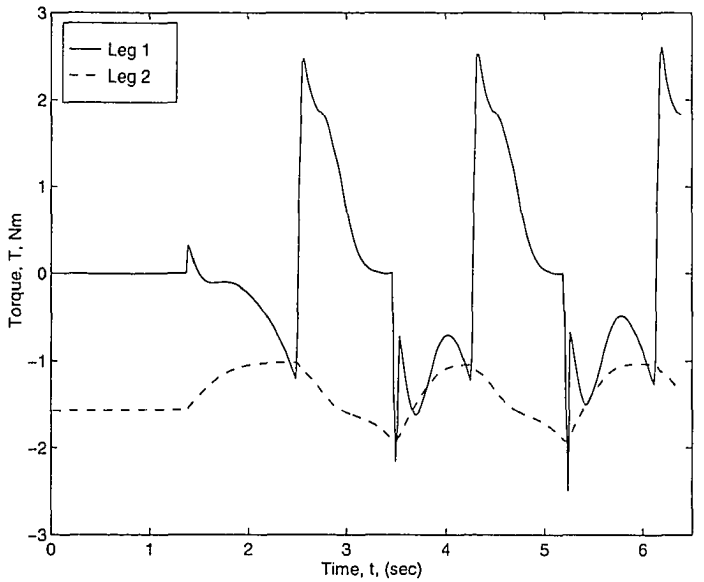

Figure 6.36 Planar 3-link biped joint torques

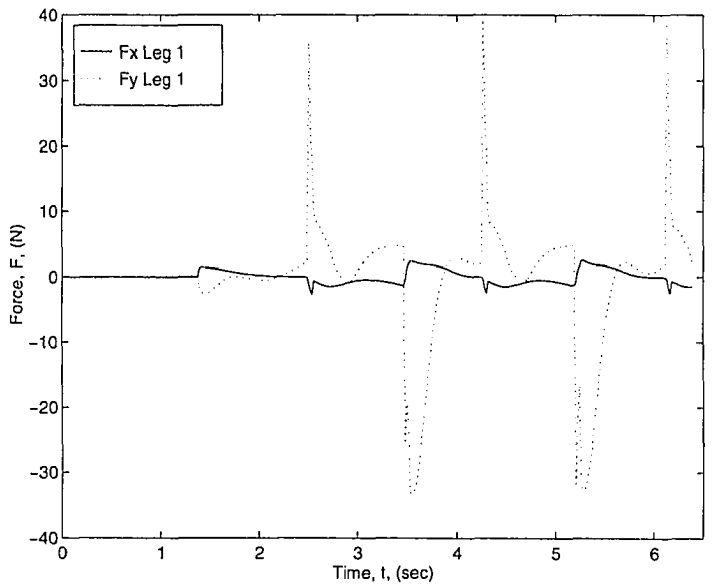

Figure 6.37 Planar 3-link biped ground reaction forces

6.3.2 5-link Sagittal Plane Biped

The walking sequence composite for the planar 5-link biped of Figure 4.11 is shown in Figure 6.38. A detailed plot of the joint path traces is shown in Figure 6.39. Figure 6.40 through Figure 6.43 show plots of the state variables, joint torques, and ground reaction forces. The regulator method gains selected for the body posture, stance and swing phases, and knee extension for this system are given in Table 6.17. The variable parameters selected for simulation of this system are listed in Table 6.18.

Table 6.17 5-link sagittal plane biped walking gains

Parameter	Kp	Kd
body	60.0	8.0
stance leg	30.0	8.0
swing leg	30.0	8.0
knee	70.0	5.0

Table 6.18 Planar 5-link biped system parameters

Parameter	link 1	link 2	link 3	link 4	link 5
mass	2.0	0.5	0.5	0.5	0.5
length	2.0	0.5	0.5	0.5	0.5

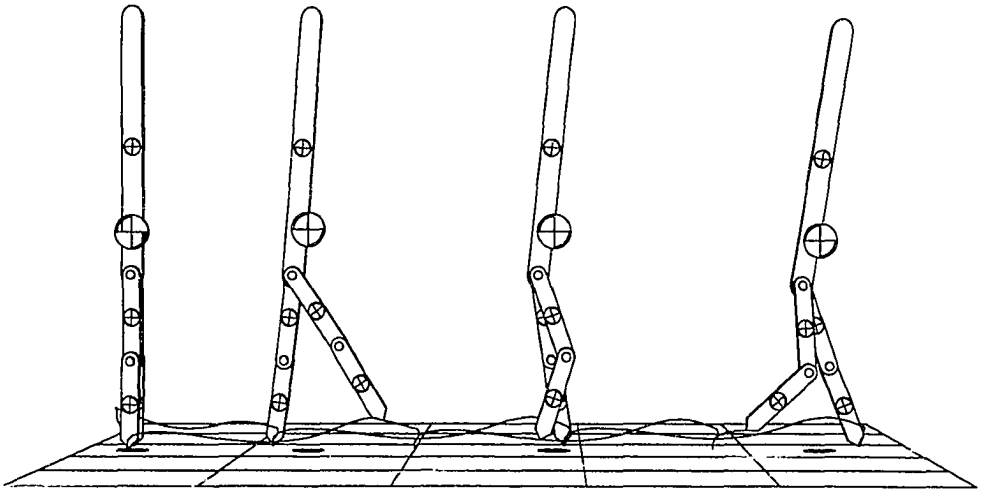

Figure 6.38 Planar 5-link biped walking sequence

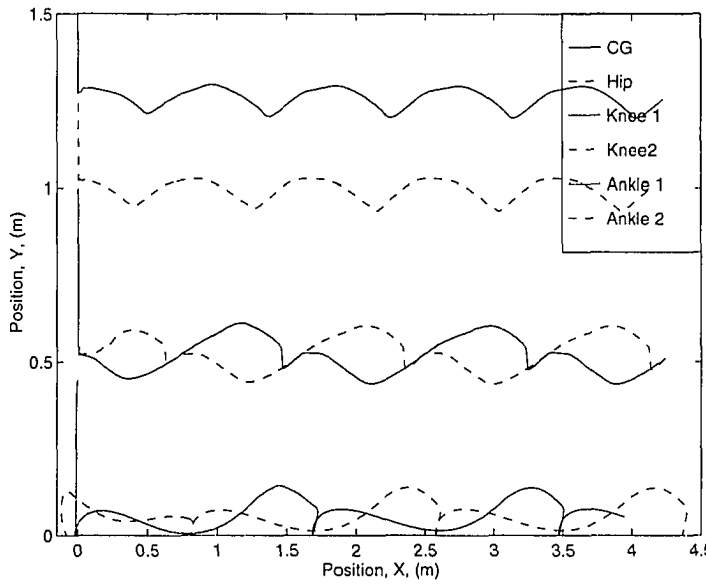

Figure 6.39 Planar 5-link biped walking sequence position data

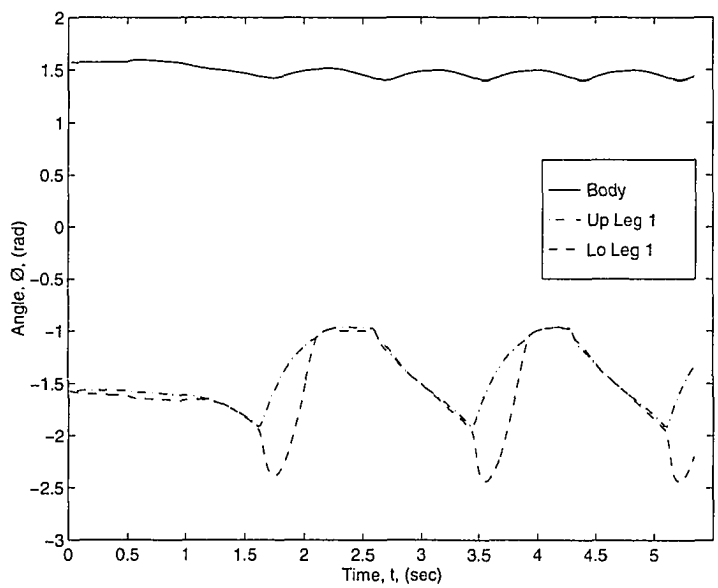

Figure 6.40 Planar 5-link biped angular positions

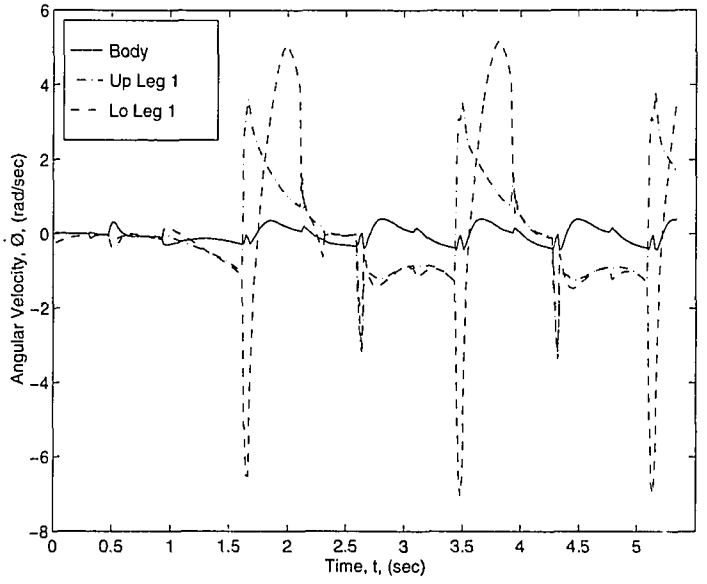

Figure 6.41 Planar 5-link biped angular velocities

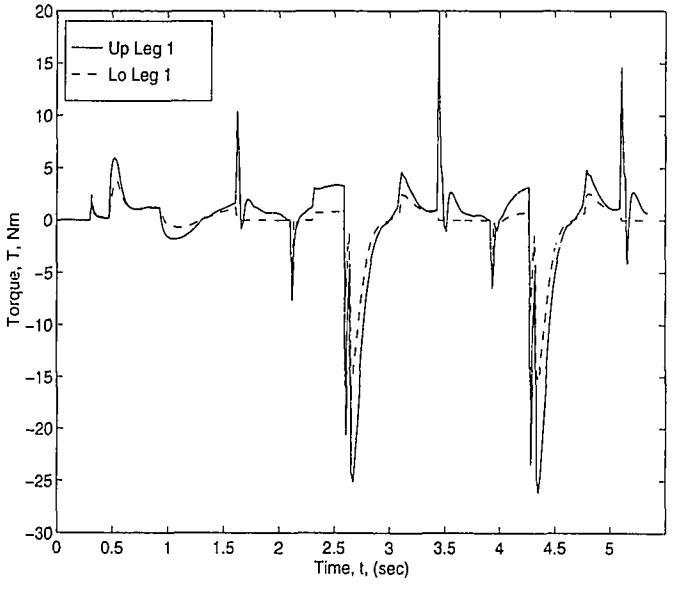

Figure 6.42 Planar 5-link biped joint torques

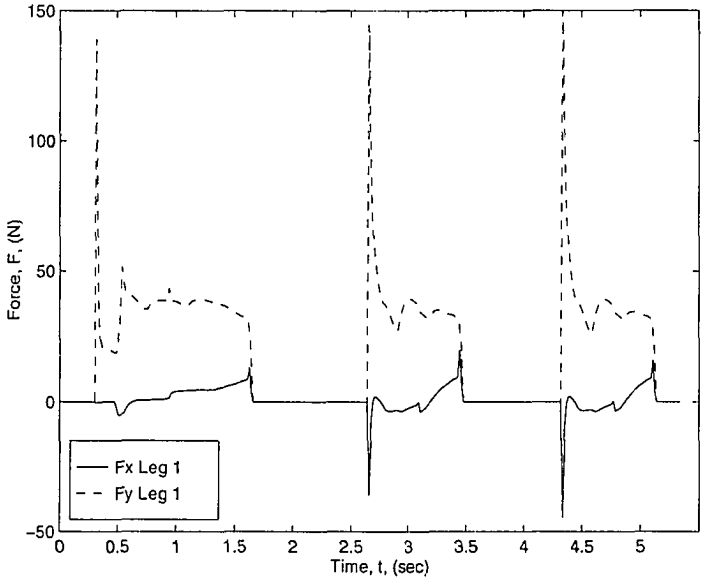

Figure 6.43 Planar 5-link biped ground reaction forces

6.3.3 7-link biped

As with the 5 and 7-link bipeds, the walking cycle of the nonlinear sagittal plane 7-link biped of Figure 4.13, is controlled by a state machine, as described in Chapter 5. The walking sequence is shown in Figure 6.44. A detailed plot of the joint path traces is shown in Figure 6.45, and in the color image of Figure D.2 of Appendix D. Angular position and angular velocity plots are given in Figure 6.46 and Figure 6.47, respectively. Joint torques are given in Figure 6.48, and the ground reaction forces transmitted through the foot to the ankles are plotted in Figure 6.49.

The PD gains selected for the body posture, stance, and swing phases, as well as the knee and foot gains for the 7-link walking cycle (for use with the regulator method) are given in Table 6.19. The variable parameters selected for simulation of this system are listed in Table 6.20.

Table 6.19 7-link sagittal plane biped walking gains

Parameter	Kp	Kd
body	60.0	8.0
stance leg	50.0	8.0
swing leg	50.0	8.0
knee	50.0	4.0
foot	40.0	4.0

Table 6.20 Planar 7-link biped system parameters

Parameter	link 1	link 2	link 3	link4 (foot)	link 5	link 6	link 7 (foot)
mass	2.0	0.5	0.5	0.2	0.5	0.5	0.2
length	2.0	0.5	0.5	0.3	0.5	0.5	0.3

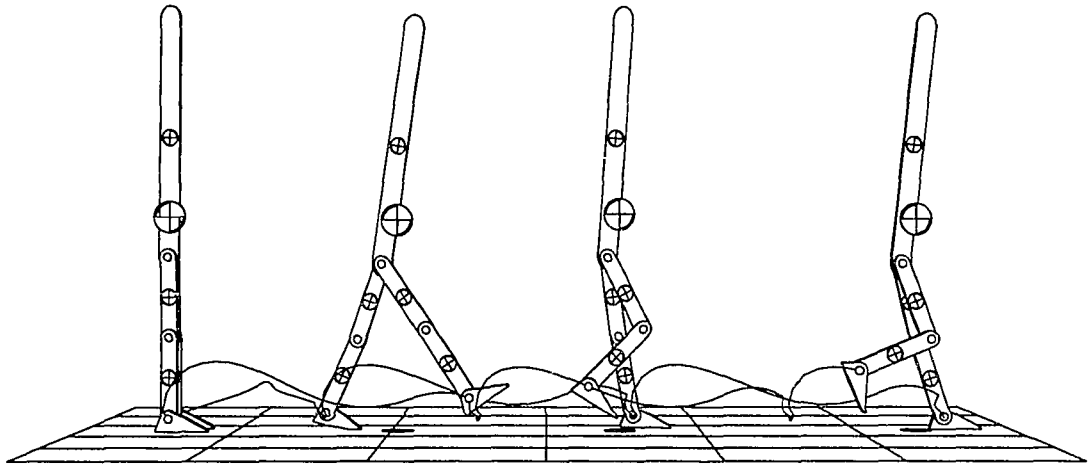

Figure 6.44 Planar 7-link biped walking sequence composite

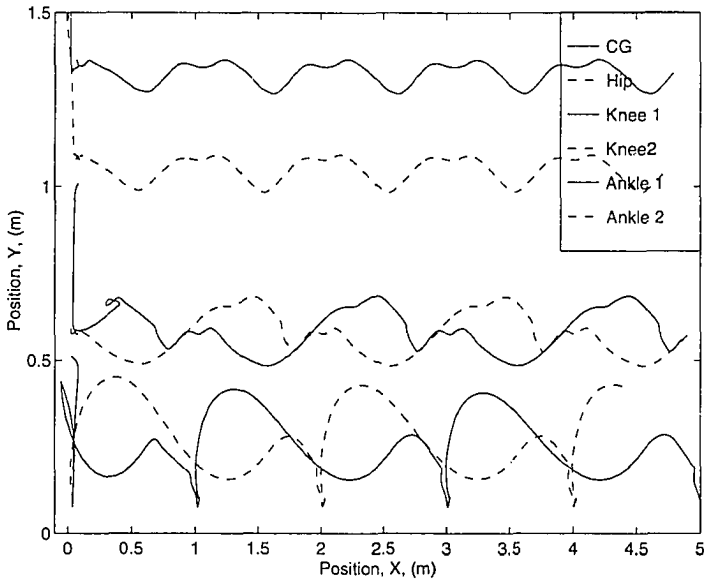

Figure 6.45 Planar 7-link biped walking sequence position data

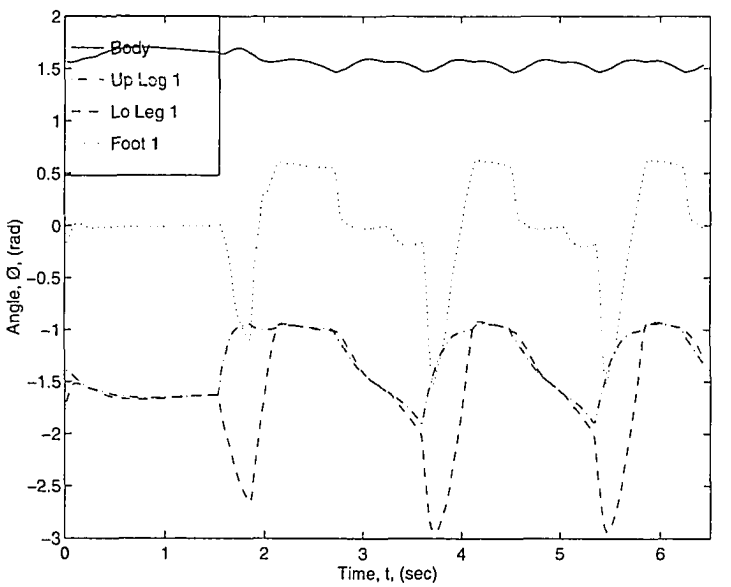

Figure 6.46 Planar 7-link biped angular positions

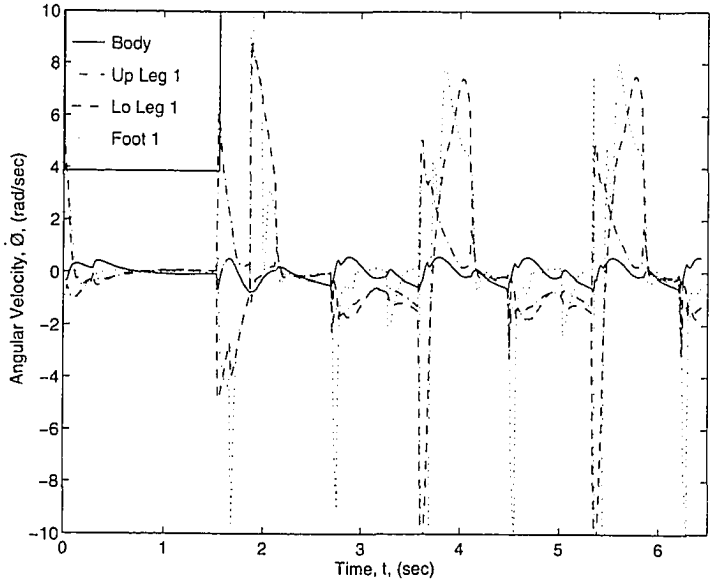

Figure 6.47 Planar 7-link biped angular velocities

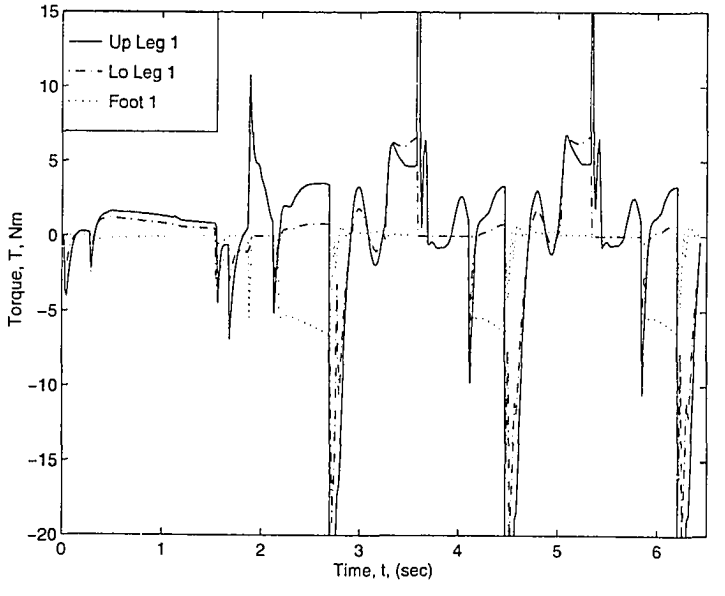

Figure 6.48 Planar 7-link biped joint torques

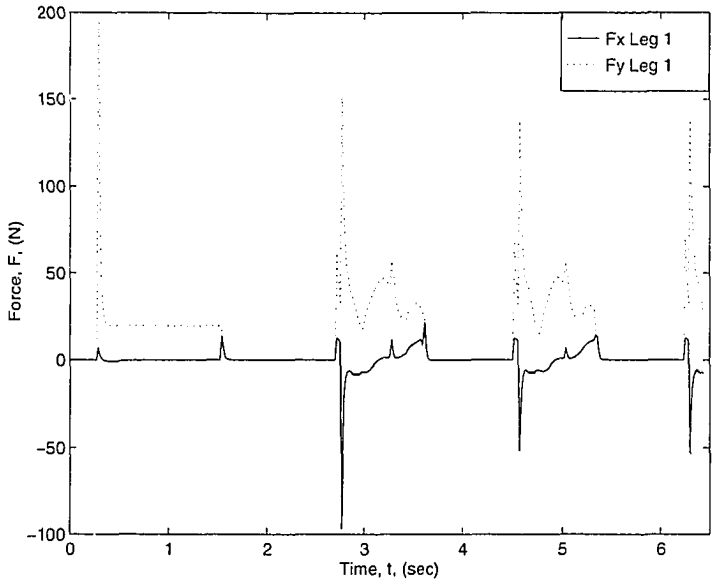

Figure 6.49 Planar 7-link biped ground reaction forces

6.3.4 Non-uniform Surfaces

All planar systems were designed to be able to respond appropriately to some degree of surface variation without modifying the feedback gains. The two examples of non-uniform surfaces that were tested are a gradually inclined surface and stairs. Figure 6.50 and Figure 6.51 show the 7-link planar biped walking down an inclined surface and down stairs, respectively. The 3-link and 5-link sagittal plane systems (not shown) were also successful at navigating these types of environments. The gains for these systems will work for inclines with gradually increasing slopes, but they will not work for ascending stairs.

In order to handle steeper slopping surfaces, the body link balancing position was modified to be a linear function of the surface slope. This method effectively moves the desired ZMP position into a range that can support a stable walking cycle. To perform the stair climbing task, the state machine must include provisions for lifting and placing the stance foot at the higher elevation. This task was not investigated here.

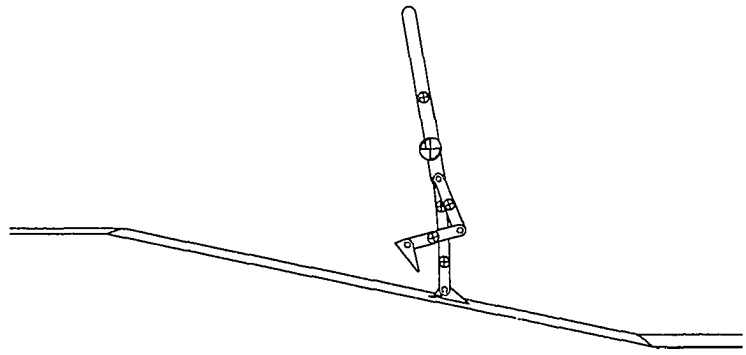

Figure 6.50 Planar 7-link biped descending an inclined surface

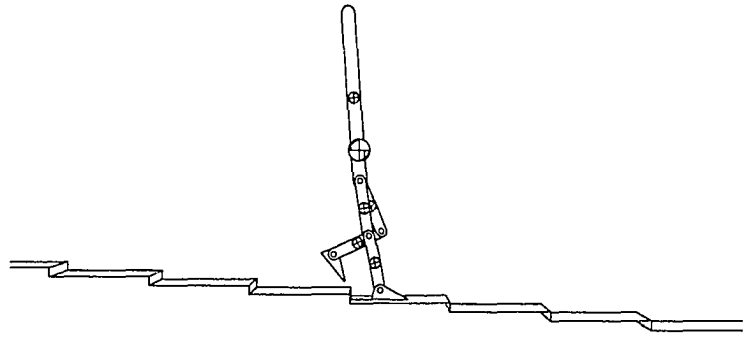

Figure 6.51 Planar 7-link biped descending stairs

6.4 Spatial Biped Balancing

Although many types of spatial bipeds were designed and presented in the chapter on modeling, only one type of spatial biped with LQR balance control will be discussed here. While the results presented here are limited to this one case, several conclusions that apply to the other spatial systems can be made. As mentioned in the chapter on control, the basic assumption for spatial biped balancing control is that separate planar control systems can operate independently.

6.4.1 3-Link Spatial Biped

The only spatial system presented here will be the nonlinear, 3-link, 8-DOF spatial biped, as described by the D-H parameters in Table 4.5 on page 57. The test case is for balancing on both feet. An image sequences for this system being dropped onto a flat surface and then establishing a symmetric balanced posture is shown in Figure 6.52(a). Since this system uses the same sagittal plane controller as the 3-link planar biped, the state variable, torque, and ground reaction for plots are nearly identical to the planar case, and will not be repeated here. This similarity is due to the symmetry of the system arrangement and the initial conditions chosen for this test case.

Figure 6.52(b) shows the same model and control system for the non-symmetric initial conditions given in Table 6.23. These conditions start the system with an initial twist in the frontal plane, with the projected CG located inside the ground support positions. Results show that the system is controllable, even without a frontal plane controller. This is due to the fact that the uncontrolled degrees of freedom in the frontal plane are stabilizable for these initial conditions. Angular positions and joint control torques for this set of initial conditions are given in Figure 6.53 and Figure 6.54, respectively.

When a larger initial twist in the frontal plane is selected that locates of the projected CG outside of the ground support points, a non-stabilizable system results. Note that an independent frontal plane controller is not possible for this 3-link configuration.

If initial conditions are selected in which the legs are separated by a relatively small angle in the sagittal plane, the system can be stabilized. A large separation angle causes the system to destabilize. This situation could possibly be corrected if an independent transverse plane controller was included. This type of controller may also prove to be useful in controlling some types of frontal plane movements.

Although a spatial 3-link model with an active frontal plane controller is not presented here (mainly due to time limitations), the basic principle that the sagittal plane balancing control can function independently of frontal plane balancing has been established.

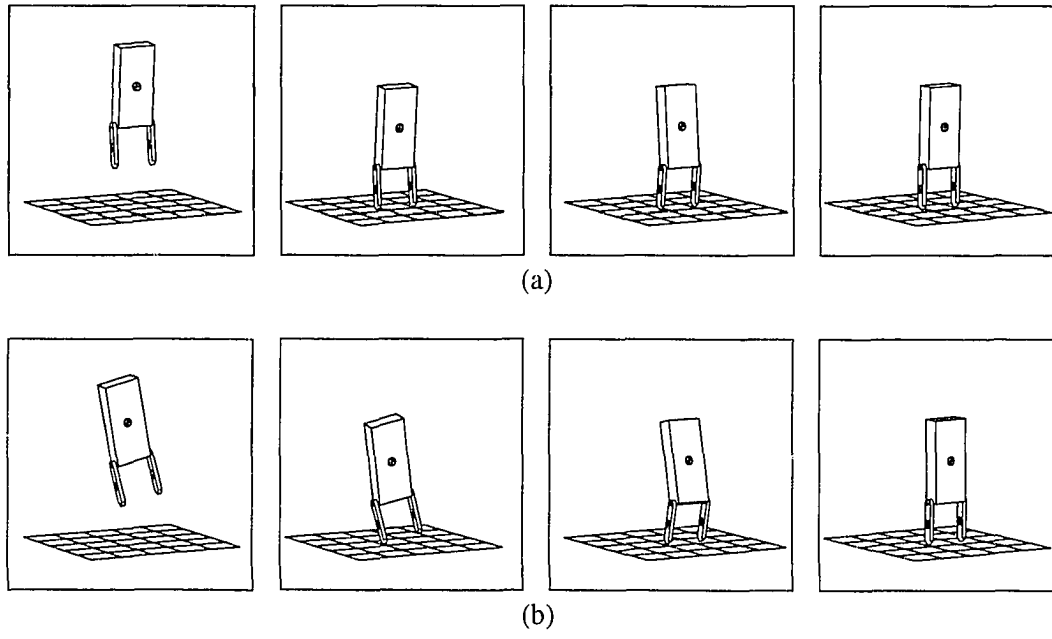

Figure 6.52 Spatial 3-link biped balancing on both feet

Table 6.21 3-link spatial biped system parameters

Parameter	link 1	link 2	link 3
mass	2.0	0.5	0.5
length	2.0	0.5	0.5

Table 6.22 Initial conditions for 3-link sagittal plane test case (a)

State Variable	Value	State Variable	Value
x	0.0	θ_2	0.1
$\dot{x}$	0.0	$\dot{\theta}_2$	0.0
y	0.0	θ_3	0.0
$\dot{y}$	0.0	$\dot{\theta}_3$	0.0
z	1.0	θ_4	0.2
$\dot{z}$	0.0	$\dot{\theta}_4$	0.0
θ_1	0.0	θ_5	0.2
$\dot{\theta}_1$	0.0	$\dot{\theta}_5$	0.0

Table 6.23 Initial conditions for 3-link sagittal plane test case (b)

State Variable	Value	State Variable	Value
x	0.0	θ_2	0.1
$\dot{x}$	0.0	$\dot{\theta}_2$	0.0
y	0.0	θ_3	0.0
$\dot{y}$	0.0	$\dot{\theta}_3$	0.0
z	1.0	θ_4	0.2
$\dot{z}$	0.0	$\dot{\theta}_4$	0.0
θ_1	0.22	θ_5	0.2
$\dot{\theta}_1$	0.0	$\dot{\theta}_5$	0.0

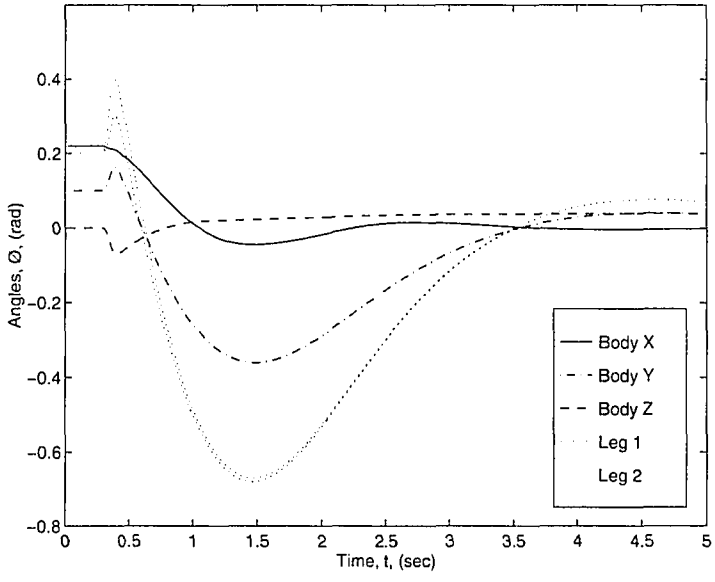

Figure 6.53 Spatial 3-link biped balancing angular positions

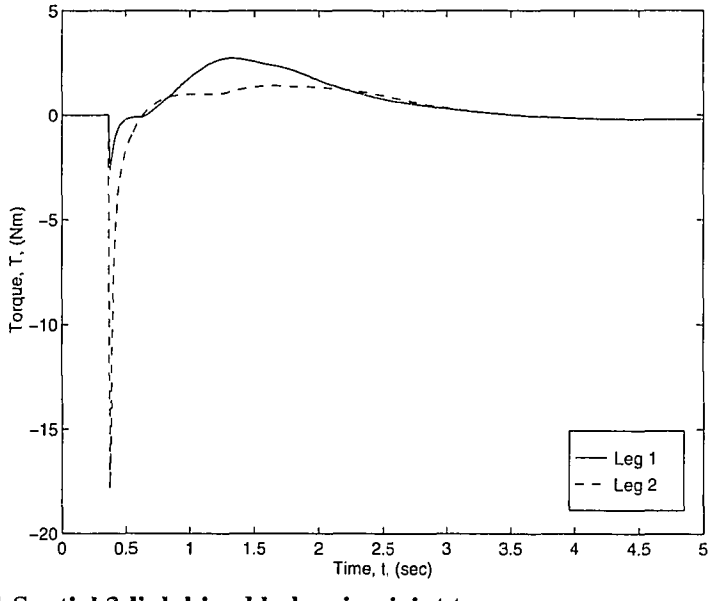

Figure 6.54 Spatial 3-link biped balancing joint torques

6.5 Spatial Biped Walking

As with spatial biped balancing, only one type spatial biped walking control will be presented. Control of the same 3-link, 8-DOF nonlinear multibody system model will be discussed with respect to steady-state walking. Transitions between balancing and walking will not be presented. At the present time, this spatial system does not operate in real-time, therefore interactive walking control will not be discussed.

6.5.1 3-Link Spatial Bipeds

Although two types of 3-link spatial biped models were developed and presented in the modeling section, only the results of the 8-DOF model with sagittal plane control will be discussed here. This system has essentially the same controller as the 3-link sagittal plane model, but has no active frontal plane control. Due to this fact, the system is very sensitive to the initial conditions, but with the right selection of these values, a steady-state walking cycle can be achieved. Figure 6.55 shows a position sequence with path traces of the feet and hip for this system. Figure 6.56 through Figure 6.63 show plots of the state variables, joint torques, and ground reaction forces. The XZ plane data is very similar to the 3-link sagittal plane results.

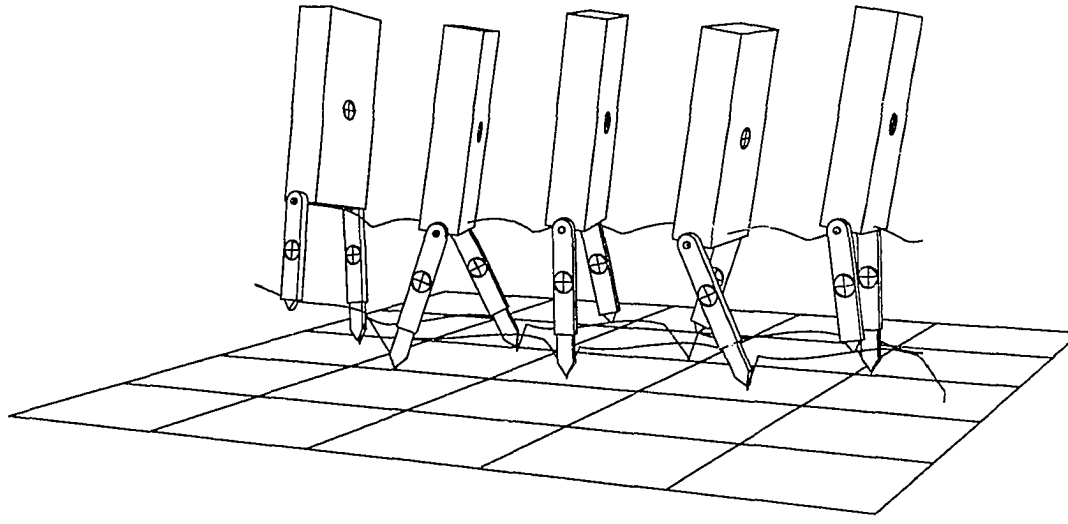

Figure 6.55 Spatial 3-link biped walking sequence

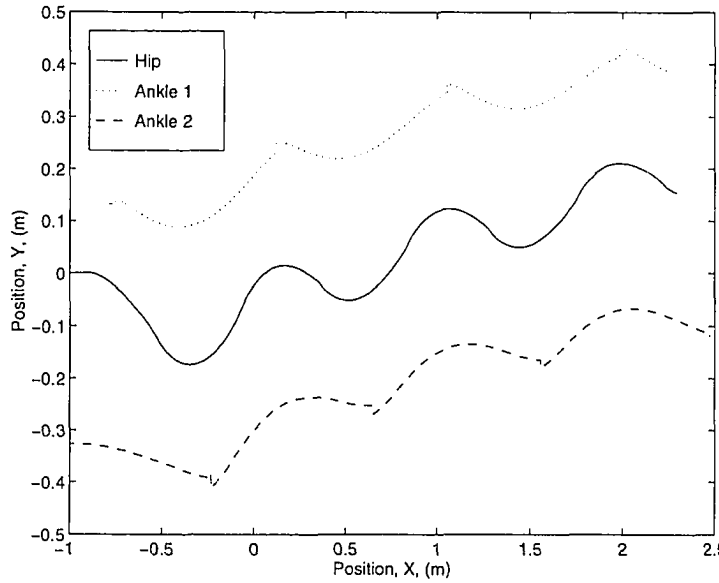

Figure 6.56 Spatial 3-link biped: X-Y plane position data

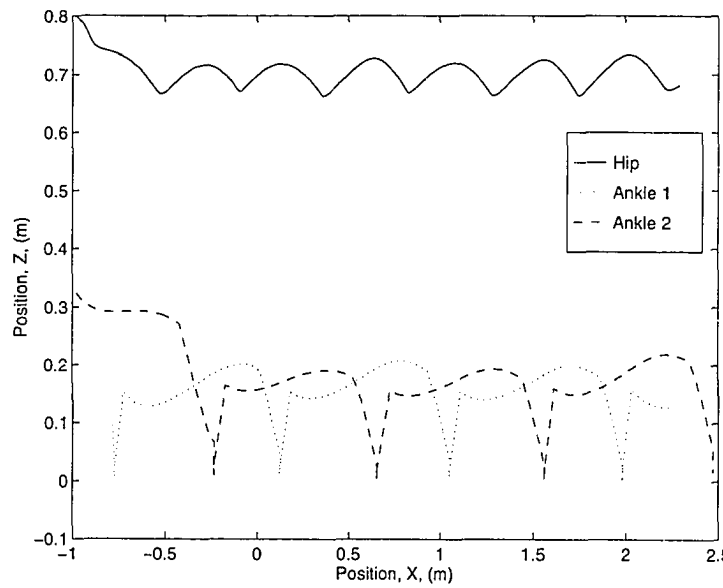

Figure 6.57 Spatial 3-link biped: X-Z plane data

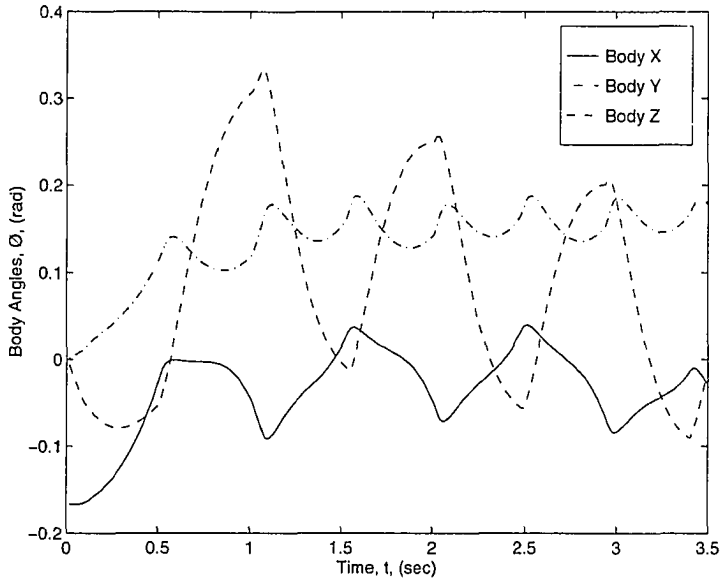

Figure 6.58 Spatial 3-link biped: body angular positions

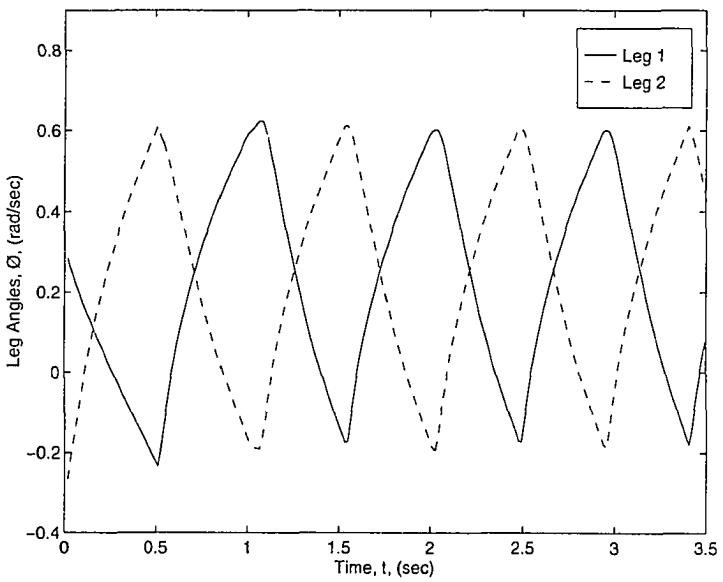

Figure 6.59 Spatial 3-link biped: leg angular positions

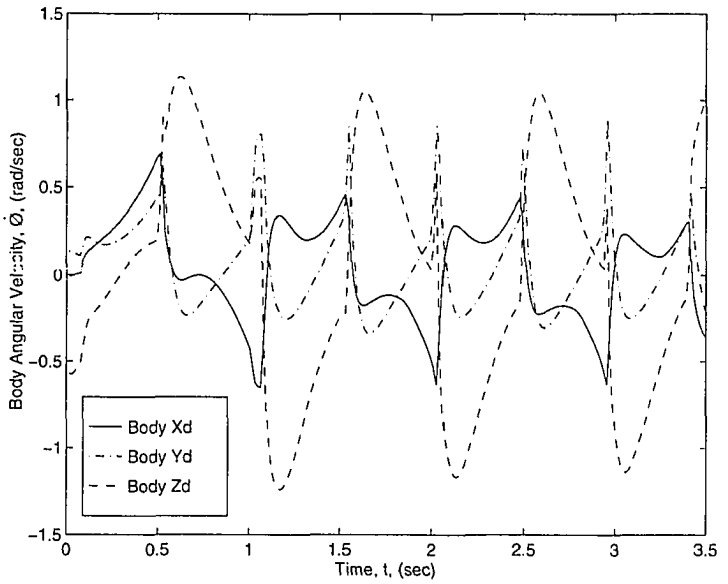

Figure 6.60 Spatial 3-link biped: body angular velocities

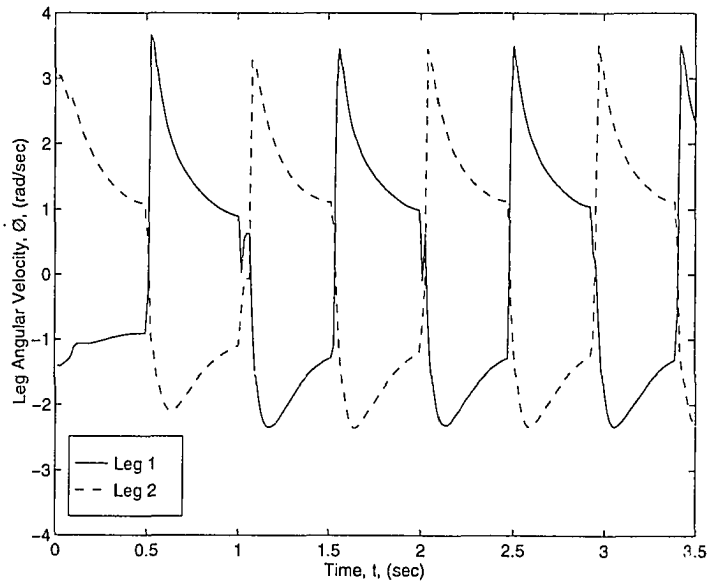

Figure 6.61 Spatial 3-link biped: leg angular velocities

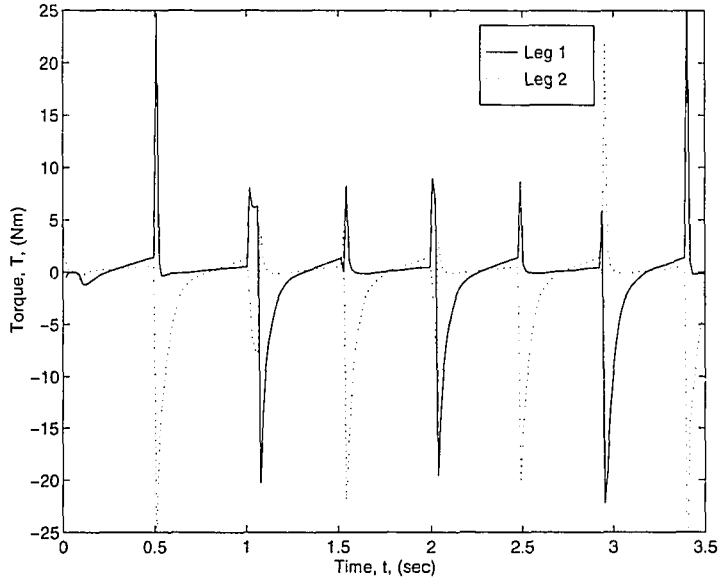

Figure 6.62 Spatial 3-link biped: joint torques

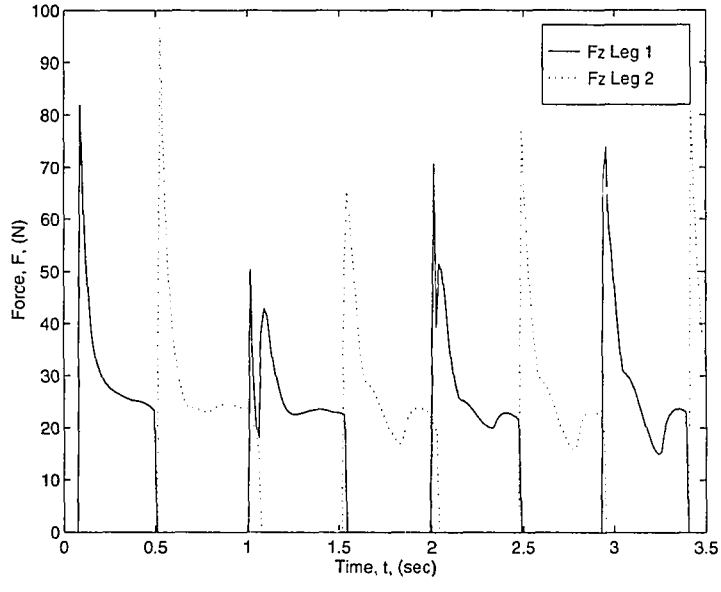

Figure 6.63 Spatial 3-link biped: ground reaction forces

In Figure 6.56, it can be seen that the system heading has a small Y-direction component. This is caused by the initial conditions chosen for this test case. To make the Y-component return to zero, a different set of initial conditions could be selected. Another option would be to implement some type of direction control algorithm. Direction control, or turning, is

accomplished for this system by making the step length for one leg longer or shorter than the other leg.

Using the same initial conditions as before, Figure 6.64 shows the 3-link spatial biped using this type of turning control. In this case, the right leg step length was shortened and the left leg step length was increased. If allowed to continue in this steady-state pattern, the system will trace out a circular path.

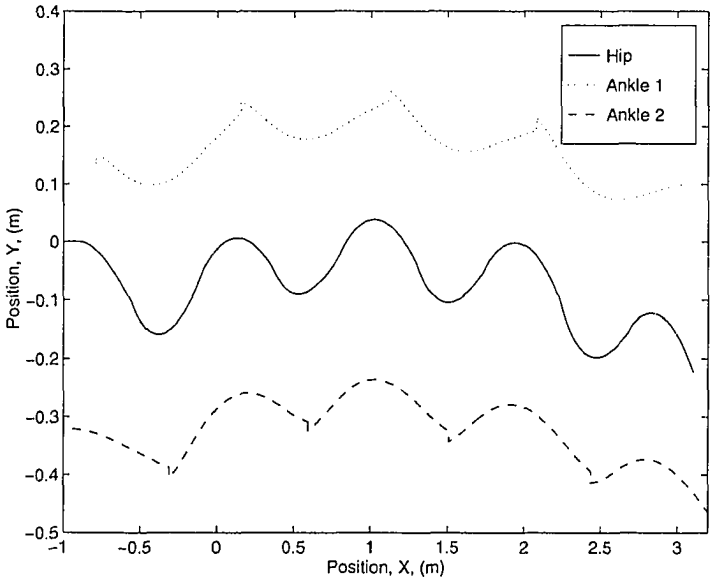

Figure 6.64 Spatial 3-link biped: X-Y plane position data, with turning

Test results from this turning experiment indicate that in addition to sagittal and frontal plane control systems, 3D bipeds will also need to have a transverse plane controller. A controller in this plane will deal primarily with turning, and would be more effective than trying to perform this operation with modifications to the sagittal plane controller as was attempted here. A transverse plane controller would also serve to manage the degree of body twist, which is an important factor in developing systems that can exhibit individual characterizations.

6.5.2 Other Spatial Bipeds

The original goal of the simulation portion of this project was to interactively control the 10-link, 22-DOF spatial biped model shown in Figure 6.65. Unfortunately, this goal was not met. This was due mainly to time constraints, but also to the realization that the serial application (i.e. non-parallelized) of the numerical form of the Newton-Euler multibody dynamics algorithm cannot produce real-time interactive simulation using current graphics workstations. A possible solutions to this problem involve parallelizing the dynamics computations for use with multi-processor computers. This is possible due to the independent nature of the numerical mass/inertia matrix calculation technique discussed in Chapter 4.

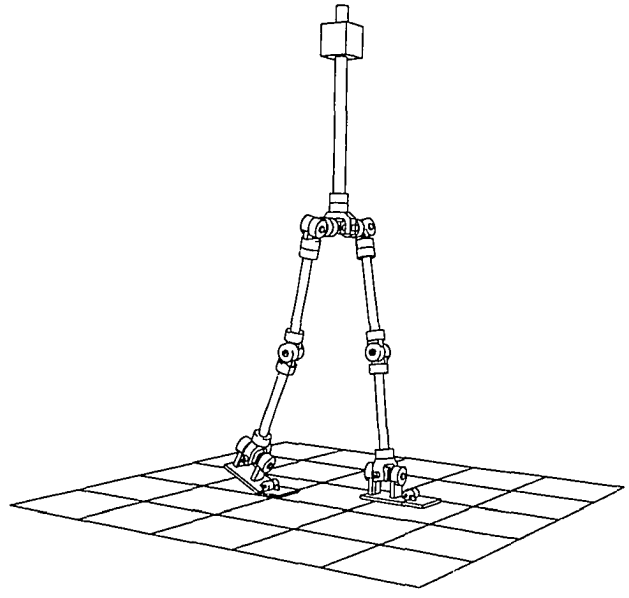

Figure 6.65 10-link, 22-DOF spatial biped model

6.6 Comparison to Human Gait Cycle

To help show the validity of the control system design, a comparison of a simulated steady-state walking cycle of the 7-link sagittal plane biped model with human walking data was made. Two types of human walking data were analyzed for this comparison.

6.6.1 Data Collection Process

Many methods have been developed that can be used to collect walking position data from human subject. One of the simplest and least expensive techniques is to record the human subject with a video camera. If 3D position data is required, multiple video cameras will be needed to simultaneously record two orthogonal views. This was the initial method used for this project. Figure 6.66 shows sagittal and frontal plane images from the treadmill walking. This data was collected using two synchronized S-VHS video cameras running at 30 frames per second. The two planes of data were converted to digital form using a digital disk recorder (DDR). Joint positions were then digitized by picking joint marker points off the computer screen.

Unfortunately, the quality of the data collected by using this technique turned out to be very noisy. And because of the blurred images produced by the slow shutter speed, it was difficult to accurately pick joint positions which resulted in the noisy data. Although data collected at 60 or 120 frames per second would give better results, the 30Hz data would be adequate for a qualitative analysis if a faster shutter speed was available to eliminate motion blur. Other issues included hidden markers and perspective distortion. Due to these problems, data from a long exposure photograph of a human with lighted joint path traces [60] was digitized instead.

(a) (b)

Figure 6.66 Images from video of human walking on treadmill: (a) sagittal plane, (b) frontal plane

6.6.2 Comparisons to Simulations

Figure 6.67 shows position data plots for one leg of the 7-link biped model along with the corresponding data for one leg of a human walking cycle digitized from [60]. The data is normalized for step length and hip height. The curves on this plot represent the hip (top), knee (middle), and ankle (bottom) positions.

Note that the amplitudes of the simulated system are larger than the human data. This is due to the overly cautious swing portion of the gait controller, which was purposely set to give a large clearance to avoid stubbing the toe of the swing leg. Other than the amplitude difference, the general trends of the human and the simulated, 2D, 7-link biped model are a fair match in overall shape.

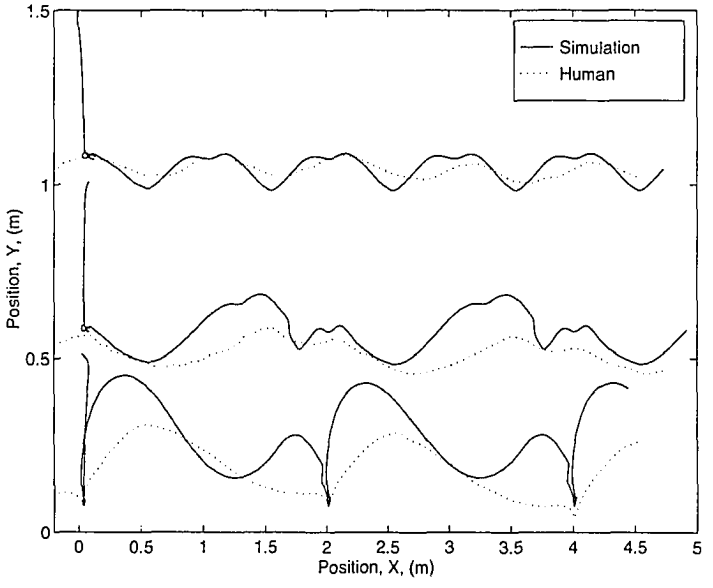

Figure 6.67 Comparison of planar 7-link sagittal position data to human data

Additional data from other human subjects collected under various conditions could be used to calibrate the mathematical biped models to create a knowledge base for a more complete human simulation tool [18]. Other data collection techniques, including magnetic position sensors, could be used to more easily and accurately collect position data. Filtering could also be used to help clean up noisy signals.

6.6.3 Ground Reaction Force Comparison

During steady-state human walking a double peak vertical ground reaction force curve is generated with a peak amplitude of approximately 1.3 times body weight on the stance foot. Figure 6.68 shows a comparison of vertical ground reaction forces for simulation and actual human walking using human data digitized from reference [31]. Although the initial impulse of the simulation curve does not match the force plate data, the remainder of the curve has a similar shape and amplitude. The hard landing impulse of the simulated data is due to the non-zero height selected by the state machine for prior to stance foot touchdown, whereas humans tend to select near zero pre-touchdown height to minimize impact. Additional fine tuning on the state machine operation could be performed to attempt to correct this discrepancy. If the initial impact spike from $t=0.0$ to $t=0.25$ is set to zero (as would be the case with a small pre-touchdown height), and the curve scaled back to $t=0.0$, the resulting double peak simulation curve would be a better match.

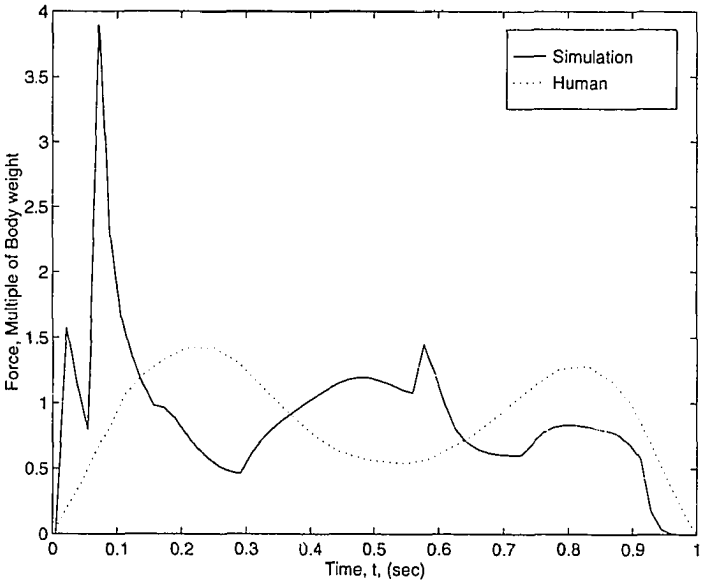

Figure 6.68 Comparison of vertical ground reaction forces

6.7 Manual Control

Interactive manual control was initially developed for testing purposes, but it can offer some additional insights that are useful in developing automatic control techniques. One interesting result of manual control testing concerns the level of user effort required to maintain balance and to initiate and sustain a steady state-gait cycle. Most users who tested the interactive software, found it almost impossible to balance even the simplest monoped or biped system for even a few seconds. On the other hand, manual walking control was accomplished by many users after several unsuccessful attempts. Like a video game, manual walking control becomes easier with practice. This type of walking control worked best for the 3-link and 5-link sagittal plane systems, but became more difficult for the 7-link system, mainly due to the limited number of input controls that a user can simultaneously manage.

The reason for the difference between the ability of the same user to operate a virtual biped in a walking mode, but fail to do so in a balancing mode has to do with the types of feedback that is received as well as the rate at which control commands can be executed. It appears that the larger motions required in walking are easier to detect than the small motions of balancing. Additional visual cues, like exaggerated motions, may help in this area. Virtual balancing also seems to require much faster human response times than that of walking, which turned out to be the same result experienced with the automatically controlled systems.

The type of input device that seemed to work best for controlling planar systems was a set of rotational dials. These input devices were used to provide commands for body posture and leg separation angles. Pedals operated by the users feet were added to control leg extension. The main drawback of dials is that users initially have a hard time remembering which way to turn the dials to get the desired movement. Dials are only useful for planar systems, a different type of input is needed for manual control of spatial systems — specifically, 6-DOF positioning devices.

Manual control of spatial systems requires input devices with a higher number of degrees of freedom than a user can achieve from a dial box. Some testing was done using 6-DOF mag-

netic sensors to control manual foot placement, but due to the non-interactive nature (in the current development state) of the more complex spatial models, manual control of these systems was not accomplished. Modifications to increase the speed of the dynamics computations may eventually allow for these type of systems to be controlled manually.

6.8 Interactive Simulation Environment

A graphical simulation environment was built for testing of the nonlinear system models using both the manual and automatic control algorithms. One of the goals of this project was to create models that could run in real-time in this type of environment (at update rates of 20-30 frames per second). This goal was realized for the planar systems, but not for the spatial systems.

The graphical environment and user interface is written in C, and uses the Silicon Graphics, Inc. (SGI) Graphics Library (GL). The user interface, shown in Figure 6.69, displays the 3D virtual environment and numerical data, as well as providing access to input commands for both the manual and automatic control systems.

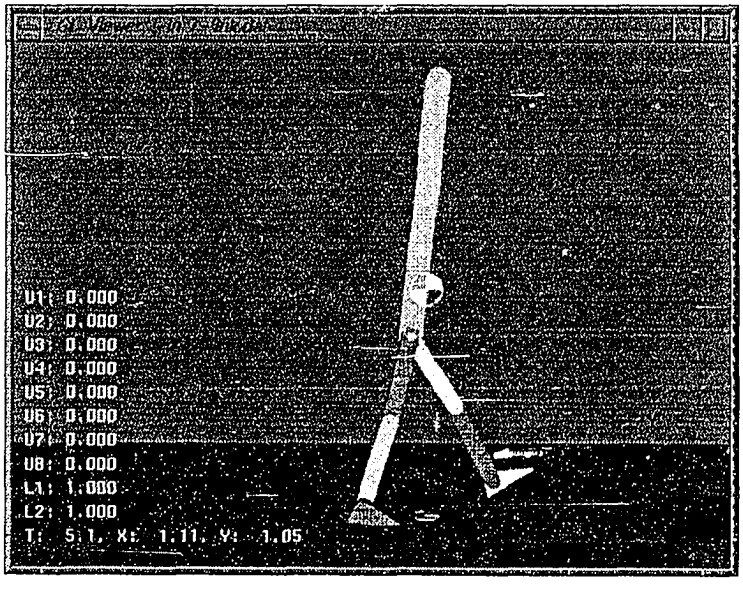

Figure 6.69 Graphical interface

Figure 6.70 shows a user sitting at workstation using the graphical simulation software along with a dial box and foot pedals to interactively control one of the biped systems. This environment allows the user to switch between manual or automatic control modes at any time.

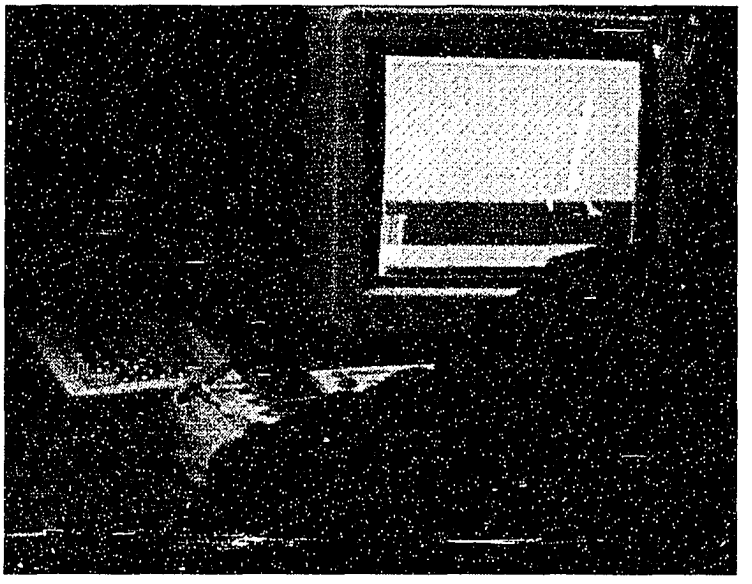

Figure 6.70 Interactive simulation environment

As mentioned earlier, the interactive simulation environment developed for this project proved to be an extremely valuable design tool for both simulation and design purposes. The ability to quickly visualize the results of a design change allowed numerous iterations to be tested in a short period of time.

7. SUMMARY AND CONCLUSIONS

This project combined several related topics to create an interactive system for balancing and locomotion control of monoped and biped mechanisms. Among these topics are, physically based modeling, multibody dynamics, feedback control, numerical integration, and computer graphics. With such a large area of subjects included in this type of research, there remains many areas for additional study. A summary of some of these areas is given at the end of this chapter.

7.1 Contributions to the Field of Bipedal Locomotion Control

Several objectives were accomplished over the course of this project, some are applications of existing theories, while others are new approaches, solutions, or working applications. These accomplishments include the development of planar and spatial, monoped and biped system models; balancing, walking, and transitional control systems using either manual or automatic control; compliant ground reaction force generation; and the creation of a real-time, interactive simulation environment.

7.1.1 Physically Based Modeling

Several types of monoped and biped systems were modeled in both planar and spatial configurations. Planar models evolved starting with a 2-link, 3-DOF monoped and proceeding through several iterations to a 7-link, 9-DOF biped. Spatial models ranged from a 2-link, 8-DOF monoped to an 8-link, 17-DOF biped.

The biped models presented here are not intended to be exact models of humans since the head and arm links are not included. Although important in human walking, they are not essential for locomotion simulation. The head and arms could easily be modeled as separate

systems that are uncoupled from the rest of the model, but this would offer little benefit in the design of either the manual or automatic control. Adding mathematically coupled head and arm components to the body link would increase the system complexity and reduce the possibility of real-time operation.

Another modeling concern deals with the type of foot model chosen. Although the added stiffness to the differential equations results in a performance penalty over hard constraint methods, the spring-damper foot model used here produced a compliant system that provided adequate results.

7.1.2 Control Systems

Balancing and walking control was accomplished for several types of planar and spatial biped systems. Monoped balancing was performed as an initial test case for biped control system design. The control system development, which evolved from completely manual to semi-automatic to completely automatic locomotion control, provided insight into the amount of user input necessary for a particular task.

Manual control

All planar models developed were controlled in real-time (i.e. 20-30 frame updates per second). Spatial models could not be simulated in real-time using the serial forms of the numeral dynamics methods on current computational hardware, and were therefore not manually controllable.

One of the many lessons learned from real-time manual control in a graphical environment is that dials are not the most intuitive input device for controlling this type of system. Although users can learn to use dials effectively, perhaps a more intuitive input device would allow for better manual control. The main result that can be drawn from this type of control is that interactive walking can be performed manually, if somewhat awkwardly, with the only type of user feedback being visual information. Other types of biped movement, like jumping and backflips, can also be performed using manual control. In general, manual control is good

for testing and speciality movements, but it is not practical for realistic walking or balancing control.

The low level control methods using torque and joint positioning allow individual segment movements, but require a high degree of user effort and coordination to achieve the complex movements of a sustained gait. In fact, direct torque control by the user is much too demanding for even the simplest biped model. The joint positioning control methods proved to be much easier and more intuitive to use. A combination manual/automatic system is possible that allows individual joint control as well as accessing stored sets of open-loop sequences and automatic feedback control.

Automatic control

All planar monoped and biped systems can balance successfully in real-time using the automatic control techniques developed for this project. The planar biped systems can also perform real-time steady-state walking, as well as transitions to walking from balancing. Automatic control of spatial systems could not be performed in real-time for the same reasons discussed for manual control. One of the spatial models, the 3-link, 8-DOF biped, was successfully controlled using off-line simulation for balancing and steady-state walking. This helped to show that planar control algorithms can be used to control a spatial biped.

To verify the performance of the automatic walking controller, simulation results for the 7-link planar biped were compared to data from human gait cycles. Although some differences were noted, overall shapes the plots were similar.

Automatic feedback control allows minor disturbances and model/environment changes to occur without disabling the system. Since a single set of gains will not be sufficient for all possible situations, collections of gain sets allow a wider range of conditions to be encountered. For example, walking down a moderate incline can be handled by the same gain sequence developed for flat surfaces, but a steep slope requires a different set of gains to maintain system stability. Another reason to develop additional sets of gains is to allow customized gait cycles to be created. Customization adds "character" to the model, which is an important issue

for computer animators. Other automatic control issues investigated here include, balance in unstable equilibrium positions and transition modes between balancing and walking.

Automatic methods alleviated the high user effort required of the manual methods, but limit the flexibility to perform specific movements. For example, avoiding obstacles with manual biped control, although difficult, can be accomplished with practice, but would require special modifications to be made using the current automatic gait cycle algorithm. Although many separate control sequences can be programmed into the control logic (for cases like climbing ramps or stairs), anytime a special task is required a separate automatic control algorithm will need to be developed. Stored control values created by interactive manual input can be used to help fill in during these special circumstances. In addition, automatic control procedures often have trouble maintaining stability in the transition phases between different control sequences.

7.1.3 Interactive Control Environment

Simulation software was developed for real-time interactive control. This 3D virtual environment proved to be a valuable tool for both system dynamics modeling and control system design. The use of this tool in model development allowed quick modifications of system parameters and interactive simulation of various "what if" scenarios. Control system design iterations were quickly simulated with interactive inputs. In addition, an interactive virtual environment is the only way to test manual walking control concepts without using actual hardware.

7.2 Applications

Possible applications for this type of interactive bipedal simulation include: generation of realistic motion for computer animation of virtual actors, analysis of human gait cycles for biomedical research, and hardware evaluation and design for robotic mechanisms.

7.2.1 Computer Graphics and Animation

In the field of computer animation of human movement, dynamic simulation and control can be a more flexible alternative to motion capture and keyframing. Realistic human motion can be obtained much faster than current animation methods.

Although acceptable for development purposes, the current interactive system needs a better graphics user interface (GUI). In order to concentrate efforts on the dynamics and controls issues, an initial research focus choice was made which did not allow much time for GUI development. Real-time control using interactive computer graphics requires an efficient environment with low overhead; including additional interface features can end up creating a bottleneck in the graphical portion of the simulation. The simple and efficient interface to the graphical environment worked well for initial design, but a more user friendly workspace will be needed if this type of environment is to be used as a practical design tool.

7.2.2 Robotics Hardware and Software

The software can be used as a tool for designing and testing of robotics and other multi-body hardware mechanisms. The current system could be adapted to work with motor models, system lag times, and sensors. Some applications include design of industrial robots, robots for the entertainment industry, and robotic-like toys.

Hardware design poses additional difficulties that are not present in a simulation. These include, sensor noise, modeling errors, and repeatability (being able to start with the same initial conditions each time). But in some ways, hardware implementation of walking machines is easier than simulation. One aspect in which this is true is in systems modeling, especially for collisions between the foot contact points and the surface, since the nonlinear system already exist in the links, joints, motors, and electronics of the actual hardware.

Simulation is useful and necessary in hardware design for testing of control algorithms, safety for both the operator and hardware, and it is a flexible, efficient, and economical design

method. A virtual environment for dynamic system design allows for much faster testing and debugging of control algorithms and system configurations.

7.2.3 Biomedical Research

This research could also be adapted to be used as a general human gait cycle analysis tool, for both medical rehabilitation use and in athletic performance enhancement. It can also be used for prosthetic limb and exoskeleton control system design.

7.3 Recommendations for Future Work

Several areas remain to be explored concerning this research topic, and many of the developments presented here can be expanded. State machines could be extended to handle running, climbing stairs, and direction control. Additional optimization methods can be evaluated for the different state machine modes just mentioned, as well as balancing, jumping, and landing. Adding motor and/or muscle models to the system would be a useful addition for both the robotics and biomedical fields. Other systems with dynamic locomotion cycles like, quadrupeds, should be possible using control techniques similar to those used for the biped mechanisms. A complete human biped system could be developed that takes advantage of a statistical database to produce accurate human simulation. And finally, a more complete user interface should be added to the real-time interactive software. The following is a partial list of suggested enhancements:

Modeling:

- full human model, including arms and head segments
- more robust and efficient foot-ground collision model with compliance
- adding joint actuator models, either in the form of motors for robotic system simulation or muscles for human motion simulation.

- more efficient application of the computational algorithms for systems requiring numerical computation of the equations of motion
- parallelize dynamic computations
- automatic parameter selection based on human segment data
- creation of additional non-human biped system models (birds for example), and non-biped systems (quadrupeds)

Control:

- finish adding sagittal and frontal plane control to the 5, 7, and 8-link system models
- develop transverse plane control algorithms
- real-time recalculation of linearized system equations based on current desired equilibrium position
- real-time recalculation of feedback control gains in addition to, or instead of table lookup methods
- optimized state machine control using LQR controllers as an alternative to PD/PID control
- additional situation modes
- better turning control

Interactive simulation

- better user interface, including options for selecting parameters, control and integration methods, and directional commands
- split up independent processes for increased performance on multi-processor workstations

BIBLIOGRAPHY

[1] Alexander, R. McN., "The Gaits of Bipedal and Quadrupedal Animals." *Int. J. Robotics Research*, vol. 3, no. 2, pp. 49-59, 1984.

[2] Alexander, R. McN., "Three Uses for Springs in Legged Locomotion." *Int. J. Robotics Research*, vol. 9, no. 2, pp. 53-61, Apr. 1990.

[3] Amirouche, F. M. L., *Computational Methods in Multibody Dynamics*, Prentice-Hall, Englewood Cliffs, NJ, 1992.

[4] Anderson, B. D. O. and Moore, J. B. *Linear Optimal Control*, Prentice-Hall, Englewood Cliffs, NJ, 1971.

[5] Armstrong, W. W., Green, M., Lake, R., "Near-Real-Time Control of Human Figure Models." *IEEE Computer Graphics and Applications*, vol. 7, no. 6, pp. 52-61, June 1987.

[6] Athens, M. and Falb, P.L. *Optimal Control an Introduction to the Theory and Its Applications*, McGraw-Hill, Yew York, 1966.

[7] Astrom, K. J., and Wittenmark, B. *Computer Controlled Systems*, 2nd ed., Prentice Hall, New Jersey, 1990.

[8] Badler, N. I. and Phillips, C. B., "Interactive Behaviors for Bipedal Articulated Figures." *Computer Graphics (proc. SIGGRAPH)*, vol. 25, no. 4, pp. 359-362, July 1991.

[9] Badler, N. I., Phillips, C. B., and Webber, B. L., *Simulating Humans: Computer Graphics Animation and Control*, Oxford University Press, New York, 1993.

[10] Bae, D. S., and Haug, E. J., "A Recursive Formulation for Constrained Mechanical Systems, Part I - Open Loop." *Mechanics of Structures and Machines*, vol. 15, no. 3, pp. 359-382, 1987.

[11] Bae, D. S., and Haug, E. J., "A Recursive Formulation for Constrained Mechanical Systems, Part II - Closed Loop" *Mechanics of Structures and Machines*, vol. 15, no. 4, pp. 481-506, 1987.

[12] Bae, D. S., Haug, E. J., and Kuhl, J. G., "A Recursive Formulation for Constrained Mechanics Systems, Part III - Parallel Procession Implementation." *Mechanics of Structures and Machines*, vol. 16, no. 2, pp. 249-269, 1988.

[13] Baraff, D. "Analytical Methods for Dynamic Simulation of Non-penetrating Rigid Bodies." *Computer Graphics (proc. SIGGRAPH)*, vol. 23, no. 3, pp. 223-231, July, 1989.

[14] Baraff, D. "Fast Contact Force Computation for Nonpenetrating Rigid Bodies." *Computer Graphics (proc. SIGGRAPH)*, vol. 28, pp. 23-34, July, 1994.

[15] Baraff, D. "Interactive Simulation of Solid Rigid Bodies." *IEEE Computer Graphics and Applications*, vol. 15, no. 5, pp. 63-75, May 1995.

[16] Bruderlin, A. and Calvert, T.W., "Goal-Directed, Dynamic Animation of Human Walking." *Computer Graphics (proc. SIGGRAPH)*, vol. 23, no. 3, pp. 233-242, July 1989.

[17] Bruderlin, A. and Calvert, T. W., "Animation of Human Gait." in *Adaptability of Human Gait Implications for the Control of Locomotion*, Patla, A.E. ed, North-Holland, Amsterdam, pp. 305-330, 1991.

[18] Bruderlin, A. and Calvert, T. W., "Knowledge-driven Animating of Human Figures." *Workshop on Simulation and Interaction in Virtual Environments (SIVE)*, pp. 199-203, July 1995.

[19] Bruderlin, A. and Williams, L., "Motion Signal Processing." *Computer Graphics (proc. SIGGRAPH)*, pp. 97-104, Aug, 1995.

[20] Burdick, J. W., "An Algorithm for Generation of Efficient Manipulator Dynamic Equations." *Proc. of the 1986 IEEE Conference on Robotics and Automation*, San Francisco, pp. 212-218, 1986.

[21] Calvert, T., Bruderlin, A., Dill, J., Schiphorst, T., and Welman, C., "Desktop Animation of Multiple Human Figures." *IEEE Computer Graphics and Applications*, vol. 13, no. 3, pp. 18-26, 1993.

[22] Clauser, C. E., McConville, J. T., and Young, J. W., "Weight, volume, and center of mass of segments of the human body." *AMRL-TR-69-70*, Wright-Patterson Air Force Base, Ohio, 1969.

[23] Cotsaftis, M. and Vibet, C., "Control Law Decoupling for 2-D Biped Walking System." *IEEE Engineering in Medicine and Biology Magazine*, pp. 41-45, Sept. 1988.

[24] Craig, J. J., *Introduction to Robotics Mechanics and Control*, Addison Wesley; Reading, MA, 1986.

[25] Craig, J. J., *Introduction to Robotics Mechanics and Control*, 2nd ed., Addison Wesley; Reading, MA, 1989.

[26] Davis, R. B, "Clinical Gait Analysis." *IEEE Engineering in Medicine and Biology Magazine*, pp. 35-40, Sept. 1988.

[27] D'Azzo, J. J, and Houpis, C. H., *Linear Control System Analysis & Design*, 3rd ed., McGraw-Hill, New York, 1988.

[28] Dempster, W. T., "Space requirements of the seated operator." *WADC-TR-55-169*, Wright-Patterson Air Force Base, Ohio, 1955.

[29] Denavit, J. and Hartenberg, R. S., "A Kinematic Notation for Lower-Pair Mechanisms Based on Matrices." *J. Applied Mechanics*, pp. 215-221, June 1955.

[30] Donner, M. D., *Real-Time Control of Walking*, R.R. Donnelley & Sons, Harrisonburg, VA, 1987.

[31] Dufek, J. S., Schot, P. K., and Bates, B. T., "Dynamic Lower Extremity Evaluation of Males and Females During Walking and Running." *J. Human Movement Studies*, (18) pp. 159-175, 1990.

[32] Dunn, E. R. and Howe, R. D., "Towards Smooth Bipedal Walking." *Proc. of the 1994 IEEE Int. Conference on Robotics and Automation*, IEEE Computer Society Press, Los Alamitos, CA, vol. 3, pp. 2489-2494, 1994.

[33] Furusho, J. and Masubuchi, M., "Control of a Dynamical Biped Locomotion System for Steady Walking." *J. Dynamic Systems, Measurement., and Control*, vol. 108, pp. 111-118, June 1986.

[34] Furusho, J. and Sano, A., "Sensor-Based Control of a Nine-Link Biped." *Int. J. of Robotics Research*, vol. 9, no. 2, pp. 83-98, Apr. 1990.

[35] Furusho, J. and Sano, A. "Development of Biped Robot." in *Adaptability of Human Gait Implications for the Control of Locomotion*, Patla, A.E. ed., North-Holland, Amsterdam, pp. 277-303, 1991.

[36] Gear, C. W., *Numerical Initial Value Problems in Ordinary Differential Equations*. Prentice-Hall, Englewood Cliffs, NJ, 1971.

[37] Goddard, R. E., Zheng, Y.F., and Hemami, H., "Control of the Heel-Off to Toe-Off Motion of a Dynamic Biped Gait." *IEEE Trans. on Systems, Man, and Cybernetics*, vol. 22, no. 1, pp 92-102, Jan/Feb 1992.

[38] Golliday, C. L. and Hemami, H., "Postural Stability of the Two-Degree-of- Freedom Biped by General Linear Feedback." *IEEE Trans. on Automatic Control*, pp 74-79, Feb. 1976.

[39] Golliday, C. L. and Hemami, H., "An Approach to Analyzing Biped Locomotion Dynamics and Designing Robot Locomotion Controls." *IEEE Trans. on Automatic Control*, Vol. AC-22, No. 6, Dec 1977.

[40] Gubina, F., Hemami, H., and McGhee, R.B., "On the Stability of Biped Locomotion." *IEEE Trans. on Bio-Medical Engineering*. vol. BME- 21, no. 2, Mar 1974, pp 102-108.

[41] Guo Y., Xu, G., and Tsuji S., "Tracking Human Body Motion Based on a Stick Figure Model." *J. Visual Communication and Image Representation*, vol. 5, no. 1, pp. 1-9, Mar., 1994.

[42] Green, M., "Using Dynamics in Computer Animation: Control and Solution Issues." in *Making Them Move*, Badler, N. I. et al. eds., pp. 281-314, Morgan Kaufmann Publishers, San Mateo, CA, 1991.

[43] Han, I. and Gilmore, B. J., "Multi-Body Impact Motion with Friction—Analysis, Simulation, and Experimental Validation." *ASME J. Mechanical Design*, vol. 115, pp. 412-422, Sept. 1993.

[44] Hatze, H., "A Mathematical Model for the Computational Determination of Parameter Values of Anthropomorphic Segments." *J. Biomechanics*, vol. 13, pp. 833-843. 1980.

[45] Hay, J. G., *The Biomechanics of Sports Techniques*, 2nd ed., Prentice-Hall, Englewood Cliffs, NJ, 1978.

[46] Hemami, H., "A Feedback On-Off Model of Biped Dynamics." *IEEE Trans. on Systems, Man, and Cybernetics*, vol. SMC-10, no. 7, pp 376-383, Jul. 1980,

[47] Hemami, H. and Dinneen, J. A., "A Marionette-Based Strategy for Stable Movement." *IEEE Trans. on Systems, Man, and Cybernetics*, vol. 23, no. 2, pp. 502-511, Mar./Apr. 1993.

[48] Hemami, H. and Farnsworth, R. L., "Postural and Gait Stability of a planar Five Link Biped by Simulation." *IEEE Trans. on Automatic Control*, Jun 1977, pp 452-458.

[49] Hemami, H. and Golliday, C. L., "The Inverted Pendulum and Biped Stability." *Mathematical Biosciences*, 34, 95-110, 1977.

[50] Hemami, H. and Jaswa, V. C., "On a Three-Link Model of the Dynamics of Standing Up and Sittion Down." *IEEE Trans. on Systems, Man, and Cybernetics*, vol. SMC-8, no. 2, pp. 115-120, Feb. 1993

[51] Hemami, H. and Wyman, B. F., "Modeling and Control of Constrained Dynamic Systems with Application to Biped Locomotion in the Frontal Plane." *IEEE Trans. on Automatic Control*, vol. AC-24, no. 4, pp. 526-535, Aug 1976.

[52] Hemami, H., and Zheng, Y.F., "Dynamics and Control of Motion on the Ground and in the Air with Applications to Biped Robots." *J. Robotic Systems*, vol. 1, no. 1, pp. 101-116, 1984.

[53] Hemami, H., Weimer, F. C., and Koozekanani, S. H., "Some Aspects of the Inverted Pendulum Problem for Modeling of Locomotion Systems." *IEEE Trans. on Automatic Control*, pp. 658-661, Dec 1973.

[54] Hemami, H., Hines M. J., Goddard, R. E., and Friedman, B., "Biped Sway in the Frontal Plane with Locked Knees." *IEEE Trans. on Systems, Man, and Cybernetics*, vol. SMC-12, no. 4, Jul/Aug 1982, pp 577-582.

[55] Hodgins, J. K., "Simulation of Human Running." *Proc. of the 1994 IEEE Int. Conference on Robotics and Automation*, vol. 3, pp. 1320-1325, 1994.

[56] Hodgins, J. K. and Raibert, M. H., "Biped Gymnastics." *Int. J. of Robotics Research*, vol. 9, no. 2, pp. 115-132, April 1990.

[57] Hodgins, J. K., Wooten, W. L., Brogan, D. C., and O'Brien J. F., "Animating Human Athletics." *Computer Graphics (proc. SIGGRAPH)*, pp. 71-78, Aug, 1995.

[58] Hollerbach, J. M., "A Recursive Lagrangian Formulation of Manipulator Dynamics and a Comparative Study of Dynamics Formulation Complexity." *IEEE Trans. on Systems, Man, and Cybernetics*, vol. SMC-10, no. 11, pp. 730-736, Nov. 1980.

[59] Huston, R. L. *Multibody Dynamics*, Butterworth-Heinemann, Boston, 1990.

[60] Inman, V. T., Ralston, H.J., and Todd, F., *Human Walking*, Williams & Wilkins; Baltimore, MD, 1981.

[61] Iqbal, K. and Hemami, H., "Simultaneous Stabilization and Decoupling of Constrained Robotic Systems with Minimal Inputs." *IEEE Trans. on Systems, Man, and Cybernetics*, vol. 22, no. 5, pp. 945-952, Sept./Oct. 1992.

[62] Isaacs, P. M. and Cohen. M. F., "Controlling Dynamic Simulation With Kinematic Constraints, Behavior Functions and Inverse Dynamics." *Computer Graphics (proc. SIGGRAPH)*, vol. 21, no. 4, July 1987.

[63] Jameson, J. W. "*The Walking Gyro.*" Robotics Age, vol. 7, no. 1, pp. 7-10, 1985.

[64] Kajita, S. and Tani, K., "Study of Dynamic Biped Locomotion on Rugged Terrain." *Proc. of the 1991 IEEE Int. Conference on Robotics and Automation*, pp. 1405-1652, Apr. 1991.

[65] Kallel, H. Hemami, H., and Simon, S., "Postural Stability of Constrained Three Dimensional Robotic Systems." *IEEE Int. Conference on Robotics and Automation*, vol. 3, pp. 2120-2124, 1990.

[66] Kane, T. R. and Levinson, D. A., "The Use of Kane's Dynamical Equations in Robotics." *Int. J. Robotics Research*, vol. 2, no. 3, pp. 3-21, 1983.

[67] Kane, T. R. and Levinson, D. A., *Dynamics: Theory and Applications*, McGraw-Hill, New York, 1985.

[68] Kearney, J. K. and Hanson, S., "Generalizing the Hop: Object-level programming for legged motion." *Proc. of the 1992 IEEE Int. Conference on Robotics and Automation*, vol. 1, pp. 136-142, May 1992.

[69] Kim, S. S, amd Vanderploeg, M. J., "A General and Efficient Method for Dynamic Analysis of Mechanical Systems Using Velocity Transformations." *J. of Mechanisms, Transmissions, and Automation Design*, vol. 108, pp. 176-182, June 1986.

[70] Kitamura, S. and Kurematsu, Y., "Autonomous Motion Planning and Learning Control of a Biped Locomotive Robot." *11th IFAC World Congress*, vol. 9, pp. 205-210.

[71] Kitamura, S., Kurematsu, Y., and Iwata, M., "Motion Generation of a Biped Locomotive robot using an Inverted Pendulum Model and Neural Networks." *Proc. of the 29th Conference on Decision and Control*, IEEE, 1990, pp. 3308-3312.

[72] Kwakernaak, H. and Sivan, R., *Linear Optimal Control Systems*, Wiley, New York, 1972.

[73] Leih, J. "Computer-Aided Modeling and Control of Multibody Systems for Robotics Applications." *Proc. of the 1991 IEEE Int. Conference on Robotics and Automation*, pp. 2385-2390, Apr. 1991.

[74] Lewis, F. L., *Optimal Controls*, Wiley, New York, 1986.

[75] Lewis, F. L., *Applied Optimal Control and Estimation*, Prentice-Hall, Englewood Cliffs, NJ, 1992.

[76] Lewis, F. L., Abdallah. C. T., and Dawson, D. M., *Control of Robot Manipulators*, Macmillan Publishing Co., New York, 1993.

[77] Lin, T. and Yae, K.H., "Recursive Linearization of Multibody Dynamics and Application to Control Design." *J. Mechanical Design*, June 1994, Vol. 116, pp. 445-451.

[78] Long, G. L. and Paul, R. P., "Singularity Avoidance and the Control of an Eight-Revolute-Joint Manipulator." *Int. J. of Robotics Research*, vol. 11, no. 6, pp. 503-515, Dec. 1992

[79] Lynch, A. G. and Vanderploeg, M. J., "A Symbolic Formulation for Linearization of Multibody Equations of Motion." in *Computers in Engineering*, Kinzel G. L. et. al. eds., ASME, New York, pp. 201-207, 1990.

[80] Maciejowski, J. M., *Multivariable Feedback Design*, Addison-Wesley, Reading, MA, 1989.

[81] Manko, D. J., "Inverse Dynamics Models of Closed-Chain Mechanisms With Contact Compliance." *ASME J. Mech. Design*, vol. 114, pp. 82-86, Mar.1992.

[82] Manko, D. J., *A General Model of Legged Locomotion on Natural Terrain.* Kluwer Academic Publishers, Boston, 1992.

[83] McGeer, T., "Passive Dynamic Walking." *Int. J. of Robotics Research*, vol. 9, no. 2, pp. 62-82, Apr. 1990.

[84] M'Closkey, R. T. and Burdick, J. W., "Periodic Motions of a Hopping Robot With Vertical and Forward Motion." *Int. J. Robotics Research*, vol. 12, no. 3, pp. 197-218, 1993.

[85] McMahon, T. A., "Mechanics of Locomotion." *Int. J. Robotics Research*, vol. 3, no. 2, pp. 4-28, 1984.

[86] Meglan, D. A. "Enhanced Analysis of Human Locomotion" Ph.D. Dissertation, Ohio State University, Columbus, OH, 1991.

[87] Meirovitch, L., *Methods of Analytical Dynamics*, McGraw-Hill, New York, 1970.

[88] Mena, D., Mansour, J.M., and Simon, S.R., "Analysis and Synthesis of Human Swing Leg Motion During Gait and its Clinical Applications." *J. Biomechanics*, vol. 14, no. 12, pp. 823-832. 1981.

[89] Meyer, A., "An efficient implementation of LU decomposition in C." *Adv. Eng. Software*, 1988, vol. 10, no 3. pp 123-130.

[90] Miller, T.W., "Real-Time Neural Network Control of a Biped Walking Robot." *Control Systems*. Feb, 1994, vol. 14, no. 1. pp. 41-48.

[91] Mita, T., Yamaguchi, T., Kashiwase, T., and Kawase, T., "Realization of a high speed biped using modern control theory." *Int. J. Control*, 1984, vol. 40, no 1. pp. 107-119.

[92] Miura, H. and Shimoyama, I., "Dynamic Walk of a Biped." *Int J. of Robotics Research*, vol. 3, no. 2, pp. 60-74, Apr. 1984.

[93] Miura, H., "Researches of the Biped Robot in Japan." *Dynamics of Controller Mechanical Systems, IUTAM/IFAC,* pp 366-377, 1988.

[94] Miyamoto, H., Israel, I., Miyamoto, H., Mori, S., Sano, A., and Sakurai, Y., "Approach to a Powered Orthosis for Paralyzed Lower Limbs.", in *Proc. of '85 Int. Conference on Advanced Robotics (ICAR)*, Robotics Society of Japan, pp. 451-458, 1985.

[95] Miyazaki, F. and Arimoto, S., "A Control Theoretic Study on Dynamical Biped Locomotion." J. *Dynamic Systems, Measurement, and Control*, vol. 102, pp. 233-239, Dec. 1980.

[96] Murphy, K.N. and Raibert, M.H., "Trotting and Bounding in a Planar Two-legged Model." in *Theory and Practice of Robots and Manipulators: Fifth Symposium*, Morecki, A., Bianchi, G., and Kedzior, K. (eds.), pp 411-420, MIT Press, Cambridge, MA, 1985.

[97] Narendra, K. S., and Parthasarathy, K., "Neural networks in dynamic systems." *Intelligent Control and Adaptive Systems*, SPIE vol. 1196, pp. 230-241, 1989.

[98] Narendra, K. S., and Parthasarathy, K., "Identification and Control of Dynamical Systems Using Neural Networks." *IEEE Trans. on Neural Networks*, vol. 1, no. 1, pp. 4-27, Mar. 1990.

[99] Narikiyo, T. and Ito, M. "Control of a biped locomotion system in a double support phase." *Robotica*, vol. 3, pp. 73-77, 1985.

[100]Nikravesh, P.E., *Computer-Aided Analysis of Mechanical Systems*, Prentice-Hall, Englewood Cliffs, NJ, 1988.

[101]Norcross, R. J., Wang, J. C., McInnis B. C., and Shieh, L. S., "Pole Placement Methods for Multivariable Control of Robotic Manipulators." *J. Dynamic Systems, Measurement, and Control.* vol. 108, pp. 340-345, Dec. 1986.

[102]Ogata, K., *Modern Control Engineering*, 2nd ed. Prentice-Hall, Englewood Cliffs, NJ, 1990.

[103]Orin, D. E. and Schrader W. W., "Efficient Computation of the Jacobian for Robot Manipulators." *Int. J. Robotics Research*, vol. 3, no. 4, pp. 66-75, 1984.

[104]Orin, D.E., McGhee, R.B., Vukobratovic, M., and Hartoch, G., "Kinematic and Kinetic Analysis of Open-Chain Linkages Utilizing Newton-Euler Methods." *Mathematical Biosciences*, (43) pp. 107-130, 1979.

[105]Pandy, M. G. and Berme, N., "Quantitative Assessment of Gait Determinants During Single Stance via a Three-Dimensional Model." *J. Biomechanics*, vol. 22, no. 6/7, pp. 717-724, 1989.

[106]Paul, R. P., *Robot Manipulators: Mathematics, Programming, and Control*, MIT Press, Cambridge, MA, 1981.

[107]Press, W. H., Flannery, B. P., Teukolsky, S. A., and Vetterling, W. T., *Numerical Recipes, The Art of Scientific Computing*, Cambridge University Press, Cambridge, 1989.

[108]Pugh, D. R., Ribble, E. A., Vohnout, V. J., Bihari, T. E., Walliser, T. M., Patterson, M. R., and Waldron, K. J., "Technical Description of the Adaptive Suspension Vehicle" *Int. J. of Robotics Research*, vol. 9, no. 2, pp. 24-42, Apr. 1990.

[109]Raibert, M.H., Brown, H. B., and Chepponis, M., "Experiments in Balance with a 3D One-Legged Hopping Machine." *Int. J. of Robotics Research*, vol. 3, no. 2, pp. 75-92, 1984.

[110]Raibert, M.H. and Murphy, K. N., "Trotting and Bounding in a Planar Two-Legged Model." *Theory and Practice of Robots and Manipulators*, Morecki, A. et. al. eds., MIT Press, Cambridge, 1985.

[111]Raibert, M.H., *Legged Robots that Balance*, MIT Press, Cambridge, MA, 1986.

[112]Raibert, M.H. and Hodgins, J. K., "Animation of Dynamic Legged Locomotion." *Computer Graphics (proc. SIGGRAPH)*, vol. 25, no. 4, pp. 349-358, July 1991.

[113]Ralston, H. J., "Energetics of Human Walking." in *Neural Control of Locomotion*, Herman, R. M., et al. eds., Plenum Press, New York, pp. 7-98, 1976.

[114]Redfern, M. S. and Schumann, T., "A Model of Foot Placement During Gait." *J. Biomechanics*, vol. 27, no. 11, pp. 1339-1346, 1994.

[115]Rose J. and Gamble J.G., *Human Walking*, 2nd ed., Williams & Wilkins; Baltimore, MD, 1994.

[116]Saito, F., Fukuda, T., and Arai, F., "Swing and Locomotion Control for a Two-Link Brachiation Robot." *Control Systems*. Feb, 1994, Vol. 14, No. 1. pp. 5-12.

[117]Shieh, L. S. and Tsay, Y. T., "Transformations of a Class of Multivariable Control Systems to Block Companion Forms." *IEEE Trans. on Automatic Control*, vol. AC-27, no. 1, Feb. 1982.

[118]Shih, C. L., Li, Y. Z., Churng, S., Lee, T. T., and Gruver, W. A., "Trajectory Synthesis and Physical Admissibility for a Biped Robot During the Single-Support Phase." *IEEE Int. Conference on Robotics and Automation*, vol. 3, pp. 1646-1652, 1990.

[119]Shih, C. L. and Gruver, W. A., "Control of a Biped Robot in the Double-Support Phase." *IEEE Trans. Systems, Man, and Cybernetics*, vol. 22, no. 4, pp. 729-735, 1992.

[120]Stitt, S. and Zheng, Y. F., "Distal Learning Applied to Biped Robots." *Proc. of the 1994 IEEE Int. Conference on Robotics and Automation*. IEEE Computer Society Press, Los Alamitos, CA, vol. 1, pp. 137-142, 1994.

[121]Symon, K. R., *Mechanics*, 3rd ed., Addison-Wesley, Reading, MA, 1971

[122]Takanishi, A., Naito, G., Ishida, M., and Kato, I. "Realization of Plane Walking by the Biped Walking Robot WL-10R" in *Theory and Practice of Robots and Manipulators: Fifth Symposium*. Morecki, A., Bianchi, G., and Kedzior, K. (eds.), pp 383-394, MIT Press, Cambridge, MA, 1985.

[123]Takanishi, A., Ishida, M., Yamazaki, Y., and Kato, I. "Realization of Dynamic Walking by the Biped Walking Robot WL-10RD" in *Proc. of '85 Int. Conference on Advanced Robotics (ICAR)*, Robotics Society of Japan, pp. 459-466, 1985.

[124]Todd, D.J., *Walking Machines an Introduction to Legged Robots*, Anchor Press, London, 1985.

[125]Townsend, M. A., "Biped Gait Stabilization via Foot Placement." *J. Biomechanics*, vol. 18, no. 1, pp. 21-38, 1985.

[126]Townsend, M. A. and Tsay, T. C., "Biomechanics and Modelling of Bipedal Climbing and Descending." *J. Biomechanics*, vol. 9, pp. 227-239, 1976.

[127]Townsend, M. A. and Seireg, A. A., "Effect of the Model Complexity and Gait Criteria on the Synthesis of Bipedal Locomotion." *Trans. Biomedical Engineering*, vol. BME-20, no. 6, pp. 433-444, Nov, 1973.

[128]Townsend, M. A. and Seireg, A. A., "The Synthesis of Bipedal Locomotion." *J. Biomechanics*, vol. 5, pp. 71-83, 1972.

[129]Trom J. D., and Vanderploeg, M. J., "Automated Linearizarion of Nonlinear Coupled Differential and Algebraic Equations." *J. Mech. Design*, vol. 113, no. 2, pp. 429-436, June, 1994.

[130]Troy, J. J. "An interactive graphical approach to off-line programming." M.S. Thesis, Iowa State University, Ames, IA, 1992.

[131]Troy, J. J., and Vanderploeg, M.J., "Interactive Simulation and Control of Planar Biped Walking Devices." *Workshop on Simulation and Interaction in Virtual Environments (SIVE)*. pp. 220-224, July 1995.

[132]Unuma, M., Anjyo, K. and Takeuchi, R. "Fourier Principles for Emotion-based Human Figure Animation." *Computer Graphics (proc. SIGGRAPH)*, pp. 91-96, Aug, 1995.

[133]Vaughan, C. L. and Sussman, M. D., "Human Gait: From Clinical Interpretation to Computer Simulation." in *Current Issues in Biomechanics*, Grabiner M. D. ed., Human Kinetics Publishers, Champaign, IL. pp. 53-68, 1993.

[134]Vukobratovic, M., Frank, A. and Juricic, D., "On the Stability of Biped Locomotion." *IEEE Trans. on Bio-Medical Engineering*, vol BME- 17, no. 1, pp 25-36, Jan 1970.

[135]Vukobratovic, M. and Stepanenko, J., "On The Stability of Anthropomorphic Systems." *Mathematical Biosciences*, vol. 15, pp. 1-37, 1972.

[136]Vukobratovic, M. and Stepanenko, J., "Mathematical Models of General Anthropomorphic Systems." *Mathematical Biosciences*, vol. 17, pp. 191-242, 1973.

[137]Vukobratovic, M., *Applied Dynamics of Manipulation Robots*, Spriner-Verlag, New York, 1989.

[138]Vukobratovic, M., Brovac, B., Surla, D., and Stokic, D., *Biped Locomotion*, Spriner-Verlag, New York, 1990.

[139]Witkin, A., and Popovic, Z., "Motion Warping." *Computer Graphics (proc. SIGGRAPH)*, pp. 105-108, Aug, 1995.

[140]Wells, D.A., *Theory and Problems of Lagrangian Dynamics*. McGraw- Hill, New York, 1967.

[141]Walker, M.W. and Orin, D.E., "Efficient dynamic Computer Simulation of Robotic Mechanisms." *J. Dynamic Systems, Measurement, and Control*, vol. 104, pp. 205-211, Sept. 1982.

[142]Yamada, M., "Dynamic Control of Walking Robot with Kick-Action." in *Proc. of '85 Int. Conference on Advanced Robotics (ICAR)*, Robotics Society of Japan, pp. 405-412. 1985.

[143]Yamaguchi, G. T., "Performing Whole-Body Simulations of Gait with 3-D, Dynamic Musculoskeletal Models." in *Multiple Muscle Systems: Biomechanics and Movement Organization,* Winters, J. M. and Woo, S. L-Y., eds, Springer-Verlag, pp. 663-679, 1990.

[144]Yamaguchi, G. T., Pandy, M. G., and Zajac, F. E., "Dynamic Musculoskeletal Models of Human Locomotion: Perspectives on Model Formulation and Control." in *Adaptability of Human Gait Implications for the Control of Locomotion*, Patla, A.E. ed, North-Holland, Amsterdam, pp. 205-240, 1991.

[145]Young, D. E. and Schmidt. R. A. "Motor Programs as Units of Movement Control." in *Making Them Move*, Badler, N. I. et al. eds., pp. 129-155, Morgan Kaufmann Publishers, San Mateo, CA, 1991.

[146]Zelder, D., "Task-level Graphical Simulation: Abstraction, Representation, and Control." in *Making Them Move*, Badler, N. I. et al. eds., pp. 3-33, Morgan Kaufmann Publishers, San Mateo, CA, 1991.

[147]Zheng, Y.F. and Hemami, H., "Impact Effects of Biped Contact With the Environment." *IEEE Trans. on Systems, Man, and Cybernetics*, vol. SMC-14, no. 3, May/June 1984, pp 437-443.

[148]Zheng, Y.F. and Hemami, H., "Mathematical Modeling of a Robot Collision with its Environment." *J. Robotic Systems*, 2(3), pp. 289-307, 1985.

[149]Zheng, Y.F. and Hemami, H., "Control of the Heel-Off to Toe-Off Motion of a Dynamic Biped Gait." *IEEE Trans. on Systems, Man, and Cybernetics*, vol. 22, no. 1, pp. 92-102, 1992.

[150]Zheng, Y.F. and Shen, J., "Gait Synthesis for the SD-2 Biped Robot to Climb Sloping Surface." *IEEE Trans. on Robotics and Automation*, vol. 6, no. 1, pp. 86-96, Feb 1990.

APPENDIX A: SUPPLEMENTAL MODELS

This Appendix contains derivations of symbolic equations of motion for planar and three dimensional bipeds and other models referred to in Chapter 4 on physically based modeling.

A.1 Preliminary Systems

Preliminary models of several types of inverted pendulum systems will be combined in various ways for form the planar monoped and biped systems. The systems developed here include: single, double, and triple link inverted pendulum; and single and double link inverted pendulum-cart systems.

A.1.1 Inverted Pendulum System

The basic model for monoped and biped systems is based on the a single link inverted pendulum model shown in Figure A.1. This system has only one degree-of-freedom (DOF). It consists of one rigid link connected to the ground by a 1-DOF revolute joint. Two external moments and distal force components are included in this model. Viscous damping the revolute joint is also included.

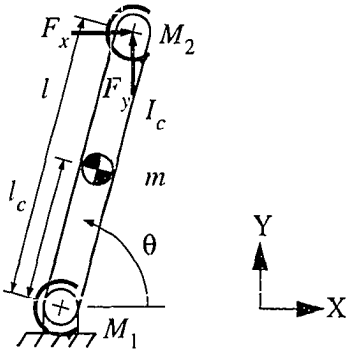

Figure A.1 Inverted pendulum

Nonlinear equations of motion

Using Lagrange's equations, the equation of motion can be derived as follows:

$$L = T - V = \frac{d}{dt}\left(\frac{\partial T}{\partial \dot{q}_i}\right) - \frac{\partial T}{\partial \dot{q}_i} + \frac{\partial V}{\partial q_i} = Q_i$$

$$T = \frac{1}{2} I_c \dot{\theta}^2 + \frac{1}{2} m\left[(-L_c \dot{\theta} \cos\theta)^2 + (-L_c \dot{\theta} \sin\theta)^2 \right] \tag{A.1}$$

$$V = mgL_c \sin\theta \tag{A.2}$$

$$(I_c + mL_c^2)\,\ddot{\theta} + mgL_c \cos\theta = M \tag{A.3}$$

Linearized equation of motion

$$(I_c + mL_c^2)\,\ddot{\theta} - mgL_c(\theta - 90°) = M \tag{A.4}$$

where system is linearized about $\theta = 90°$.

A.1.2 Inverted Pendulum-Cart Systems

The inverted pendulum-cart system is one of the most basic plant models used for balancing control development. These 2-DOF and 3-DOF systems, Figure A.2(a) and Figure A.2(b) respectively, consists of a rigid link connected to a block (cart) by a 1-DOF revolute joint. The block is either a 1-DOF or a 2-DOF frictionless translational element. Two external moments (including one at the distal end of the last link in the chain), external block forces, and distal force components are included in this model. Viscous damping of the revolute joint is also included.

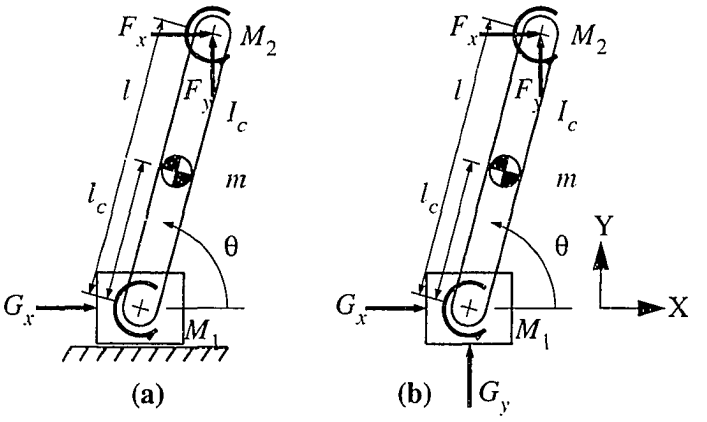

Figure A.2 Inverted pendulum-cart systems: (a) sliding on ground, (b) in space

Nonlinear equations of motion

The nonlinear equations of motion for the 2-DOF inverted pendulum-cart system of Figure A.2(a) sliding on a frictionless surface are derived using Lagrange methods below:

$$T = \frac{1}{2} I_c \dot{\theta}^2 + \frac{1}{2} m_1 \left[(\dot{x} - L_c \dot{\theta} \cos\theta)^2 + (-L_c \dot{\theta} \sin\theta)^2 \right] + \frac{1}{2} m_2 \dot{x}^2 \tag{A.5}$$

$$V = -mgL_c (1 - \cos\theta) \tag{A.6}$$

$$(I_c + mL_c^2)\ddot{\theta} - (m_1 L_c \cos\theta)\ddot{x} - mgL_c \sin\theta = M_1 + M_2 \tag{A.7}$$

$$(m_1 + m_2)\ddot{x} - (m_1 L_c \cos\theta)\ddot{\theta} + (m_1 L_c \sin\theta)\dot{\theta}^2 = G_x \tag{A.8}$$

The same system with the surface replaced with an explicit vertical force component resulting in the 3-DOF system of Figure A.2(b), is derived below:

$$T = \frac{1}{2} I_c \dot{\theta}^2 + \frac{1}{2} m_1 \left[(\dot{x} - L_c \dot{\theta} \cos\theta)^2 + (\dot{y} - L_c \dot{\theta} \sin\theta)^2 \right] + \frac{1}{2} m_2 (\dot{x}^2 + \dot{y}^2) \tag{A.9}$$

$$V = -mgL_c (1 - \cos\theta) + m_2 g y \tag{A.10}$$

$$(I_c + mL_c^2)\ddot{\theta} - (m_1 L_c \cos\theta)\ddot{x} - mgL_c \sin\theta = M_1 + M_2 \tag{A.11}$$

$$(m_1 + m_2)\ddot{x} - (m_1 L_c \cos\theta)\ddot{\theta} + (m_1 L_c \sin\theta)\dot{\theta}^2 = G_x \tag{A.12}$$

$$(m_1 + m_2)\,\ddot{y} - (m_1 L_c \sin\theta)\,\ddot{\theta} - (m_1 L_c \cos\theta)\,\dot{\theta}^2 = G_y - (m_1 + m_2)\,g \qquad \text{(A.13)}$$

Linearized equations of motion

$$(I_c + mL_c^2)\,\ddot{\theta} - m_1 L_c \ddot{x} - mgL_c\theta = M_1 + M_2 \qquad \text{(A.14)}$$

$$(m_1 + m_2)\,\ddot{x} - m_1 L_c \ddot{\theta} = G_x \qquad \text{(A.15)}$$

$$(m_1 + m_2)\,\ddot{y} = G_y - (m_1 + m_2)\,g = G_y \qquad \text{(A.16)}$$

A.1.3 Double Inverted Pendulum System

This 2-DOF open chain system (Figure A.3) consists of two rigid links connected together and to the ground by 1-DOF revolute joints. Three external moments (including one at the distal end of the last link in the chain) and final link distal force components are included in this model. Viscous damping at each revolute joint is also included.

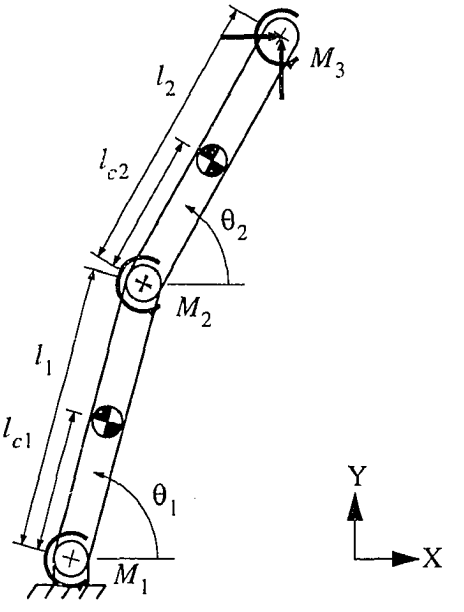

Figure A.3 Double inverted pendulum system

Nonlinear equations of motion

```
m1*Add*Lc1^2+m2*Add*L1^2+m2*L1*Bdd*Lc2*cos(A-B)+
m2*L1*Bd^2*Lc2*sin(A-B)+m1*g*Lc1*cos(A)+m2*g*cos(A)*L1

m2*Lc2*(Add*L1*cos(A-B)-Ad^2*L1*sin(A-B)+Bdd*Lc2+g*cos(B))
```

A.1.4 Double Inverted Pendulum-Cart Systems

The 4-DOF and 5-DOF open chain systems of Figure A.4(a) and Figure A.4(b) respectively, consist of two rigid links connected together and to the block (cart) by 1-DOF revolute joints. The block is either a 1-DOF or a 2-DOF frictionless translational element. Three external moments (including one at the distal end of the last link in the chain), cart external forces, and final link distal force components are included in this model. Viscous damping at each revolute joint is also included.

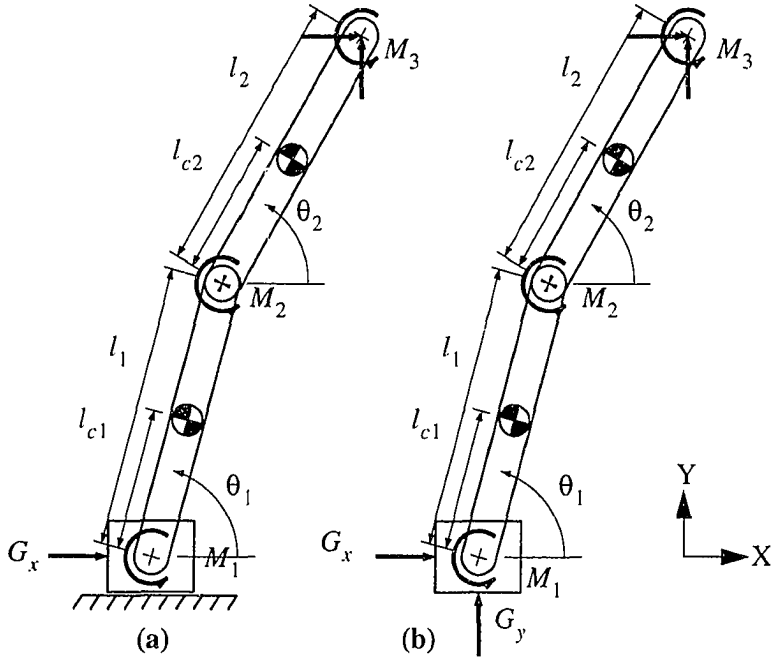

Figure A.4 Double inverted pendulum systems: (a) sliding on ground, (b) in space

Nonlinear equations of motion

The nonlinear equations of motion for the 4-DOF inverted pendulum-cart system of Figure A.4(a) sliding on a frictionless surface are derived using Lagrange methods below (due to time constraints some equations were entered as text instead of the usual equation format):

```
Ic1*Add+m1*Add*Lc1^2+m2*Add*L1^2+m2*L1*Bdd*Lc2*cos(A-B)
+m2*L1*Bd^2*Lc2*sin(A-B)+m1*g*Lc1*cos(A)+m2*g*cos(A)*L1

Ic2*Bdd+m2*Add*L1*Lc2*cos(A-B)-m2*Ad^2*L1*Lc2*sin(A-B)
+m2*Bdd*Lc2^2+m2*g*cos(B)*Lc2
```

Linearized equations of motion

```
(-m1*g*Lc1*sin(A)-m2*g*sin(A)*L1)*del_A
+Add*(Ic1+m1*Lc1^2+m2*L1^2)  +m2*L1*Bdd*Lc2*cos(A-B)

-m2*g*sin(B)*Lc2*del_B+m2*Add*L1*Lc2*cos(A-B)
+Bdd*(Ic2+m2*Lc2^2)
```

The same system with the surface replaced with an explicit vertical force component resulting in the 5-DOF system of Figure A.2(b), is derived in a manner similar to the single inverted pendulum.

```
(-m2*sin(A)*L1-m1*sin(A)*Lc1)*Add+(m2+m1)*Xdd-
m2*Ad^2*cos(A)*L1-m2*Bdd*sin(B)*Lc2-m2*Bd^2*cos(B)*Lc2-
m1*Ad^2*cos(A)*Lc1

(m1*cos(A)*Lc1+m2*cos(A)*L1)*Add+(m2+m1)*Ydd+m2*Bdd*cos(B)*Lc2
-m1*Ad^2*sin(A)*Lc1+m1*g-m2*Ad^2*sin(A)*L1-m2*Bd^2*sin(B)*Lc2
+m2*g
```

```
(m2*L1^2+Ic1+m1*Lc1^2)*Add+(m1*cos(A)*Lc1+m2*cos(A)*L1)*Ydd
+(-m2*sin(A)*L1-m1*sin(A)*Lc1)*Xdd+m2*L1*Bd^2*Lc2*sin(A-B)
+m1*g*cos(A)*Lc1+m2*g*cos(A)*L1+m2*L1*Bdd*Lc2*cos(A-B)

(m2*Lc2^2+Ic2)*Bdd+m2*Add*L1*Lc2*cos(A-B)+m2*Ydd*cos(B)*Lc2-
m2*Xdd*sin(B)*Lc2-m2*Ad^2*L1*Lc2*sin(A-B)+m2*g*cos(B)*Lc2
```

A.1.5 Triple Pendulum System

This 3-DOF open chain system (Figure A.5) consists of three rigid links connected together and to the ground by 1-DOF revolute joints. Four external moments (including one at the distal end of the last link in the chain) and final link distal force components are included in this model. Viscous damping at each revolute joint is also included.

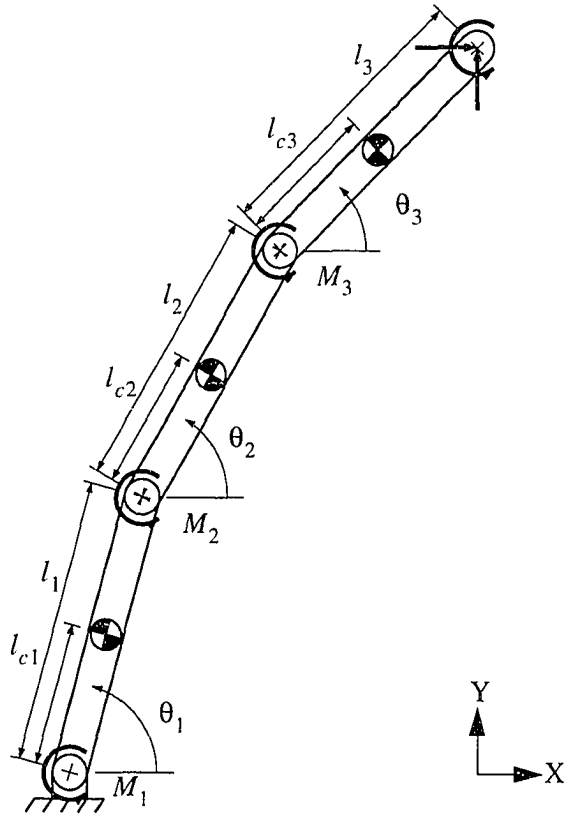

Figure A.5 Triple inverted pendulum system

Equations of motion

```
(m3*L1*L2*cos(A-B)+m2*L1*Lc2*cos(A-B))*Bdd
+(m2*L1^2+m3*L1^2+Ic1+m1*Lc1^2)*Add+m3*L1*Bd^2*L2*sin(A-B)
+m3*L1*Cdd*Lc3*cos(A-C)+m1*g*Lc1*cos(A)+m2*L1*Bd^2*Lc2*sin(A-
B) +m3*L1*Cd^2*Lc3*sin(A-C) +m2*g*cos(A)*L1 +m3*g*cos(A)*L1

(L2^2*m3+Lc2^2*m2+Ic2)*Bdd+(m3*L1*L2*cos(A-B)+
m2*L1*Lc2*cos(A-B))*Add-m2*Ad^2*L1*Lc2*sin(A-B)-
m3*L2*Cd^2*Lc3*sin(B+C)+m3*L2*Cdd*Lc3*cos(-B+C)-
m3*Ad^2*L1*L2*sin(A-B)+m3*g*cos(B)*L2+m2*g*cos(B)*Lc2

(m3*Lc3^2+Ic3)*Cdd-m3*Ad^2*L1*Lc3*sin(A-C)
+m3*Add*L1*Lc3*cos(A-C)+m3*Bd^2*L2*Lc3*sin(-B+C)
+m3*Bdd*L2*Lc3*cos(-B+C)+m3*g*cos(C)*Lc3
```

Linearized equations of motion

```
(-m3*L1-m1*Lc1-m2*L1)*g*sin(A)*del_A
+(Ic1+m1*Lc1^2+m3*L1^2+m2*L1^2)*Add+L1*cos(A-B)*
(m2*Lc2+m3*L2)*Bdd +m3*L1*Cdd*Lc3*cos(A-C)

(-m3*L2-m2*Lc2)*g*sin(B)*del_B+L1*cos(A-B)*(m2*Lc2+m3*L2)*Add
+(L2^2*m3+Lc2^2*m2+Ic2)*Bdd+m3*L2*Cdd*Lc3*cos(-B+C)

-m3*g*sin(C)*Lc3*del_C+m3*Add*L1*Lc3*cos(A-C)
+m3*Bdd*L2*Lc3*cos(-B+C)+(m3*Lc3^2+Ic3)*Cdd
```

Equilibrium position calculation

```
th2 = [-phi+2*atan((B-(B^2+A^2-M21^2)^(1/2))/(A+M21))]

[-phi+2*atan((B+(B^2+A^2-M21^2)^(1/2))/(A+M21))]
```

```
M31 = [C*cos(-phi+2*atan((B-(B^2+A^2-M21^2)^(1/2))/
(A+M21)))+D*sin(-phi+2*atan((B-(B^2+A^2-M21^2)^(1/2))/
(A+M21)))-M21]

[C*cos(-phi+2*atan((B+(B^2+A^2-M21^2)^(1/2))/(A+M21)))
+D*sin(-phi+2*atan((B+(B^2+A^2-M21^2)^(1/2))/(A+M21)))-M21]

th3 = [-2*atan((F+(F^2+E^2-M31^2-2*M31*M32-M32^2)^(1/2))/(-
E+M31+M32))]
```

A.2 2-Link Monoped

Nonlinear equations of motion

```
(m1+m2)*Xdd-m1*Lc1*sA*Add-m2*Lc2*sB*Bdd = -(-m1*Lc1*cA*Ad*Ad-
m2*Lc2*cB*Bd*Bd-Gx

(m1+m2)*Ydd+m1*Lc1*cA*Add+m2*Lc2*cB*Bdd = -(-m1*Lc1*sA*Ad*Ad
+(m1+m2)*g-m2*Lc2*sB*Bd*Bd-Gy)

-m1*Lc1*sA*Xdd+m1*Lc1*cA*Ydd+(Ic1+m1*Lc1*Lc1)*Add = -
(m1*g*Lc1*cA-M)

-m2*Lc2*sB*Xdd+m2*Lc2*cB*Ydd+(Ic2+m2*Lc2*Lc2)*Bdd = -
(m2*g*Lc2*cB+M+Gx*L2*sB-Gy*L2*cB)
```

A.3 3-Link Monoped

Nonlinear equations of motion

```
m1*Xdd-m1*Lc1*sA*Add-m1*Lc1*cA*Ad*Ad+(m2+m3)*Xdd-
(m2*Lc2+m3*L2)*sB*Bdd-(m2*Lc2+m3*L2)*cB*Bd*Bd-m2*Lc3*sC*Cdd-
m2*Lc3*cC*Cd*Cd-Gx3 = 0
```

```
m1*Ydd+m1*Lc1*cA*Add-m1*Lc1*sA*Ad*Ad+m1*g+(m2+m3)*Ydd
+(m2*Lc2+m3*L2)*cB*Bdd -(m2*Lc2+m3*L2)*sB*Bd*Bd+m3*Lc3*cC*Cdd-
m3*Lc3*sC*Cd*Cd+(m2+m3)*g-Gy3 = 0

(Ic1+m1*Lc1*Lc1)*Add-m1*Lc1*sA*Xdd+m1*Lc1*cA*Ydd+
m1*g*Lc1*cA+M21 = 0

(Ic2+m2*Lc2*Lc2+m3*L2*L2)*Bdd+m3*Lc3*L2*cos(C-B)*Cdd-
m3*Lc3*L2*sin(C-B)*Cd*Cd+(m2*Lc2+m3*L2)*g*cB-
(m2*Lc2+m3*L2)*sB*Xdd+(m2*Lc2+m3*L2)*cB*Ydd+Gx3*L2*sB-
Gy3*L2*cB -M21+M31 = 0

(Ic3+m3*Lc3*Lc3)*Cdd+m3*Lc3*L2*cos(C-B)*Bdd +m3*Lc3*L2*sin(C-
B)*Bd*Bd +m3*Lc3*g*cC-m3*Lc3*sC*Xdd+m3*Lc3*cC*Ydd+Gx3*L3*sC-
Gy3*L3*cC-M31-M32 = 0
```

Equations of motion for constrained linearized system

```
(-m1*g*Lc1*sin(A)-m2*g*sin(A)*L1-m3*g*sin(A)*L1)*del_A
+(m3*L1^2+Ic1+m1*Lc1^2+m2*L1^2)*Add +L1*cos(A-
B)*(m2*Lc2+m3*L2)*Bdd +m3*L1*Cdd*Lc3*cos(A-C)

(-m3*g*sin(B)*L2-m2*g*sin(B)*Lc2)*del_B +L1*cos(A-
B)*(m2*Lc2+m3*L2)*Add +(m2*Lc2^2+Ic2+m3*L2^2)*Bdd
+m3*L2*Cdd*Lc3*cos(-B+C)

-m3*g*sin(C)*Lc3*del_C +m3*Add*L1*Lc3*cos(A-C)
+m3*Bdd*L2*Lc3*cos(-B+C) +(m3*Lc3^2+Ic3)*Cdd
```

A.4 3-Link Sagittal Plane Biped

The 3-link frontal plane biped non-linear and linearized equations for the foot-ground constrained system are given below.

Nonlinear equations of motion

```
(m2+m3+m1)*Xdd-m1*Lc1*sA*Add-m2*Lc2*sB*Bdd-m3*Lc3*sC*Cdd=-(-
m1*Lc1*cA*Ad^2-m2*Lc2*cB*Bd^2-Gx2-m3*Lc3*cC*Cd^2-Gx3)

(m2+m3+m1)*Ydd+m1*Lc1*cA*Add+m2*Lc2*cB*Bdd+m3*Lc3*cC*Cdd=-(-
m1*Lc1*sA*Ad^2+m1*g-Gy2-Gy3-m2*Lc2*sB*Bd^2+m2*g+m3*g-
m3*Lc3*sC*Cd^2)

-m1*Lc1*sA*Xdd+m1*Lc1*cA*Ydd+(Ic1+m1*Lc1^2)*Add=-
(m1*g*Lc1*cA+M22+M32)

-m2*Lc2*sB*Xdd+m2*Lc2*cB*Ydd+(Ic2+m2*Lc2^2)*Bdd=-((-
Gy2*L2+m2*g*Lc2)*cB-M22-M21+Gx2*Lc2*sB)

-m3*Lc3*sC*Xdd+m3*Lc3*cC*Ydd+(Ic3+m3*Lc3^2)*Cdd=-((-
Gy3*L3+m3*g*Lc3)*cC-M32-M31+Gx3*Lc3*sC)
```

Equations of motion for constrained linearized system

$$\begin{bmatrix} r11 & r12 & r13 \\ r21 & r22 & r23 \\ r31 & r32 & r33 \end{bmatrix} \begin{bmatrix} Add \\ Bdd \\ Cdd \end{bmatrix} = \begin{bmatrix} RHS1 \\ RHS2 \\ RHS3 \end{bmatrix}$$

```
a = Ic1 + m1*Lc1*Lc1 + (m2+m3)*L1*L1;

b = -m2*Lc2*L1*cos(B-A);

c = -m3*Lc3*L1*cos(C-A);

d = ic2 + m2*Lc2*Lc2;

e = ic3 + m3*Lc3*Lc3;

f = (m1*Lc1 + (m2+m3)*L1)*g*sin(A);
```

```
h = m2*Lc2*g*sin(B);

i = m3*Lc3*g*sin(C);

j = m2*Lc2*L1*sin(B-A)*Bd*Bd;

k = m3*Lc3*L1*sin(C-A)*Cd*Cd;

n = m2*Lc2*L1*sin(B-A)*Ad*Ad;

p = m3*Lc3*L1*sin(C-A)*Ad*Ad;

den = a*d*e-b*b*e-c*c*d;

R11 = d*e/den;

R12 = -b*e/den;

R13 = -c*d/den;

R21 = -b*e/den;

R22 = (a*e-c*c)/den;

R23 = b*c/den;

R31 = -c*d/den;

R32 = b*c/den;

R33 = (a*d-b*b)/den;

RHS1 = -f - j - k + U[0] - U[1] - U[3] - (vf11+vf12)*Ad-
vf22*Bd+(vf12+vf22)*Cd;

RHS2 = h + n - U[3] + vf22*(Cd-Bd);

RHS3 = i + p + U[1] + U[3]+ vf12*(Ad-Cd) + vf22*(Bd-Cd);
```

A.5 3-Link Frontal Plane Biped

The 3-link frontal plane biped variable definitions for the foot-ground constrained system are given in Figure A.6. As mentioned earlier, only one type of frontal plane system was developed.

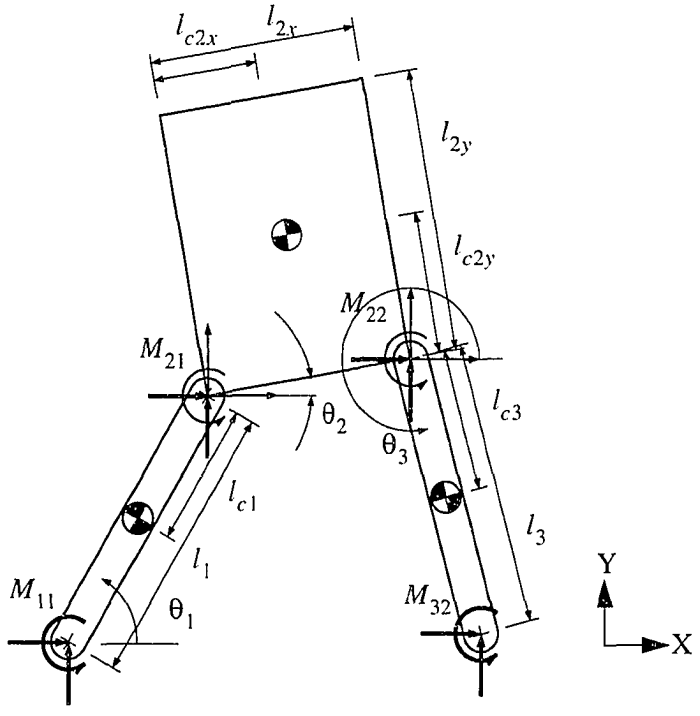

Figure A.6 3-link frontal plane biped variable definitions

Nonlinear equations of motion for constrained system

```
(m1*Lc1^2+m3*L1^2+m2*L1^2+Ic1)*Add+(m3*L1*L2*cos(A-
B)+m2*L1*Lcy2*sin(A-B)+m2*L1*Lcx2*cos(A-B))*Bdd
+m3*L1*Lc3*cos(A-C)*Cdd=-(m2*g*cos(A)*L1+m3*g*cos(A)*L1
+m2*L1*Bd^2*Lcx2*sin(A-B)+m3*L1*Cd^2*Lc3*sin(A-C)
+m3*L1*Bd^2*L2*sin(A-B)-m2*L1*Bd^2*Lcy2*cos(A-B)
+m1*g*Lc1*cos(A))+M1-M2
```

```
(m3*L1*L2*cos(A-B)+m2*L1*Lcy2*sin(A-B)+m2*L1*Lcx2*cos(A-
B))*Add +(m3*L2^2+m2*Lcy2^2+m2*Lcx2^2+Ic2)*Bdd+m3*L2*Lc3*cos(-
B+C)*Cdd=-(m2*Ad^2*L1*Lcy2*cos(A-B)-m3*L2*Cd^2*Lc3*sin(-B+C)-
m3*Ad^2*L1*L2*sin(A-B)+m2*g*Lc2*cos(B+Q)+m3*g*cos(B)*L2-
m2*Ad^2*L1*Lcx2*sin(A-B))+M2-M3

m3*L1*Lc3*cos(A-C)*Add+m3*L2*Lc3*cos(-B+C)*Bdd
+(m3*Lc3^2+Ic3)*Cdd=-(m3*Bd^2*L2*Lc3*sin(-B+C)-
m3*Ad^2*L1*Lc3*sin(A-C)+m3*g*cos(C)*Lc3)+M3
```

Equations of motion for linearized system

```
(m1*Lc1^2+m3*L1^2+m2*L1^2+Ic1)*Add+L1*(m3*L2*cos(A-B)
+m2*Lcy2*sin(A-B)+m2*Lcx2*cos(A-B))*Bdd+m3*L1*Lc3*cos(A-
C)*Cdd=-(-m2*g*sin(A)*L1-m3*g*sin(A)*L1-
m1*g*Lc1*sin(A))*del_A+M1-M2

L1*(m3*L2*cos(A-B)+m2*Lcy2*sin(A-B)+m2*Lcx2*cos(A-B))*Add
+(m3*L2^2+m2*Lcy2^2+m2*Lcx2^2+Ic2)*Bdd+m3*L2*Lc3*cos(-
B+C)*Cdd=-(-m2*g*Lc2*sin(B+Q) -m3*g*sin(B)*L2)*del_B+M2-M3

m3*Add*L1*Lc3*cos(A-C)+m3*Bdd*L2*Lc3*cos(-B+C)
+(m3*Lc3^2+Ic3)*Cdd=m3*g*sin(C)*Lc3*del_C+M3
```

APPENDIX B: NUMERICAL TECHNIQUES

This Appendix discusses procedures for setting up a system of ordinary differential equations (ODEs) to be solved by numerical integration techniques, and iterative solutions techniques to solve algebraic equations.

B.1 Numerical Solutions to Ordinary Differential Equations

This section presents three examples of setting up an ordinary differential equations (ODEs) initial value problem to be solved by numerical techniques.

B.1.1 System setup

The general system of (B.1) is decoupled into the system of (B.2) and then transformed into a series of first order systems. For typical multibody dynamics problems this usually means converting coupled second order systems into $2n$ first order equations. Three examples will serve to explain the procedure in more detail.

$$A\ddot{X} = B \tag{B.1}$$

$$\ddot{X} = A^{-1}B \tag{B.2}$$

Example #1: A 1-DOF second order system

The mass-spring-damper system of Figure B.1 is an example of a simple (i.e. non-coupled) single degree of freedom second order system.

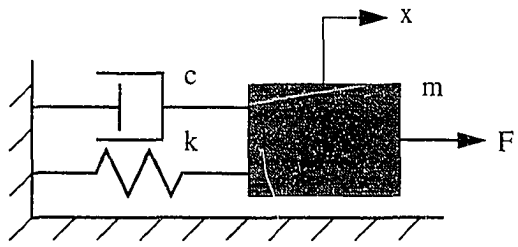

Figure B.1 A 1-DOF second order system

The second order equation of motion for this system is:

$$m\ddot{x} + c\dot{x} + kx = F \tag{B.3}$$

Since only one second order equation is needed to represent this system, the matrix inversion decoupling step is not needed. Converting this to two first order equations proceeds as follows:

$$y_1 = x$$

$$\dot{y}_1 = \dot{x} = y_2$$

$$\dot{y}_2 = \ddot{x} = \frac{F - c\dot{x} - kx}{m} = \frac{F - cy_2 - ky_1}{m}$$

The resulting first order series of equations in matrix form is:

$$\dot{Y} = \begin{bmatrix} \dot{y}_1 \\ \dot{y}_2 \end{bmatrix} = \begin{bmatrix} 0 & 1 \\ -\frac{c}{m} & -\frac{k}{m} \end{bmatrix} \begin{bmatrix} y_1 \\ y_2 \end{bmatrix} + \begin{bmatrix} 0 \\ \frac{1}{m} \end{bmatrix} F \tag{B.4}$$

Example #2: A 2-DOF second order system

The mass-spring-damper system of Figure B.2 is a more complex example in which contains multiple degrees of freedom.

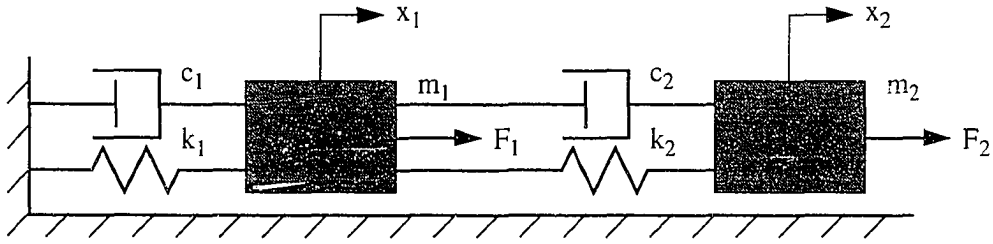

Figure B.2 A 2-DOF second order system

The second order equations of motion for this system are:

$$m_1\ddot{x}_1 + (c_1 + c_2)\dot{x}_1 - c_2\dot{x}_2 + (k_1 + k_2)x_1 - k_2x_2 = F_1 \tag{B.5}$$

$$m_2\ddot{x}_2 + c_2\dot{x}_2 - c_1\dot{x}_1 + k_2x_2 - k_1x_1 = F_2 \tag{B.6}$$

In matrix form:

$$\begin{bmatrix} 1 & 0 \\ 0 & 1 \end{bmatrix}\begin{bmatrix} \ddot{x}_1 \\ \ddot{x}_2 \end{bmatrix} + \begin{bmatrix} c_1 + c_2 & -c_2 \\ -c_2 & c_2 \end{bmatrix}\begin{bmatrix} \dot{x}_1 \\ \dot{x}_2 \end{bmatrix} + \begin{bmatrix} k_1 + k_2 & -k_2 \\ -k_2 & k_2 \end{bmatrix}\begin{bmatrix} x_1 \\ x_2 \end{bmatrix} = \begin{bmatrix} 1 & 0 \\ 0 & 1 \end{bmatrix}\begin{bmatrix} F_1 \\ F_2 \end{bmatrix} \tag{B.7}$$

Solving for the acceleration terms:

$$\ddot{X} = \begin{bmatrix} \ddot{x}_1 \\ \ddot{x}_2 \end{bmatrix} = \begin{bmatrix} 1 & 0 \\ 0 & 1 \end{bmatrix}\begin{bmatrix} F_1 \\ F_2 \end{bmatrix} - \begin{bmatrix} c_1 + c_2 & -c_2 \\ -c_2 & c_2 \end{bmatrix}\begin{bmatrix} \dot{x}_1 \\ \dot{x}_2 \end{bmatrix} - \begin{bmatrix} k_1 + k_2 & -k_2 \\ -k_2 & k_2 \end{bmatrix}\begin{bmatrix} x_1 \\ x_2 \end{bmatrix} \tag{B.8}$$

Note that since the mass matrix is the identity matrix, the decoupling step is not needed. Converting this to four first order equations proceeds as follows:

$$y_1 = x_1$$

$$\dot{y}_1 = \dot{x}_1 = y_2$$

$$\dot{y}_2 = \ddot{x}_1 = \frac{F_1 - (c_1 + c_2)\dot{x}_1 + c_2\dot{x}_2 - (k_1 + k_2)x_1 + k_2x_2}{m_1}$$
$$= \frac{F_1 - (c_1 + c_2)y_2 + c_2y_4 - (k_1 + k_2)y_1 + k_2y_3}{m_1}$$

$$y_3 = x_2$$

$$\dot{y}_3 = \dot{x}_2 = y_4$$

$$\dot{y}_4 = \ddot{x}_2 = \frac{F_2 - c_2\dot{x}_2 + c_2\dot{x}_1 - k_2x_2 + k_2x_1}{m_2}$$
$$= \frac{F_2 - c_2y_4 + c_2y_2 - k_2y_3 + k_2y_1}{m_2}$$

The resulting four first order equations in matrix form:

$$\dot{Y} = \begin{bmatrix} \dot{y}_1 \\ \dot{y}_2 \\ \dot{y}_3 \\ \dot{y}_4 \end{bmatrix} = \begin{bmatrix} 0 & 1 & 0 & 0 \\ -\frac{(k_1 + k_2)}{m_1} & -\frac{(c_1 + c_2)}{m_1} & \frac{k_2}{m_1} & \frac{c_2}{m_1} \\ 0 & 0 & 0 & 1 \\ \frac{k_2}{m_2} & \frac{c_2}{m_2} & -\frac{k_2}{m_2} & -\frac{c_2}{m_2} \end{bmatrix} \begin{bmatrix} y_1 \\ y_2 \\ y_3 \\ y_4 \end{bmatrix} + \begin{bmatrix} 0 & 0 \\ \frac{1}{m_1} & 0 \\ 0 & 0 \\ 0 & \frac{1}{m_2} \end{bmatrix} \begin{bmatrix} F_1 \\ F_2 \end{bmatrix} \qquad \text{(B.9)}$$

Example #3: A coupled second order system

The coupled inverted pendulum-cart system in Figure B.3 (see Appendix A for equation development) is a more complex example in which the uncoupling step of (B.2) will need to be performed prior to converting the system to first order equations. After the decoupling step is performed, the system can be solved using numerical integration.

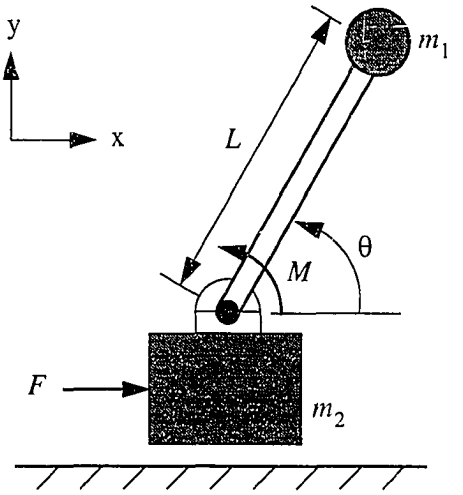

Figure B.3 A 2-DOF, coupled second order system

The equations of motion for this system are:

$$m_1 L^2 \ddot{\theta} - (m_1 L \cos\theta)\,\ddot{x} - mgL\sin\theta = M \tag{B.10}$$

$$(m_1 + m_2)\,\ddot{x} - (m_1 L \cos\theta)\,\ddot{\theta} + (m_1 L \sin\theta)\,\dot{\theta}^2 = F \tag{B.11}$$

In matrix form:

$$\begin{bmatrix} m_1 L^2 & -m_1 L\cos\theta \\ -m_1 L\cos\theta & m_1 + m_2 \end{bmatrix} \begin{bmatrix} \ddot{\theta} \\ \ddot{x} \end{bmatrix} = \begin{bmatrix} mgL\sin\theta \\ -m_1 L \sin\theta \dot{\theta}^2 \end{bmatrix} + \begin{bmatrix} 1 & 0 \\ 0 & 1 \end{bmatrix} \begin{bmatrix} M \\ F \end{bmatrix} \tag{B.12}$$

Note that since the mass matrix is non-diagonal, the decoupling step is required. Converting this systems to first order equations proceeds as follows:

$$\begin{bmatrix} \ddot{\theta} \\ \ddot{x} \end{bmatrix} = \begin{bmatrix} m_1 L^2 & -m_1 L\cos\theta \\ -m_1 L\cos\theta & m_1 + m_2 \end{bmatrix}^{-1} \left(\begin{bmatrix} mgL\sin\theta \\ -m_1 L \sin\theta \dot{\theta}^2 \end{bmatrix} + \begin{bmatrix} 1 & 0 \\ 0 & 1 \end{bmatrix} \begin{bmatrix} M \\ F \end{bmatrix} \right) = \begin{bmatrix} r_{11} & r_{12} \\ r_{21} & r_{22} \end{bmatrix}^{-1} \begin{bmatrix} R_1 \\ R_2 \end{bmatrix}$$

$$\begin{bmatrix} \ddot{\theta} \\ \ddot{x} \end{bmatrix} = \frac{\begin{bmatrix} r_{22}R_1 - r_{12}R_2 \\ -r_{12}R_1 + r_{11}R_2 \end{bmatrix}}{r_{11}r_{22} + r_{12}^2}$$

Converting into first order equations:

$$y_1 = x_1$$

$$\dot{y}_1 = \dot{x}_1 = y_2$$

$$\dot{y}_2 = \frac{r_{22}R_1 - r_{12}R_2}{-r_{12}R_1 + r_{11}R_2}$$

$$y_3 = x_2$$

$$\dot{y}_3 = \dot{x}_2 = y_4$$

$$\dot{y}_4 = \frac{-r_{12}R_1 + r_{11}R_2}{-r_{12}R_1 + r_{11}R_2}$$

The nonlinear[1] first order equations to be used for numerical integration are:

$$\dot{y}_1 = y_2 \tag{B.13}$$

$$\dot{y}_2 = \frac{r_{22}R_1 - r_{12}R_2}{-r_{12}R_1 + r_{11}R_2} \tag{B.14}$$

$$\dot{y}_3 = y_4 \tag{B.15}$$

1. Note that in order to represent this system in matrix form, the equations will need to be linearized first.

$$\dot{y}_4 = \frac{-r_{12}R_1 + r_{11}R_2}{-r_{12}R_1 + r_{11}R_2} \tag{B.16}$$

B.2 Numerical Solutions to Algebraic Equations

This section describes the use of Newton-Raphson iteration to obtain numerical solutions to algebraic equations.

B.2.1 Newton-Raphson Iteration

The numerical method discussed here is referred to as Newton-Raphson iteration. This method, which is mathematically similar to the gradient decent optimization technique, involves minimizing a set of residual functions, f_i. The method involves calculating the residual function and the first derivative of the residual function evaluated at an initial guess. These values are used in the first order Taylor series approximation, (B.17), to predict the solution. The process is repeated using the previous solution as the guess for the next iteration.

$$\theta = \theta - \frac{f}{df} \tag{B.17}$$

Example #4: An algebraic problem requiring a numerical solution

Suppose the nonlinear algebraic problem of (B.18) needs to be solved for θ, and a valid closed form solution can not be found. The problem and be reformulated into a residual function and its derivative as shown in (B.19) and (B.20). An initial guess for the solution is chosen and (B.17) is used to predict the solution.

$$-6\cos\theta + 18\sin\theta + 4\,(12 + 5\,(\cos\theta + \sin\theta))\,(1 - \cos\theta) = 7 \tag{B.18}$$

$$f = -6\cos\theta + 18\sin\theta + 4\,(12 + 5\,(\cos\theta + \sin\theta))\,(1 - \cos\theta) - 7 \tag{B.19}$$

$$df = 34\sin\theta + 38\cos\theta + 20\sin(2\theta) - 20\cos(2\theta) \tag{B.20}$$

Programming a numerical algebraic problem

Below is an example program for applying the solution of Example #4.

```
% newton-raphson iteration example (matlab)
ftol=0.001;

A = 0.;      %initial guess

maxiter=100;
iter=0;
while 1,
  iter=iter+1;
  f = -6*cos(A)+18*sin(A)+4*(12+5*(cos(A)+sin(A)))*(1-cos(A))-7;
  df = 34*sin(A)+38*cos(A)+20*sin(2*A)-20*cos(2*A);
  if abs(f)<ftol
    break;
  end
  if iter>maxiter
    iter
    break;
  end
  A=A-f/df;
end;
```

APPENDIX C: SOFTWARE SUMMARY

This appendix is intended as a summary of programs and documentation developed for this project, this includes software written specifically for this research, in-house software, and commercially available software. All computer work, both research and documentation, was performed on Silicon Graphics, Inc. (SGI) workstations.

C.1 Software Summary

C.1.1 C and Matlab Programs

There is too much code to be printed here. This section is intended as a listing and brief description of the main programs developed for this research, specifically, monoped and biped dynamics and control. Other secondary programs for image processing, data digitizing, simulation playback: control, and graphing are also listed. Various converters, translators, and other in-house programs were also used, but are too numerous to discuss here.

Planar monoped programs:

- m2d-2link — 2-link, 4-DOF planar monoped
- m2d-3link — 3-link, 5-DOF planar monoped
- m2d-4link — 4-link, 6-DOF planar monoped

Sagittal plane biped programs:

- b2d-3link — 3-link, 5-DOF planar biped
- b2d-5link — 5-link, 7-DOF planar biped
- b2d-7link — 7-link, 9-DOF planar biped

Frontal plane biped programs:

- bf2d-3link — 3-link, 5-DOF frontal plane biped

Spacial bipeds programs

- b3d-3link — 3-link, 9-DOF spacial biped

Other miscellaneous programs

- moviepts — program for digitizing data from a series of images
- viewgeo — geometry viewer and animation program

C.1.2 Commercial Software

This is a list of the commercial software packages used in this project.

Matlab®

Matlab® is numeric computation software (by MathWorks, Inc.) used for initial gain calculations and simulation verification. Several Matlab.m files were created for each of the monoped and biped models discussed. A summary of these programs is given in section X.

Ernie/VisLab™

Ernie and its commercial counterpart VisLab™ (by EAI) are animation software packages used to create some of the color images.

Gigit/Vismodel™

Gigit and its commercial version Vismodel™ (by EAI) are simple solid modelers. Many of the less complex solid models use in this research were created and of modified using Gigit/ Vismodel. (Elaborate solid models we not a high priority, but are obviously important in other aspects or applications of this work.)

Showcase™

Showcase is a simple drawing and mixed media presentation system (by SGI) used for creating some of the 2D graphics images used in this dissertation.

FrameMaker®

FrameMaker® version 4.0 is a word processor/ document publishing system (by Frame Technology Corporation). Several FrameMaker templates were created for the Abstract, Appendix, Bibliography, Front pages, Chapter, and Title page as specified by the Iowa State University Thesis Office. These templates will be made available for use in the ISU Visualization Laboratory.

I-DEAS™

The I-DEAS Solid Modeling™ module, by Structural Dynamics Research Corporation (SDRC), was used to create some of the geometry models used in the virtual environment display.

Iris GL™

Iris GL™ (Graphics Library) is a collection of hardware specific graphics commands written in C for use on Silicon Graphics, Inc. (SGI) workstations. Iris GL was used to create the interactive environment for the dynamic simulations.

Inventor SceneViewer™

The Inventor SceneViewer™ (SGI) is a 3D object editor and viewer for Inventor™ models. SceneViewer was used to create the postscript images of the 3D models presented in this dissertation.

C.2 On-Line Documentation

C.2.1 World-Wide Web

On-line files associated with this research are located on the Iowa State University Visualization Laboratory World-Wide Web server at `http://www.vislab.iastate.edu/`. Files available include the Ph.D. Abstract, results summary, images, and animations[1]. Figure C.1 shows the initial page. Additional files will be temporally available on the Iowa State University public homepage server at `http://www.public.iastate.edu/~troy/`

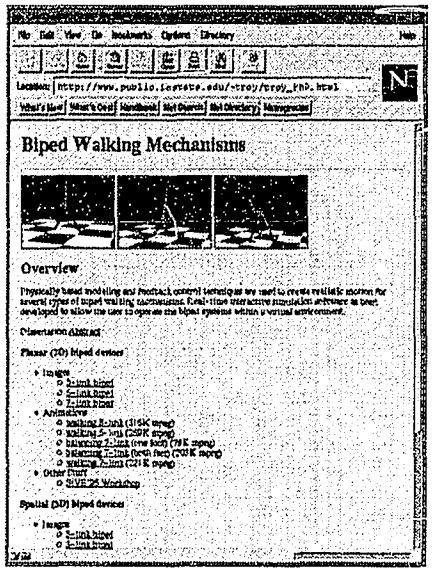

Figure C.1 On-line documentation

1. At the time of the final deposit of this dissertation, all files were available and in working order. (See comments in the Introduction about the volatility of electronic repositories.)

APPENDIX D: COLOR IMAGES

This appendix contains color images of some of the planar and spatial system models developed in this dissertation.

D.1 Planar System Images

- Figure D.1 shows planar (2D) monoped and biped system models
- Figure D.2 shows a composite walking sequence for the 7-link sagittal plane biped

D.2 Spatial System Images

- Figure D.3 shows spatial (3D) monoped and biped system models
- Figure D.4 shows a comparison of the gait cycle path traces for the three sagittal plane bipeds and one spatial biped

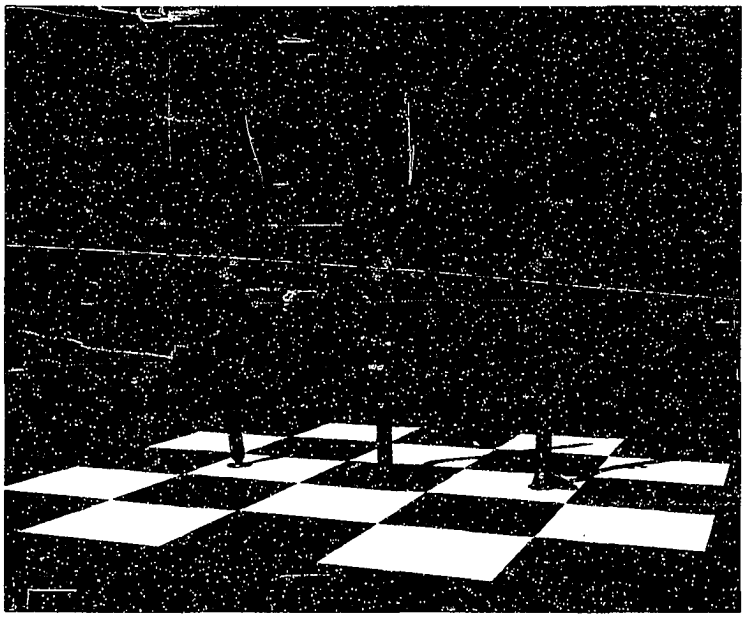

(a)

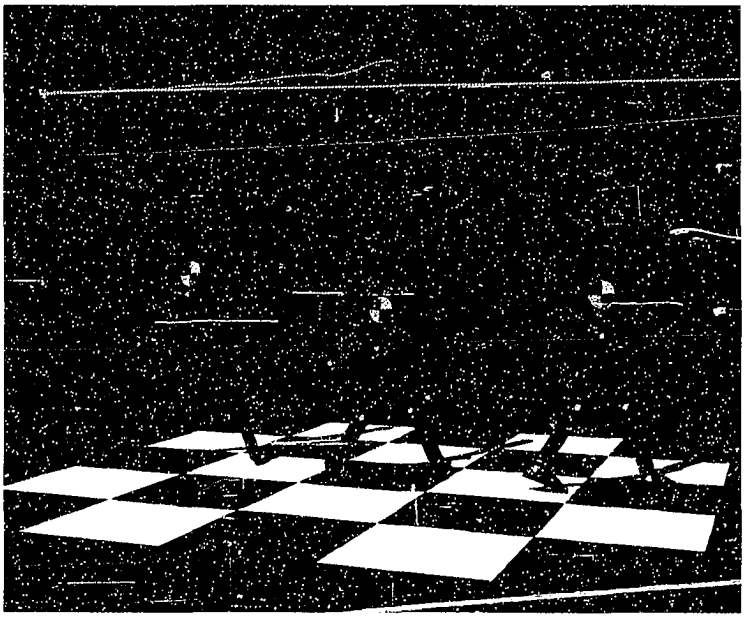

(b)

Figure D.1 Planar models: (a) monopeds, (b) bipeds

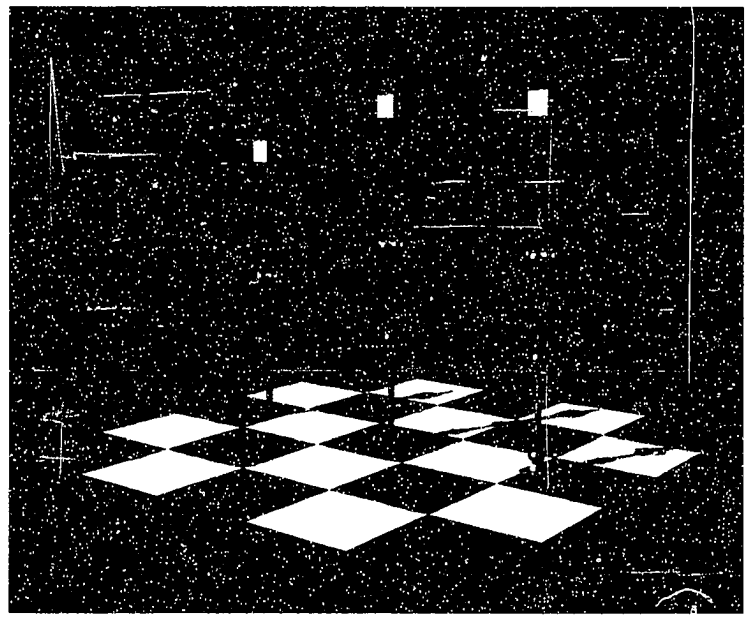

(a)

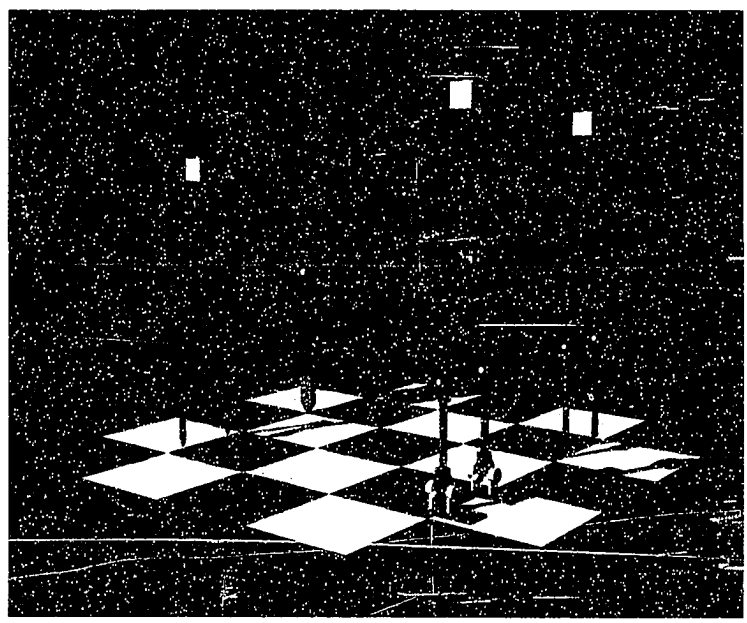

(b)

Figure D.3 Spatial models: (a) monopeds, (b) bipeds

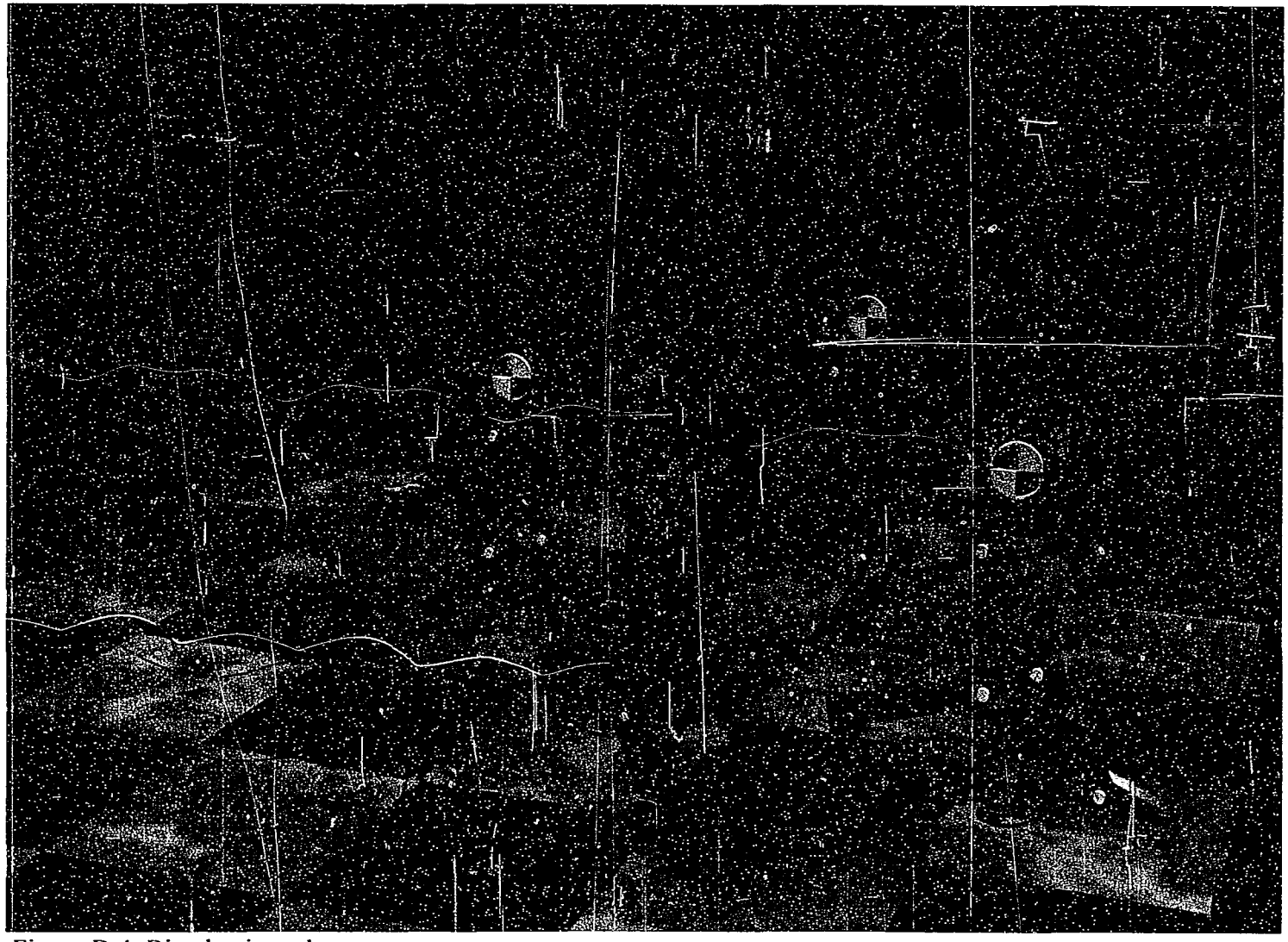

Figure D.4 Biped gait cycles